

■ DISSERTATIONES SCHOLAE DOCTORALIS AD SANITATEM INVESTIGANDAM
UNIVERSITATIS HELSINKIENSIS

34/2016

BÁRBARA HERRANZ BLANCO

**Multi-Approach Design and Fabrication of Hybrid
Composites for Drug Delivery and Cancer Therapy**

DIVISION OF PHARMACEUTICAL CHEMISTRY AND TECHNOLOGY
FACULTY OF PHARMACY
DOCTORAL PROGRAMME IN DRUG RESEARCH
UNIVERSITY OF HELSINKI

Department of Pharmaceutical Chemistry and Technology
University of Helsinki
Finland

Multi-Approach Design and Fabrication of Hybrid Composites for Drug Delivery and Cancer Therapy

by

Bárbara Herranz Blanco

ACADEMIC DISSERTATION

To be presented, with the permission of the Faculty of Pharmacy of the University of Helsinki, for public examination in Auditorium 1, Infocenter Korona (Viikinkaari 11, Helsinki), on 27th May 2016, at 12 noon.

Helsinki 2016

Supervisors Docent Hélder A. Santos
Division of Pharmaceutical Chemistry and Technology
Faculty of Pharmacy
University of Helsinki
Finland

Professor and Dean Jouni Hirvonen
Division of Pharmaceutical Chemistry and Technology
Faculty of Pharmacy
University of Helsinki
Finland

Reviewers Professor Christian Celia
Department of Pharmacy
Faculty of Pharmacy
University of Chieti –Pescara “G. d’Annunzio
Italy

Doctor Ciro Chiappini
Faculty of Engineering
Imperial College of London
United Kingdom

Opponent Professor Leigh Canham
PSiMedica Ltd, Malvern, United Kingdom
and
School of Physics and Astronomy
University of Birmingham
United Kingdom

© Barbara Herranz Blanco 2016
ISBN 978-951-51-2057-1 (pbk.)
ISBN 978-951-51-2058-8 (PDF)
ISSN 2342-3161

Helsinki University Printing House
Helsinki 2006

Abstract

Drug delivery systems (DDS) have been developed in the last decades to improve the pharmacological properties of free drugs by modifying their pharmacokinetic profile and biodistribution. Major limitations for newly developed drug molecules are the poor water solubility and stability, which can be addressed by DDS. These can protect the drugs from the potentially harsh external conditions found in the biological fluids, and improve their dissolution rate by different strategies, overall increasing the therapeutic activity of the drugs. Additionally, chemotherapeutic agents are nonspecific in nature, leading to deleterious off-target side effects, and poor therapeutic efficacy. Therefore, targeted therapy plays a very important role in cancer treatment, although not without obstacles, since DDS have to overcome a number of biological barriers following their intravenous administration, including renal clearance or opsonization-mediated phagocytosis and efficient extravasation to the tumor.

Mesoporous silicon (PSi) micro- and nanoparticles offer numerous benefits for biomedical applications, in particular for drug delivery. Along with a great biocompatibility and biodegradability, PSi possess mesopores (2–50 nm), where the drugs can be easily loaded and confined in their amorphous state avoiding extensive crystallization, thus, increasing their dissolution rate. However, the release of drugs from this platform is uncontrolled and fast, necessitating the use of strategies to tune the drug release.

In this thesis, multiple approaches were used for the design and fabrication of hybrid composites for drug delivery and cancer therapy, including PSi and polymer–drug conjugate-based DDS produced by different modalities of the microfluidics technology and pH-switch nanoprecipitation.

First, the loading and release of drugs with different solubility characteristics from PSi were investigated, and further PSi-lipid and polymer-composites were developed to control the drug release profiles. Overall, it was achieved both a sustained release of hydrophilic and hydrophobic molecules loaded on the PSi and also a reduced initial ‘burst release’ from the bare PSi particles.

Next, PSi-based nanovectors were envisaged for antitumoral applications. A smart PSi-based hybrid nanocomposite with stealth properties was developed, consisting of a pH-responsive polymeric structure assembled on the surface of drug-loaded PSi nanoparticles. This nanocomposite was extremely efficient avoiding drug release from PSi under physiological conditions, while allowing the release of the drug upon acidification of the medium. Remarkably, the nanocomposites avoided extensive macrophage recognition and phagocytosis.

Thereupon, a tumor targeted theranostic nanoplatform with dual pH- and magnetic-response capacity was designed. The DDS consisted of a polymeric-drug conjugate nanoparticle containing an imaging agent and decorated with a tumor homing peptide for targeted drug delivery, which was successfully applied for intracellular triggered drug release.

Overall, the hybrid composites based on PSi and a polymer-drug conjugate represented an advanced contribution to the field of drug delivery and cancer therapy, and in particular to the development of PSi as a platform for advanced drug delivery applications.

Acknowledgements

This work was carried out at the Division of Pharmaceutical Chemistry and Technology, Faculty of Pharmacy, University of Helsinki during the years 2012-2016. This period has been challenging but greatly stimulating and flourishing, and could not have been achieved without the financial and personal support received.

I would like to acknowledge the founding sources that made this work possible: Academy of Finland, University of Helsinki Research Funds, Biocentrum Helsinki, and the European Research Council.

I would like to express my deepest gratitude to my supervisor, Docent Hélder A. Santos, for giving me the fantastic opportunity of pursuing my doctoral studies under his supervision, and for supporting, encouraging, and believing in my abilities from the beginning and at every step, even in the moments I doubted them. His positive attitude, enthusiasm, and generosity, both personally and scientifically, have always inspired me and have paved the way of my accomplishments.

I am extremely grateful to my supervisor, Professor Jouni Hirvonen, for warmly admitting me to join his research group, and for his unwavering support. I deeply admire his kindness and generosity that have made this journey truly pleasant.

I would like to express my gratitude to all my co-authors for sharing their knowledge and expertise with me. Particularly, I would like to thank Docent Jarno Salonen, Ermei Mäkilä, Dr. Vimalkumar Balasubramanian, and Dr. Mohammad-Ali Shahbazi for their invaluable advice that has greatly help me to develop this work; and specially to Dr. Dongfei Liu for helping me to overcome the first obstacles in the “lab”, and for sharing his expertise with me in so many occasions.

I would like to thank Dr. Ciro Chiappini and Professor Christian Celia for reviewing this thesis and for their constructive comments that have truly helped me to improve it.

I am very grateful to all my colleagues from the Division of Pharmaceutical Chemistry and Technology for the warm welcome and for always creating a positive atmosphere that moves you to share and do your best.

I would like to express my most sincere gratitude to my colleagues and friends Elisa, Alexandra, Neha, Francisca, Ali, Riky, Patrick, Mónica, and Flavia for their friendship, and for sharing with me the best and the worst of these years, always cheering-me up, and for the well-deserved moments of fun.

I would like to dedicate this work to my parents, Jesús and Nieves, to whom I owe my deepest gratitude for their love and unconditional support with every decision I have made, always encouraging me to pursue my dreams; to my brother and sister-in-law, Jesús and Lupe, for lighting up my life and for their positive wishes; and to my grandmother, Leonor, for her unlimited love.

Finally, I would like to express my everlasting gratitude to my boyfriend and comrade Eloy, for his patience and selfless dedication to me. Always overcoming all odds side by side. I cannot thank you enough.

Helsinki, May 2016.
Bárbara Herranz Blanco

Contents

Abstract	i
Acknowledgements	ii
List of original publications	vi
Abbreviations and symbols	vii
1 Introduction	1
2 Review of the literature	3
2.1 Particulate drug delivery systems (DDS)	3
2.1.1 Overview and challenges	3
2.1.2 Porous silicon (PSi)	5
2.1.2.1 Fabrication and surface chemistry modification of PSi	6
2.1.2.2 Biocompatibility and biodegradability	7
2.1.2.3 Biomedical applications: drug delivery	9
2.1.2.4 Progress in PSi-based DDS	11
2.1.3 Lipid and polymer-based DDS	13
2.1.3.1 Fabrication of lipid- and polymer-based DDS	14
2.1.3.2 Progress in lipid- and polymer-based DDS	20
2.2 Nanomedicines for tumor therapy	22
2.2.1 Biological barriers for nanomedicines in tumor therapy	22
2.2.2 Strategies for nanomedicines tumoral therapy	24
3 Aims of the study	27
4 Experimental	28
4.1 Fabrication of glass capillary microfluidic chips (I-III)	28
4.1.1 Single emulsion flow-focusing (I) and nanoprecipitation co-flow (III) glass capillary devices	28
4.1.2 Double emulsion glass capillary device (II)	28

4.2 Fabrication of the DDS (I-IV)	29
4.2.1 Fabrication of PSi micro- and nano-particles (I-III)	29
4.2.2 Single emulsion-based fabrication of solid lipid microcomposites (SLMCs) (I)	29
4.2.3 Double emulsion-based fabrication of PSi–lipid vesicles (II)	30
4.2.4 Nanoprecipitation-based fabrication of PSi–Polymer composite (PSi–PC) (III)	31
4.2.5 pH-Switch nanoprecipitation of IO@PNP (IV)	32
4.3 Characterization of the DDS (I-III)	33
4.4 Loading degree and drug release studies (I-III)	35
4.4.1 Loading degree (I-III)	35
4.4.2 <i>In vitro</i> drug release (I-IV)	35
4.5 Human plasma stability of nanocarriers (III)	36
4.6 <i>In vitro</i> cell-based studies (I-IV)	36
4.6.1 Cell lines and cell culture (I-IV)	36
4.6.2 Cytotoxicity (I–IV)	37
4.6.3 Cell–particle interactions and intracellular trafficking (III and IV)	37
4.6.3.1 Flow cytometry analysis (III and IV)	37
4.6.3.2 Confocal fluorescence microscopy analysis (III and IV)	38
4.7 Hemotoxicity (IV)	38
4.8 <i>Ex vivo</i> studies (IV)	39
5 Results and discussion	40
5.1 Single-emulsion microfluidic templated THCPsi MPs–SLMCs for sustained drug delivery (I)	40
5.1.1 Characterization and cytocompatibility	40
5.1.2 Drug loading and release	42
5.2 Double-emulsion microfluidic templated THCPsi MPs–lipid vesicles for sustained drug delivery (II)	44

5.2.1 Microfluidic encapsulation of THCPSi MPs in lipid vesicles and characterization	45
5.2.2 Cytocompatibility and sustained drug release	45
5.3 Microfluidic nanoprecipitation self-assembly of PSi-based hybrid nanocomposites with pH-responsive properties (III)	46
5.3.1 Characterization	46
5.3.2 pH-Triggered drug delivery and cell growth inhibition	47
5.3.3. <i>In vitro</i> stealth properties	49
5.4 pH-Switch nanoprecipitation of polymeric solid NPs for tumor theranostics (IV)	50
5.4.1 Characterization and toxicity assessment	51
5.4.2 iRGD-Mediated cell uptake	53
5.4.3 Lysosomal escape and intracellular drug delivery	54
5.4.4 <i>In vitro</i> cell growth inhibition	57
6 Conclusions	58
References	59

List of original publications

This thesis is based on the following publications:

- I** Liu, D.*, **Herranz-Blanco, B.***, Mäkilä, E., Arriaga, L.R., Mirza, S., Weitz, D. A., Sandler, N., Salonen, J., Hirvonen, J., Santos, H. A. Microfluidic templated mesoporous silicon–solid lipid microcomposites for sustained drug delivery. *ACS Applied Materials & Interfaces*, 2013. 5(22), 12127–12134.
- II** **Herranz-Blanco, B.**, Arriaga, L. R., Mäkilä, E., Correia, A., Shrestha, N., Mirza, S., Weitz, D. A., Salonen, J., Hirvonen, J., Santos, H. A. Microfluidic assembly of multistage porous silicon–lipid vesicles for controlled drug release. *Lab On a Chip*, 2014. 14, 6, 1083–1086.
- III** **Herranz-Blanco, B.**, Liu, D., Mäkilä, E., Shahbazi, M. A., Ginestar, E., Zhang, H., Aseyev, V., Balasubramanian, V., Salonen, J., Hirvonen, J., Santos, H. A. On-chip self-assembly of a smart hybrid nanocomposite for antitumoral applications. *Advanced Functional Materials*, 2015. 25, 10, 1488–1497.
- IV** **Herranz-Blanco, B.**, Shahbazi, M. A., Correia, A., Balasubramanian, V., Hirvonen, J., Santos, H. A. pH-switch nanoprecipitation of polymeric nanoparticles for multimodal cancer targeting and intracellular triggered delivery of doxorubicin. *Advanced Healthcare Materials*, 2016 (in press).

The publications are referred to in the text by their roman numerals (**I–IV**). Reprinted with the kind permission of American Chemical Society (**I**), Royal Society of Chemistry (**II**), and John Wiley & Sons, Inc. (**III** and **IV**).

*In publication **I** the first two authors contributed equally to the work.

Abbreviations and symbols

AF	Alexa Fluor 647/ Alexa Fluor 488
APSTCPSi	3-aminopropyltriethoxysilane modified thermally carbonized porous silicon
APTS	3-aminopropyltriethoxysilane
BBB	Blood brain barrier
DAPI	4, 6-diamidino-2-phenylindole
DDS	Drug delivery system(s)
DHPE-Rh	1, 2-dioleyl-sn-glycero-3-phosphoethanolamine-N-(lissamine rhodamine B sulfonyl)
DLS	Dynamic light scattering
DMEM	Dulbecco's Modified Eagle's Medium
DMSO	Dimethylsulfoxide
DOX	Doxorubicin
D-PBS	Dulbecco's PBS
EDC	1-Ethyl-3-(3-dimethylaminopropyl) carbodiimide
EDTA	Ethylenediaminetetraacetic acid
EPR	Enhanced permeability and retention
EtOH	Ethanol
FBS	Fetal bovine serum
FITC	Fluorescein isothiocyanate
GI	Gastrointestinal
HBSS	Hank's balanced salt solution
HEPES	4-(2-Hydroxyethyl)-1-piperazineethanesulfonic acid
HF	Hydrofluoric acid
HPLC	High pressure liquid chromatography
i.v.	Intravenous
IO@AF-PNP-DOX	AF-labeled and DOX-conjugated IO@PNP
IO@iRGD-PNP	iRGD-decorated IO@PNP
IO@iRGD-PNP-DOX	iRGD-decorated and DOX-conjugated IO@PNP
IO@PNP	SPION encapsulated in polymeric nanoparticle
IO@PNP-DOX	DOX-conjugated IO@PNP
MES	2-(N-morpholino) ethanesulfonic acid
MFI	Mean fluorescence intensity
MP	Microparticle
mPEG	Methoxy poly(ethylene) glycol
mPEG-PHIS	Methoxy-terminated PEG-PHIS
MPS	Mononuclear phagocytic system
MRI	Magnetic resonance imaging
Ms	Magnetization saturation
NH ₂ -PEG-PHIS	Amino-terminated PEG-PHIS
NHS	N-Hydroxysuccinimide

NP	Nanoparticle
PBS	Phosphate buffer saline
PDI	Polydispersity index
PDMS	Poly(dimethylsiloxane)
PEG	Poly(ethylene) glycol
PEG-PHIS	PEG-block-poly(L-histidine)
PEG-PLA	PEG-block-poly(lactide methyl ether)
PLGA	Poly(lactic-co-glycolic acid)
PSi	Mesoporous silicon / porous silicon
PSi-PC	PSi-Polymer composite(s)
PVA	Polyvinyl alcohol
RBC	Red blood cell
Re	Reynolds number
SEM	Scanning electron microscopy
SFN	Sorafenib
SFN-PSi	SFN-loaded PSi
SFN-PSi-PC	SFN-loaded PSi-PC
SLMC	Solid lipid microcomposite
SPION	Superparamagnetic iron oxide nanoparticle
Sulfo-SMCC	sulfosuccinimidyl 4-(N-maleimidomethyl) cyclohexane-1-carboxylate
TCPSi	Thermally carbonized PSi
TEM	Transmission electron microscopy
THCPSi	Thermally hydrocarbonized PSi
THCPSi-SLMC	THCPSi-solid lipid microcomposite
TOPSi	Thermally oxidized PSi
UnTHCPSi	Undecylenic modified thermally hydrocarbonized PSi
τ_{agg}	Aggregation time
τ_{mix}	Mixing time

1 Introduction

Drug delivery systems (DDS) have been developed in the last decades to improve the pharmacological properties of free drugs [1-3] by modifying their pharmacokinetic profile and biodistribution [4], or by acting as drug reservoirs for sustained drug release. The poor water solubility of drugs is one of the major problems in drug development. For instance, for oral administration, the dissolution rate of practically insoluble drugs may be slower than the gastrointestinal (GI) transit time, resulting in therapeutically unacceptable bioavailability [5]. Even more challenging is the intravenous (i.v.) administration of poorly water-soluble anticancer drugs, necessitating the application of organic solvents to dissolve them prior to their administration [6]. In addition, many of the newly developed drugs consist of peptides or other biomacromolecules, which often suffer from degradation in the biological fluids, thus losing their activity [7]. Drugs integrated within DDS are protected from potentially harsh external conditions, such as acidic pH or enzymes that may degrade them, and their release may be tuned by different strategies, thus increasing the bioavailability of the drug [8-10].

In particular, chemotherapeutic agents generally suffer from low solubility and stability, and are nonspecific, leading to deleterious off-target side effects and poor therapeutic efficacy. Therefore, targeted therapy in cancer plays a very important role [11]. For this reason, DDS have been extensively used as a tool for nanomedicine in the treatment of solid tumors. Nowadays, there are a number of examples of nanomedicines in the market, such as Daunoxome[®] (liposomal daunorubicin), Doxil[®] (liposomal doxorubicin; DOX), Depocyt[®] (liposomal cytarabine), or the recently approved Lypusu[®], which represents the first paclitaxel-based liposomal formulation on the market. However, DDS have to overcome various biological barriers following their i.v. administration. The first of these is the renal clearance or opsonization-mediated phagocytosis by the mononuclear phagocytic system (MPS), which is influenced by the size and stealth properties of the DDS [12, 13]. Thereafter, the DDS have to extravasate to the tumor either passively, taking advantage of the leaky vasculature of the tumor angiogenic blood vessels; or actively, by targeting to the tumor vasculature using ligands that specifically bind to receptors expressed by the tumor-related cells. Tumor accumulation of the NPs is, in both cases, is boosted by DDS presenting long blood circulation times, by increasing the chances of the NPs to contact with the tumoral endothelial vascular cells and undergo active or passive extravasation [14-16].

As a result of the abovementioned challenges, DDS have evolved towards high loading capacity of therapeutic compounds, and controlled and targeted drug release. It is, nonetheless, crucial that the DDS are biocompatible and biodegradable in order to avoid any DDS-associated toxicity. Consequently, the biocompatibility and biodegradability of natural lipids have been widely exploited in this respect [17, 18]. In addition, a great effort is directed towards the development of biocompatible and biodegradable polymeric and inorganic materials which in turn offer great versatility for the development of advanced DDS [19]. These include polymers, such as polyglycolide, polylactide, polycaprolactone, polydioxane, poly(lactide-co-glycolide), or poly(trimethylene carbonate); and inorganic nanoparticles made out of silicon or calcium phosphate, among others [20, 21].

Among the materials exploited for drug delivery applications, porous silicon (PSi) stands out because of its many ideal characteristics in drug delivery and biomedicine [22-24]. First, and most importantly, PSi is biocompatible and its biodegradability in biological fluids is well established and can be easily tuned. In addition, due to the micro- or nanometric dimensions and the high porosity, PSi presents a large surface area. Together with a great pore volume, PSi can be loaded with considerable amounts of drug molecules, overcoming some of the greatest challenges that DDS have to address. In addition, the mesopores provide PSi with some exciting characteristics. For example, highly PSi was found to emit visible photoluminescence upon excitation with a green or blue laser, due to the two-dimensional quantum size effect [25]. Another exciting characteristic about PSi is that the drug molecules loaded are stabilized within the confined pores by limiting their arrangement in crystal lattices, providing loaded molecules with different physicochemical properties than the ones found in the bulk. This translates into improved dissolution of poorly water-soluble molecules and sustained dissolution of water soluble molecules [26]. Finally, the surface chemistry of PSi can be modified, rendering the particles with different properties [27].

However, PSi does not allow the controlled drug delivery of payloads. Upon administration, the mesopores are readily accessible by the body fluids, which can displace the payload, resulting in off-target premature drug release and, possibly, subsequent drug degradation, side effects, and loss of therapeutic efficacy. To overcome this hurdle, PSi particles decorated with a number of moieties or PSi-based hybrid composites have been designed in order to cap the pores and obtain drug release in a sustained or triggered fashion [28, 29]. Among the methods reported to produce lipid or polymer-based DDS, the microfluidics technology has shown great potential [30, 31]. This technique is used to precisely manipulate fluids in the micrometric scale in a highly reproducible way [32]. Two approaches are used for the fabrication of DDS by microfluidics: (1) droplet-based [32] and (2) and mixing-based microfluidics [33, 34]. The former generally renders DDS in the micrometric range, while the latter is based on the nanoprecipitation principle, rendering DDS in the nano-range. Remarkably, the microfluidics production of DDS ensures high encapsulation efficiency, while enabling a precise control of the size and dispersity.

In this dissertation, different materials and methodologies were developed for the fabrication of advanced DDS, and their potential applications were tested *in vitro*. PSi was loaded with different drug molecules to subsequently fabricate lipid and polymer-based PSi micro- and nano-composites. First, single and double emulsion droplet-based microfluidics technology was applied for the formation of PSi-lipid composites. The drug release profiles from these DDS were studied *in vitro* to assess the sustained drug release properties. Further steps were given towards the *in vitro* evaluation of the potential of DDS for cancer applications. For this purpose, different designs of polymer-based DDS were explored, aiming at accomplishing stimuli-triggered drug release, avoiding macrophage recognition, and achieving active targeting, while attaining good biocompatibility and stability in biological fluids. The DDS consisted of a PSi-polymer composite produced by fast mixing-based microfluidics, and a polymer-drug conjugate nanoparticle (NP) produced by bulk nanoprecipitation.

2 Review of the literature

2.1 Particulate drug delivery systems (DDS)

2.1.1 Overview and challenges

DDS have been developed in the last decades to improve the pharmacological properties of free drugs [2, 3]. In particular, some of the properties that might be improved by formulating drugs into DDS and that directly affect their bioavailability are the solubility of poorly water-soluble drugs and their stability in biological fluids [35]. Therefore, poorly water-soluble molecules may be formulated into DDS, such as cyclodextrins, porous structured materials, or other lipid- and polymer-based supramolecular structures to improve their dissolution rate [36-39]. In addition, DDS may also protect the loaded drugs from potentially harsh external conditions, such as acidic pH or enzymes that could degrade them [8-10]. However, when loading drugs into the DDS, the potency of the drug and the loading capacity of the DDS have to be taken into account in such a manner that drugs with low potency should be formulated into DDS with high loading capacity in order to maintain a reasonable dose in the DDS [1]. **Table 1** shows the potential problems associated with drug molecules and some of the solutions provided by their formulation in DDS.

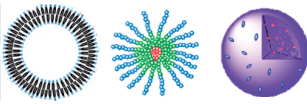
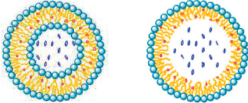

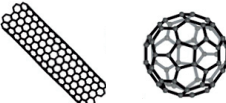
Table 1. *Pharmacological problems of drugs and some solutions provided by DDS. Modified with permission from ref. [1].*

<i>Problem</i>	<i>Implication</i>	<i>Effect of DDS</i>
Poor solubility	A convenient pharmaceutical format is difficult to achieve, as hydrophobic drugs may precipitate in aqueous media. Toxicities are associated with the use of excipients	DDS such as lipid micelles or liposomes provide both hydrophilic and hydrophobic environments, enhancing drug solubility
Tissue damage on extravasation	Inadvertent extravasation of cytotoxic drugs leads to tissue damage	Regulated drug release from the DDS can reduce or eliminate tissue damage on accidental extravasation
Rapid breakdown of the drug <i>in vivo</i>	Loss of activity of the drug following administration	DDS protects the drug from premature degradation and functions as a sustained release system. Lower doses of drug are required
Unfavorable pharmacokinetics	Drug is cleared too rapidly, for example by the kidney, requiring high doses or continuous infusion	DDS can substantially alter the pharmacokinetics of the drug and reduce clearance. Rapid renal clearance of small molecules is avoided
Poor biodistribution	Drugs that have widespread distribution in the body can affect normal tissues, resulting in dose-limiting side effects	The particulate nature of DDS lowers the volume of distribution and helps to reduce side effects in sensitive, non-target tissues

The DDS have been classified in three generations according to their properties [4, 40]. The first generation of DDS are systems capable of delivering an active substance to a target site when implanted close to it. The second generation, smart delivery systems, consist of smart polymers and hydrogels and nanoparticles (NPs) capable of carrying the drug to the target site after administration, protecting the drug along the delivery route and passively accumulating at the target site. Besides zero-order controlled drug release, peptide and protein delivery have also been demonstrated. The third generation of DDS, in addition to the previously mentioned properties, present the capacity to deliver poorly water-soluble drugs in a disease-targeted manner [4, 40].

In addition, DDS are classified according to their composition and structure. Generally, lipids, polymers, carbon, or inorganic materials, such as metal oxides, or silicon have been utilized for the fabrication of particulate DDS [40] in the formulations of liposomes, lipid emulsions, lipid-drug complexes, micelles, polymer-drug conjugates, and inorganic NPs, among others (**Table 2**).

Table 2. Summary of some of the particles used for drug delivery applications. Modified with permission from refs. [41, 42].

Composition	Particle type	Properties	
Polymer		Polymersome Micelles Nanospheres Nanocapsules	Drug delivery Some biodegradable
Lipid		Liposomes Micelles Solid lipid particles	Drug delivery Biocompatible Carrying hydrophobic cargos
Inorganic particles, e.g. silicon and silica		Spheres Shells Mesoporous	Drug delivery Luminescence Contrast agents Biocompatible Biodegradable
Carbon-based		Carbon nanotubes Graphene	Drug delivery Biocompatible

The DDS are designed to improve the pharmacological properties of free drugs by modifying their pharmacokinetic profile and biodistribution [4], or by acting as drug reservoirs for sustained drug release [1, 43]. DDS can be configured to present prolonged residence time in the body, either by reducing the clearance from the bloodstream, or by prolonging the retention in the GI tract, eye, skin, etc. [44-46]. Moreover, the volume of distribution of the DDS compared to free drugs is decreased due to the limited permeation of particles across the biological barriers [47], meaning that the volume of distribution of the drug formulated into a DDS is determined by the release rate of the drug [1]. An example

for this pharmacological improvement is given by the PEGylated liposomal formulation of DOX (Doxil[®]). Due to the prolonged circulation time of the PEGylated liposomes, the half-life of DOX was increased to up to 79 h, and the volume of distribution was limited to almost the plasma volume [48], overall rising the drug levels found in malignant effusions compared to free DOX [49].

DDS can be applied to different administration routes, each of them with a number of factors to consider and potential applications. The i.v. administration of DDS allows the drug to reach otherwise inaccessible sites in the body, and be rerouted away from the sites where the drug is toxic [40]. The blood vessels do not permit the extravasation of DDS, except through the discontinuous capillary endothelium found in the liver, spleen, and bone marrow [50]. In addition, pathological conditions, such as inflammation or solid tumors, render capillary endothelia particularly leaky, which has given place to the development of a number of DDS exploiting this characteristic [51, 52]. DDS administered orally, as a general rule, cannot reach the blood circulation, and are designed to protect labile drugs from degradation in the GI tract and to increase the bioavailability of poorly water-soluble drugs by enhancing their dissolution rate, localizing the delivery of the drug, and increasing the residence time of the system in the GI tract, while reducing the toxic effects of drugs [53]. Another administration route of DDS that holds great potential is the eye. Bioadhesive DDS have demonstrated to be retained in the eye and penetrate through the corneal epithelium [54, 55]. Other administration routes, such as subcutaneous, intramuscular, and topical have shown greater retention times for the DDS at the administration site compared to free drugs [40].

Probably, the greatest challenge that DDS have to face is their access to the clinic. Besides purely regulatory and industrial limitations [56], some of the technological barriers that the DDS have to overcome are the complexity of the systems and production, the safety and efficacy, the cost, and the storage stability [1, 57]. In terms of expenses, although the cost per treatment for DDS can be higher than for the free drugs, if one sums up the expenses related to side effects, DDS have demonstrated to be more cost-competitive than the free drugs [1, 58]. However, there is still much to understand about the pharmacokinetic of DDS [59] and the safety of the novel molecules used in their manufacture. Therefore, validated techniques for evaluating their pharmacokinetic profile and safety have to be implemented. In addition, the heterogeneity of complex multicomponent products must be minimized and controlled to ensure the reproducible manufacture at the industrial scale [57]. Despite the great challenge ahead, DDS have reached the market, mostly in the form of PEGylated lipid-based DDS for monotherapy [1, 2].

2.1.2 Porous silicon (PSi)

Mesoporous silicon (PSi), consisting of a crystalline silicon (Si) structure with pores in the size range of 2 to 50 nm, was first reported by Uhlir in 1956. In his search for a technique to shape semiconductor materials, Uhlir described the electrolytic etching of Si, through which PSi was obtained [60]; however, it was not until 1971 when the porosity of the structure of PSi was described [61]. Thereafter, highly PSi wires were found to emit visible photoluminescence upon excitation with a green or blue laser, owed to the two-dimensional

quantum size effect [25]; and, later on, PSi demonstrated to be biocompatible *in vitro* [62], this finding being the stepping stone for the following studies about this material as a tool for biomedicine, especially in the field of drug delivery.

2.1.2.1 Fabrication and surface chemistry modification of PSi

The production of PSi is commonly carried out by the electrochemical dissolution of bulk Si in a hydrofluoric acid (HF) based electrolyte [27, 63, 64]. For this, a Si wafer is placed between two HF resistant electrolyte cells, in which platinum electrodes are located on both sides of the Si wafer, and an electrical current is applied between them. The upper side of the Si substrate acts as the anode, where the oxidation and chemical etching of the Si surface takes place, with the subsequent dissolution of Si and formation of a PSi layer. The lower side of the wafer is the cathode, which is in contact with a conductive metal. Here, the proton reduction takes place, leading to the formation and evacuation of hydrogen (H₂) [64]. Therefore, in this setup, the dissolution of Si and formation of the porous layer occurs exclusively at the anode.

The final characteristics of the PSi layer obtained, such as porosity, thickness, and pore size and shape, directly depend on the conditions of the fabrication [27], which are finely tuned in order to get a specific and reproducible structure. These include the voltage and density of the electrical current applied to the electrodes, the concentration of HF in the electrolyte solution, the type, doping, resistivity, and crystallographic orientation of the Si wafer, the temperature, and the time [27].

Freshly etched PSi presents on its surface hydrophobic Si-H, Si-H₂, and Si-H₃ groups, that tend to oxidize under atmospheric conditions upon few months of storage, rendering a hydrophilic surface [27]. The application of native PSi for drug delivery is limited, since surface hydrides have been found to be strong reducing agents and incompatible with redox-active payloads [63, 65]. For this reason, the surface of PSi is generally stabilized through different methods, such as oxidation, hydrosilylation, or carbonization [27].

Oxidation is one of the most common ways to stabilize the surface of PSi, because of its simplicity, and the biocompatibility of the oxidized surface [66]. There are different oxidation methods, such as anodic [67], photo [68], chemical [69], and thermal oxidation [63]. Among them, thermal oxidation at low temperatures has been extensively used, through which two types of surface oxidation take place, *i.e.*, Si-Si back-bond oxidation and Si-H bond oxidation, to render -O_ySiH_x, Si-O-Si, and Si-OH surface species [70]. The PSi obtained by this method has received the name of thermally oxidized PSi (TOPSi). Oxidation provides stability and hydrophilicity to the surface of PSi, which are key factors for drug delivery applications. However, it might not be favorable for the loading of certain drugs or some drugs may react with the oxidized surface [71]. In addition, oxidation of the back-bond of Si, leads to the expansion of the structure and reduction in the pore diameter [71]. This phenomena has been exploited in drug delivery for the oxidation-trapping post-loading of drugs into native PSi [72].

Hydrosilylation of alkenes or alkynes on the surface of PSi [73-75], consists of the reaction of surface species SiH_x with compounds containing C=C, C≡C, or C=O to yield Si-C-C, Si-C=C, or Si-C-O. These modifications have been used to increase the stability of PSi

and to attach molecules with specific functional groups at the opposite end of the chain. Methodologies including, Lewis acid catalyzed, white light promoted, cathodic electrografting, and thermal hydrosilylation, have been applied for the hydrosilylation of PSi [64]. In particular, thermal hydrosilylation is a simple technique that has been used to produce, among others, hydrophilic derivatized undecylenic acid PSi [76].

Carbonization of the surface of PSi refers to the substitution of the Si-H bonds for Si-C bonds, providing PSi with stability towards harsh chemical conditions and oxidation [77, 78]. The most commonly used method is the thermal carbonization of PSi in the presence of acetylene. Due to the rapid diffusion of the small molecules of acetylene through the pores, a complete carbonization of the surface can be achieved. Depending on the temperature used, two types of surface chemistries are obtained. These are, Si-CH, when the treatment temperature is below 650 °C, rendering thermally hydrocarbonized PSi (THCPSi), with hydrophobic surface properties; and hydrogen-free Si-C species, when the treatment temperature is above 700 °C, generating thermally carbonized PSi (TCPSi) with hydrophilic surface properties [77, 79]. Similarly to the hydrosilylation of native PSi, the surface of the THCPSi NPs has been functionalized by thermal treatment of the particles in undecylenic acid to obtain undecylenic acid modified THCPSi (UnTHCPSi). The presence of -COOH groups allow easy covalent attachment of other biopolymers, macromolecules, or fluorescent dyes, having a great impact for drug delivery applications [80].

2.1.2.2 Biocompatibility and biodegradability

The first *in vitro* incursion into the biocompatibility of PSi was successfully performed by Canham in 1995 [62]. Later, encompassing the increased interest in PSi in the field of biomedicine, great efforts have been dedicated to the investigation of the biocompatibility of this material [81-84], as well as to its fate in the body [82, 85-88]. Although *in vitro* models are a good tool to understand the interactions and effects of a biomaterial over different cell lines, they do not account for the possible effects of the biomaterial over the complex systems of a human body. Therefore, *in vivo* studies are also required to determine the biosafety of a material. In this respect, *in vitro* and *in vivo* models have been applied to determine the biocompatibility of PSi, revealing that a number of parameters, including size [84], pore size [83], and surface chemistry [89] have an effect on its toxicity.

The biocompatibility of PSi for oral administration has been widely studied *in vitro* with GI-related cell models [90, 91]. For example, the toxic effects of TOPSi NPs with different pore sizes, between 17 and 58 nm, and amine functionalized PSi NPs incubated with a co-culture of Caco-2/HT29-MTX cells have been evaluated [83]. The results revealed that increasing the pore size of TOPSi NPs might enhance the cytotoxicity of the particles; however, this was justified either by the pore size of the particles or by the different methodology used to produce the TOPSi NPs with different pore sizes. TOPSi NPs with larger pore sizes were annealed in order to increase the pore size prior to their thermal oxidation, which has been found to decrease the density of -OH groups on the surface, and that could have influenced the toxicity of the NPs. Besides, amine functionalized PSi NPs were more cytotoxic than TOPSi NPs with similar pore size [83].

The biocompatibility of PSi *in vivo* in the rat eye has also been tested [81, 92, 93]. In one study, hydrosilylated PSi and TOPSi with sizes between 1 and 270 μm were injected into the rabbit's vitreous and observed until their total degradation in 3-4 weeks [92]. The authors reported no signs of toxicity in the different parts of the eye of the animals. Moreover, chemical modification of the particles and pores' surface by hydrosilylation or by thermal oxidation dramatically increased the stability and vitreous residence time of the particles, thus revealing the feasibility of using PSi as a long-lasting intravitreal drug-delivery vehicle.

Recently, a study presented the toxic effects of various surface modified PSi NPs assessed *in vitro* in blood immune and red blood cells (RBCs), and also *in vivo*, based on histopathological and biochemical parameters [89]. Overall, the *in vitro* studies showed that the toxicity was greatly dependent on the surface charge of the PSi NPs, and to a lesser extent on their hydrophobicity. Thus, positively charged 3-aminopropyltriethoxysilane modified thermally carbonized porous silicon (APSTCPSi) or the more hydrophobic UnTHCPSi, showed the greatest impact on RBCs' morphology, and APSTCPSi the greatest damage to the DNA, compared to TOPSi, TCPSi, and THCPSi. *In vivo*, the histopathological and biochemical parameters assessed after the i.v. injection of PSi revealed the biosafety of TOPSi, TCPSi, and THCPSi, showing mild histological changes in kidney, liver, and spleen, whereas APSTCPSi and UnTHCPSi presented greater toxicity.

The biocompatibility of PSi micro- and nano-particles have also been studied for their application in drug delivery to the heart tissue to treat myocardial infarction [84]. THCPSi and TOPSi microparticles (MPs) and NPs were evaluated, showing good *in vivo* biocompatibility and no alterations on the cardiac function or the hematological parameters. However THCPSi MPs activated inflammatory cytokines and fibrosis promoting genes. Thus, THCPSi and TOPSi MPs and TOPSi NPs could as well serve as vehicles for improving the cardiac delivery of therapeutic agents.

A further concern about the biocompatibility of any substance introduced in the body is its biodegradability, as well as the biocompatibility and rate of production of the degradation products [94]. In this respect, PSi degrades in aqueous solutions to orthosilicic acid through oxidative hydrolysis [95], which has been corroborated *in vivo*, demonstrating also to be biocompatible [86, 96, 97] and cleared from the body through the urinary pathway [87]. Furthermore, the degradation rate of PSi directly depends on the degree of crystallinity [98], the porosity and surface area [99], the surface chemistry [100, 101], and the pH of the medium [95]. Therefore, increasing the porosity and surface area of PSi accelerates its degradation rate by increasing the surface contact for hydrolysis [99]. Moreover, the surface chemistry affects in two ways to the degradation rate of PSi. First, it determines the hydrophilicity, and thus, the wettability of the surface of the pores; and second, it is related to the chemical resistance to hydrolysis [95]. By modifying the hydrogen termination of freshly etched PSi to oxidized, hydrosilylated, or hydrocarbonized surfaces, the stability and biodegradability of PSi can be tuned, rendering less reactive species towards oxidation and hydrolysis [102, 103]. Lastly, an increase in the pH value of the medium accelerates the degradation rate of PSi due to the presence of OH^- mediating the hydrolysis of the Si-H and Si-Si bonds [95, 99]. Thus, all these parameters should be taken into consideration when designing PSi for biomedical application, in order to obtain the most adequate degradation rate according to the particular potential application.

2.1.2.3 Biomedical applications: drug delivery

From the first reference in the literature to the potential applicability of PSi *in vivo* [62], numerous *in vitro* and *in vivo* studies have boosted the development of this material for biomedical applications, such as implants [104], biosensors [105], *in vivo* imaging agents [86, 88, 106], and drug carriers [83, 107, 108]. In particular, the beneficial biocompatibility and biodegradability of PSi, along with the vast surface area-to-volume ratio and pore volume, makes them ideal candidates as drug delivery vehicles [81, 85, 101, 109].

In this regard, the loading and adsorption of drugs into the pores of PSi and their release is ruled by many factors that can be tuned in order to successfully load and release different kinds of cargos. Among these factors are the surface area and the pore volume, which determine the amount of drug that can potentially be loaded; the degradation rate of PSi itself (*Section 2.1.2.2*) [110]; and the surface chemistry, which determines the physicochemical properties of the surface of the pores and the interactions between the pore wall, the solvent used to load the drug, and the drug [111, 112]. Other parameters that have an impact on the loading of drugs into the pores of PSi are related to the solvent used and the properties of the drug. The wettability of the pores is dependent, in addition to the surface properties of the pores, on the surface tension and the viscosity of the drug solution. Low viscosity and surface tension allow better filtration of the solvent into the pores and, hence improving the drug loading. Furthermore, the physicochemical properties of the drugs and the concentration also play a role in drug loading into PSi. However, although these parameters are understood, predicting the loading degree of a certain drug molecule in the pores of PSi is still rather challenging [111].

Drug loading within PSi can be achieved by immersion, impregnation, or covalent attachment, among others. The most commonly used, the immersion method [26, 111], although unpredictable, is reproducible as long as the properties of PSi remain invariable [111]. This method consists of the immersion of PSi in a drug solution for a certain period of time, usually in the range of hours, to allow the solvent to diffuse into the pores carrying the drug, which is adsorbed on the pore walls driven by geometrical and chemical interactions. The solvent is then removed and PSi can be carefully rinsed with an appropriate solvent to remove the drug bound to the external surface. Loading can be performed at room temperature, which is very convenient when handling thermosensitive molecules, such as peptides. However, relatively high concentration of drug solutions are required for the loading, thus rendering the immersion method not optimal for the loading of valuable drugs [26, 111]. Therefore, other methods to incorporate drugs into PSi, such as impregnation or covalent grafting, might be advisable when handling these drugs [111]. In the impregnation method, the drug solution is mixed with the mesoporous material and the solvent is dried, forcing the diffusion of drug into the pores [111, 113, 114]. In this way, the drugs may be efficiently loaded, although the adsorption of the drug on the surface is difficult to control [64].

Drug molecules loaded in the mesopores of PSi are stabilized by the confined pore space that limits their arrangement in crystal lattices. Thus, drugs remain in their amorphous state or form nanocrystals, providing to these molecules with different physicochemical properties than the ones found for the bulk drug. This has been translated into improved dissolution of poorly water-soluble molecules and sustained dissolution of water-insoluble

molecules loaded into surface stabilized TOPSi and TCPSi [26]. In this respect, the dissolution rate of a number of poorly water-soluble drugs has been enhanced, including furosemide [26, 115], griseofluvin [26, 116], ibuprofen [117, 118], indomethacin [119], itraconazole [120], sorafenib [121], ethionamide [122], celecoxib [83], or saliphenylhalamide [123].

Along with the properties of the drugs, the pore size, surface chemistry, and loading degree, have also demonstrated to affect the kinetics of the delivery of drugs. In one study, PSi MPs with varying pore sizes (17–58 nm) were loaded with different amounts of the poorly water-soluble drug celecoxib (5–36%) in order to study how these parameters affected to the physical form of the drug, as well as to its *in vitro* and *in vivo* performance [83]. It was reported that while celecoxib loaded in the PSi MPs with smaller pore size was found in a non-crystalline form, the larger pore size and loading degree favored the crystallization of celecoxib in the pores with formation of bigger drug crystals with increasing pore size. However, pore size, and thus, celecoxib crystal formation did not have a major effect on the *in vitro* release of celecoxib, since the crystal growth inside the pores of PSi was limited by the pore dimensions, thus yielding nanocrystals with high surface area, which aided drug dissolution. Alternatively, the drug loading degree showed to influence the release rate of the drug. The lower drug loading degrees were found to enhance the release rate *in vitro* compared to higher drug loading degrees, by preventing the local accumulation of large amounts of drugs at the pore opening during the drug release, which might recrystallize on the external surface of the particles forming bigger drug crystals with slower dissolution rate profiles, and thus, blocking the pores. Accordingly, low drug loading degree was also found to improve the bioavailability of celecoxib in rats after oral administration [83].

Relative to the surface chemistry, a study comparing the effect of PSi with six different surface chemistries on the loading and release of ibuprofen was carried out [117]. The studied were as-anodized PSi particles, TCPSi, TOPSi, annealed TCPSi, annealed TOPSi, and THCPsi. The release profiles showed that the surface chemistry affected the dissolution enhancing properties of these particles. In particular, TCPSi MPs presented the highest capacity to improve drug dissolution. Likewise, in another study, acyclovir release profiles from UnTHCPsi, TOPSi, and native PSi were assessed [124]. UnTHCPsi particles with more stable Si–C chemistry showed a steadier drug release than TOPSi and native PSi, showing that acyclovir release could be modified by changing the surface chemistry of PSi.

Another approach for the loading of drugs into PSi, which further allows a better control of the drug delivery, is the covalent grafting of drug molecules onto its surface [125, 126]. The release of drugs from these PSi–drug conjugates is mediated by the cleavage of the covalent bond between the PSi and the drug, or by the degradation of the Si structure. In this respect, drug release can be controlled by tuning both the liability of the chemical bonds or the degradation rate of PSi [111]. However, this methodology admits a reduced drug loading degree compared to the physical adsorption, since it is limited by the number of moieties available for the conjugation of the drug [111]. Moreover, the activity of the released drug has to be confirmed. Following this methodology, methotrexate was conjugated to PSi NPs through an ester bond rendering PSi-methotrexate conjugates capable of sustaining the release of the drug for up to 96 h [127]. In addition, the combination of the

drug with PSi enabled improved cellular uptake of methotrexate and *in vitro* antiproliferative effect in a cell culture.

2.1.2.4 Progress in PSi-based DDS

In addition to the promising features that PSi offers, further modifications can be done to this material to enrich its application in the drug delivery field. The most relevant modifications on PSi have been done towards the controlled and targeted drug delivery [128], along with magnetic or *in vivo* imaging properties [88, 129].

A major drawback limiting the application of PSi particles for the delivery of drugs is the uncontrolled release of the loaded cargo. Upon administration, the pores of PSi are readily accessible by the body fluids that can rapidly displace the payload resulting in uncontrolled and off-target premature drug release. This issue has been addressed by capping the pores of PSi by different methods, such as oxidation-induced trapping [72], grafting pore gating systems [107, 130], or by physically capping the pores or encapsulating the PSi particles within other carriers [107, 108].

Oxidation-induced trapping of drug molecules into the pores of PSi uses the contraction of the mesopores occurring during oxidation of the Si matrix to increase the retention of drugs [72]. In this way, two model compounds, cobinamide and rhodamine B, were loaded into a PSi film, together with sodium nitrite, which enabled the oxidation of Si. Subsequently, the drug-loaded films were fractured by ultrasonication into MPs, and the release rates of the compounds were found to be prolonged by 20-fold compared to PSi samples loaded with the compounds after oxidation.

Especially interesting are the DDS capable of responding to external stimuli as the trigger for drug release in order to achieve spatiotemporal control of this process (*Section 2.1.3.2*). This approach has also been used in combination with PSi particles. For example, a smart DDS combining PSi NPs with a pH-triggered nanovalve system was recently reported [107]. The nanocomposite was prepared by grafting a pH-responsive cationic polymer, poly(beta-amino ester), to PSi NPs loaded with DOX. In addition, due to the hydrophobic nature of the grafted polymer, the system was further stabilized with F127, a triblock copolymer containing poly(ethylene) oxide and poly(propylene glycol). First, F127 was used to prepare micelles loaded with paclitaxel that were, subsequently, assembled on the surface of the polymer grafted PSi NPs. The resulting nanocomposite achieved sequential combination therapy through the steady release of paclitaxel along with a pH-triggered release of DOX upon acidification of the release medium (pH 5) for the site-specific release of DOX. The nanocomposite also demonstrated enhanced colloidal stability and good cytocompatibility.

Regarding the physical pore capping or encapsulation of PSi particles to control the delivery of drugs, a number of polymers and lipids have been used, such as poly lactide-co-glycolide [131, 132], glycerol monostearate, and phosphatidylcholine [28]; or stimuli responsive compounds, such as hydroxypropylmethylcellulose [90, 128], acetalated dextran [133], or poly(N-isopropylacrylamide-co-diethylene glycol divinyl ether) [131]. For example, PSi has been functionalized with a polymer film to achieve sustained and temperature-dependent delivery of drugs [108]. Therefore, PSi loaded with the anticancer

drug camptothecin was coated with the temperature-responsive poly(N-isopropylacrylamide-co-diethylene glycol divinyl ether) that underwent physical transitions when heated beyond the lower critical solution temperature of 32 °C. In this fashion, the composite achieved to quench the burst release of the drug from bare PSi, as well as to sustain the release of drug along the time at 25 and 37 °C, when this effect was more pronounced at 25 °C.

PSi has also been used as a vehicle for other DDS. For example, APTS-modified PSi MPs ($1.6 \pm 0.1 \mu\text{m}$) with a pore size of 30 nm were loaded with liposome encapsulated paclitaxel for the targeted delivery of the payload to endothelial cells and bone marrow tissue [134] mediated by APTS binding to E-selectin receptors. Similarly, hemispherical PSi particles have been loaded with DDS to create NP-in-MP multistage vectors [135, 136]. In this respect, the size, shape, and surface chemical properties of the PSi particles were analyzed in order to tune their i.v. tissue distribution, revealing that the hemispherical PSi MPs were more likely to accumulate in the tumor endothelial and perivascular depots where the therapeutic payload was then released. This accumulation was achieved by the optimal hydrodynamic forces and interfacial interaction of these particles with the tumor vasculature, thus representing the best configuration as a vector for delivery of nanotherapeutics [137, 138].

PSi particles have also been targeted to certain organs or diseases, including bone marrow, mediated by APTS binding to E-selectin receptors [134]; subcutaneous MDGI-expressing tumors, mediated by a homing-peptide [139]; neuroblastoma, glioblastoma and B lymphoma cells, mediated by antibodies [140]; and prostate cancer, mediated by the homing-peptides RGD and iRGD [141]. However, efficient targeting of i.v. administered PSi particles is still compromised by the rapid clearance from the blood stream, therefore it is highly advisable to combine such targeted systems with other methods to prolong their blood circulation time. For example, dual-PEGylated TOPSi NPs presenting a high-density of Poly(ethylene) glycol (PEG) coating with both brush-like and mushroom-like conformations have been developed [142], demonstrating improved colloidal stability in salt solutions and reduction in both protein adsorption and macrophage uptake, features that could potentially be beneficial for the i.v. administration of PSi.

Other interesting properties in the field of drug delivery have been implemented in PSi, like magnetic properties for remote-guided targeted drug delivery (**Figure 1**). In this respect, PSi MPs were simultaneously loaded with superparamagnetic iron oxide NPs (SPIONs) and the anticancer drug DOX [129]. These particles were incubated with a cell culture and magnetically guided to promote the concentration of the particles in the vicinity of the magnetic field resulting in a high concentration of drug being released in that region of the Petri dish, which in turn resulted in localized cell death as confirmed by fluorescence cellular viability assay.

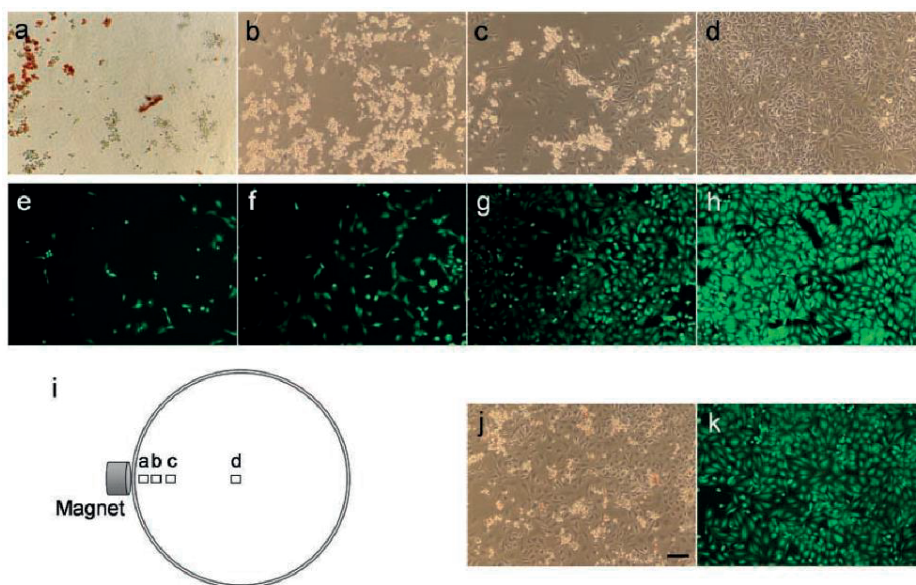


Figure 1 *In vitro* remote-guided targeted drug delivery. (a–d) Phase contrast microscope images of HeLa cells corresponding to different regions of the petri dish after 24 h incubation with DOX-loaded magnetic PSi MPs under the influence of a magnetic field placed on one side of the Petri dish (refer to figure i). (e–f) Fluorescence microscope images of HeLa cells stained with calcein acetomethoxy corresponding to the same positions as a–d images, respectively. (i) Representation of the relative position of the magnet and each image (a–d) in the Petri dish. (j, k) Phase contrast and fluorescence microscope images of a negative control dish of HeLa cells. Scale bar for all images is 100 μm . Reprinted with permission from ref. [129].

2.1.3 Lipid and polymer-based DDS

The first DDS to reach the market was PEGylated liposomal DOX in 1995, approved by the Food and Drug Administration [143], and, to date, lipid-based DDS have still been the most successful candidates in the race for clinical approval [1]. One of the reasons for the success of lipids in the formulation of DDS is their biocompatibility and biodegradability [17, 18]. However, biodegradable polymers are considered a good alternative to lipids because of their improved *in vivo* stability and tunable degradability [19].

In the past few years, lipid based particulate systems have been increasingly reported, such as nanostructured lipid carriers [144], emulsions [145], lipid–drug conjugates, lipid nanoparticulates [146], and polymer-lipid hybrid NPs [147]; but the major focus has been on liposomes and solid lipid NPs [148]. Most of these lipid-based DDS have been used to solubilize poorly water-soluble molecules to improve their bioavailability in the body [149], and one example of this are the liposomes, which have demonstrated excellent loading capacity and retention of hydrophilic drugs within their aqueous core through remote loading, guided by chemical gradients [150–152]. In addition, hydrophobic molecules have been successfully loaded and solubilized within the lipid bilayer of the liposomes [153].

Meanwhile, polymers hold the advantage of versatility, existing a number of natural and synthetic polymers with varying backbones to alter the release rate of drugs, and presenting the capacity to attach ligands for active targeting purposes. Among them, biodegradable polymers are desirable [19]. Polymeric NPs or self-assembled micelles from amphiphilic block copolymers are of particular interest in the drug delivery field, together with polymer-based DDS and polymer-drug conjugates, which are becoming widely utilized standard method to improve the circulation and bioavailability of biomacromolecules, such as antibodies [19].

In the following sections, the fabrication of different lipid- and polymer-based DDS related to this work will be discussed, as well as some of their advanced drug delivery applications.

2.1.3.1 Fabrication of lipid- and polymer-based DDS

Numerous approaches have been applied for the production of lipid- and polymer-based particles for drug delivery applications, often making use of amphiphile lipidic and polymeric molecules, which are capable of self-assembling in water to produce supramolecular structures. The most commonly used methods to drive and tune the self-assembly of these molecules are [32, 154-156]:

- solvent-switch method, in which the amphiphiles are dissolved in a solvent that is gradually switched for another solvent where one of the blocks of the amphiphile is not soluble;
- film rehydration method, which is based on the dissolution of the amphiphiles in an organic solvent, further removed to obtain a film that is then rehydrated with aqueous-based solutions;
- direct dissolution method, where the bulk lipid or polymer is directly dispersed in the aqueous solutions;
- microfluidics technology, which consists on the formation of particles from a single, double, or more, emulsion template produced inside microchannels;
- and nanoprecipitation method, in which a solute-containing solvent is mixed with a non-solvent, becoming the solute highly supersaturated and spontaneously nucleating.

In particular, the microfluidics technology and the nanoprecipitation method were the approaches used in this thesis for the production of lipid and polymer-based MPs and NPs, and will be described in detail in the following sections.

Microfluidics technology

The microfluidics technology consists of the manipulation of small volumes of fluids in the order of 10^{-9} to 10^{-18} L, making use of microchannels [157]. It has been exploited for a variety of applications, such as high throughput separation and detection of compounds [158], chemical synthesis [159], fluid optics [160], manipulation of cells [161], biomimetics [162], microbiotic systems [161], and manipulation of fluids [163]. Microfluidics offers

possibilities that are non-existent in the bigger scale, like the capacity to use tiny quantities of samples and reagents, detect and separate compounds with high resolution and sensitivity, and exploit the laminar flow occurring at the microchannels; while reducing the cost time and footprint of the process [164].

Particularly relevant to this work is the application of microfluidics for the manipulation of multi-phase flows in order to produce lipidic and polymeric-based particles. In this field there are a number of approaches used, among which are: (i) single emulsion-templation [165, 166]; (ii) double emulsion-templation [163], (iii) and rapid mixing [33]. The first two techniques render single or double emulsion drops in the micrometric range, while the last is based on the mixing pattern of fluids, allowing the production of particles in the nanometric range. By controlling the flow rates of the fluids pumped inside the capillaries, the viscosity and interfacial tension of the fluids, and the type and concentration of the polymers or lipids used to stabilize the droplets or form the NPs, the size of the droplets and NPs can be finely tuned. Moreover, highly monodisperse droplets and NPs, with high encapsulation efficiency are obtained [33, 167-169].

Two of the most representative devices used in microfluidics for the production of particles typically consist of microchannels etched primarily on a Si rubber of poly(dimethylsiloxane) (PDMS) using soft lithography [157], and chemically attached to a glass slide; or a circular capillary or a series of them inserted concentrically into another capillary and co-axially aligned and glued to a glass slide [170]. A difference between these two techniques in terms of the resulting flows achieved is that the glass capillary chips allow the production of truly three-dimensional flows [32] compared to the PDMS chips (**Figure 2**). Additionally, the chemical compatibility of PDMS devices is very limited, hindering the utilization of PDMS device with strong solvents. In contrast, glass capillary devices are very robust and compatible with a wide variety of solvents [171]. However, the etching of microchannels in PDMS can be performed in parallel, rendering a high production efficiency, compared to glass capillary devices, which have to be assembled individually by hand.

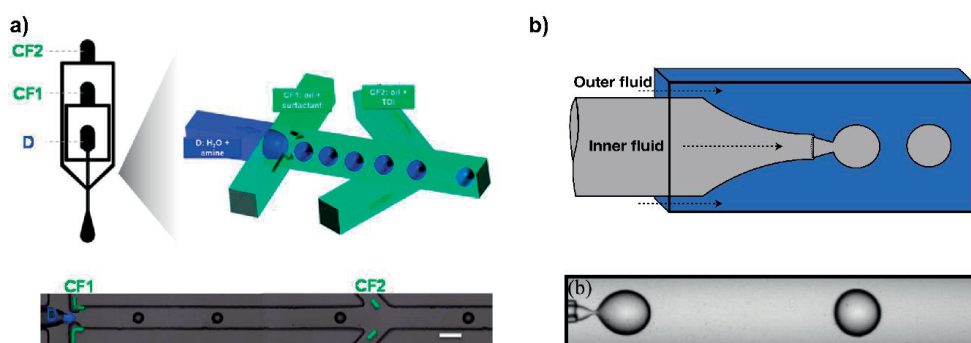


Figure 2 Schematic illustration of the geometry of droplet formations in (a) a PDMS microfluidic device. D: dispersed fluid, CF: continuous fluid for emulsification, CF2: continuous fluid for encapsulation. (b) Glass capillary flow-focusing microfluidic device. It can be observed how with the glass capillary devices truly 3D flows can be achieved compared to the PDMS device. Reprinted with permission from refs. [32, 172] and from ref. [173]. Copyright 2014 American Chemical Society.

Single and double emulsion microfluidic fabrication of microcarriers

Single and double-emulsion microfluidic templated production of MPs is based on the formation of two or three phases emulsion droplets, usually oil-in-water or water-in-oil-in-water droplets, stabilized by amphiphilic molecules, which after the evaporation of the oil phase render the MPs. The principle of droplet formation in the micrometric channels lays on the hydrodynamic instability of the inner flow [174]. Droplets might be formed by two different regimes called dripping or jetting. In the first one, the droplets form when the surface tension of the incipient droplet leaving the inner capillary is overcome by the viscous drag of the outer fluid. In the second regime, droplets are formed from a stream of fluid that eventually breaks down, based on the Rayleigh-Plateau instability [32]. When the inner fluid jet is slightly disturbed a thinner region is formed, leading to the curvature of the interface between the two fluids and the increase in the internal pressure of the water, as explained by the Laplace pressure, pushing the fluid within the jet to the sides and forcing the narrowing of the thinner part of the jet until it breaks up into droplets [32].

The glass capillary microfluidics devices offer the possibility of building a variety of geometries (**Figure 3**) for the production of single and double emulsion droplets. Single-emulsion microfluidics devices consist of an inner circular capillary tapered to a certain diameter and inserted into another glass capillary with which two fluid geometries can be achieved: co-flow and flow-focusing. In the co-flow geometry (**Figure 3a**) the inner phase is pumped into the inner capillary and the outer phase into the outer capillary, through the space between the inner and the outer capillaries, and in the same direction as the inner phase [175]. In the flow-focusing geometry (**Figure 3b**) the inner and outer phases are pumped into the outer capillary in opposite directions. When the fluids come into contact, they form an interphase and the outer fluid focuses the inner phase into the collection inner capillary where the droplets are formed [175].

Double emulsion microfluidics devices combine both the geometries, although different configuration of the capillaries can be used to achieve similar results [163, 176]. A design for double emulsion production is given in **Figure 3c**, consisting of two tapered capillaries, injection and collection, inserted at each side of an outer capillary. The inner and middle phases co-flow pumped into the inner injection and outer capillaries, respectively; while the outer phase, flowing in the opposite direction, focuses both inner and middle phases into the collection capillary, forming the double emulsion droplets [175].

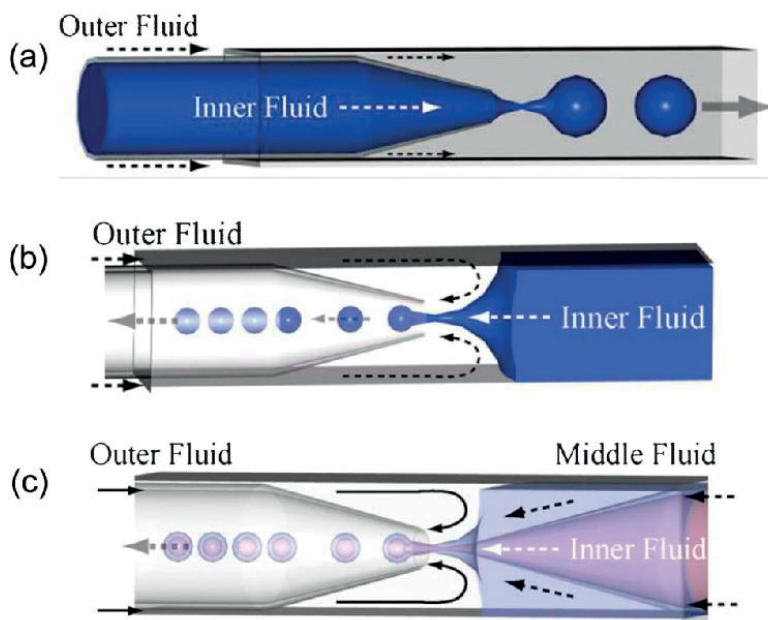


Figure 3 Schematic representation of glass capillary microfluidics devices. (a) Co-flow single-emulsion production approach. (b) Flow-focusing single-emulsion production approach. (c) Double-emulsion production approach combining co-flow and flow-focusing. Reprinted with permission from ref. [175].

Fabrication of nanocarriers based on nanoprecipitation

The nanoprecipitation technique was first patented by Fessi *et al.* [177] and described as “a process for the preparation of dispersible colloidal systems of a substance in the form of spherical particles of the matrix type and of a size less than 500 nm”. Following, in the same document, the process was described. For this, two liquid phases are needed: the first is a solution of the substance in a solvent or a mixture of solvents, and the second is a non-solvent or a mixture of non-solvents for the substance; being both miscible and containing or not surfactants. Either of the liquid phases may be added to the other with moderate stirring to produce a colloidal suspension of NPs almost instantaneously, and optionally the solvent may be removed from the final NP suspension. According to this patent, practically any substance sufficiently soluble in a given solvent can be used to produce NPs in this fashion. Based on this phenomenon, a large number of drug carriers have been produced, from classical polymers, such as poly(lactide) [178, 179], poly(caprolactone) [180], and poly(lactic-co-glycolic acid) (PLGA) [181]; to amphiphilic copolymers forming a core-shell structure [182, 183].

The formation of NPs by this method has been suggested to be triggered by the so-called “Ouzo effect” by Vitale and Katz [184, 185]. Based on a ternary phase diagram of the concentration of solute, solvent, and non-solvent, the Ouzo region represents the composition of these three components where only NPs are obtained (**Figure 4a**) [186].

This effect occurs because, upon mixing with a non-solvent, the solute becomes greatly supersaturated in certain regions where the nuclei of the solute are formed spontaneously, depleting the solute close to them, and limiting further nucleation in the close vicinity. The nucleation ends when there are not supersaturated regions remaining [184].

Nucleation has been explained by the classical nucleation theory. On the ternary phase diagram, the Ouzo region is a metastable region delimited by the spinodal and binodal curves, representing the limit of thermodynamic stability of the solution and the miscibility limit upon solvent composition, respectively (**Figure 4a**) [187]. When a critical supersaturation of the solute is reached (the supersaturation is defined as the ratio of the solute concentration to the equilibrium solubility) in the metastable Ouzo region, nuclei form spontaneously from small local fluctuations in the concentration of the solute [186]. Particles with a radius smaller than the critical radius, r^* , corresponding to the maximum of free energy, vanish, whereas above r^* , particles are stable and can grow further [186]. Growth may happen through two mechanisms, both resulting in monodispersed NPs (**Figure 4b and 4c**) [188]. The first of them is limited by the diffusion coefficient of the solute molecules and by the supersaturation, when the growing nuclei stick solute molecules around them until the solute equilibrium concentration is reached (**Figure 4b**); the second mechanism takes place mostly when the nuclei concentration is very high, since the probability of collision is proportional to the square of the number of particles. Therefore, the nuclei collide and rearrange forming dense structures (**Figure 4c**) [186, 188].

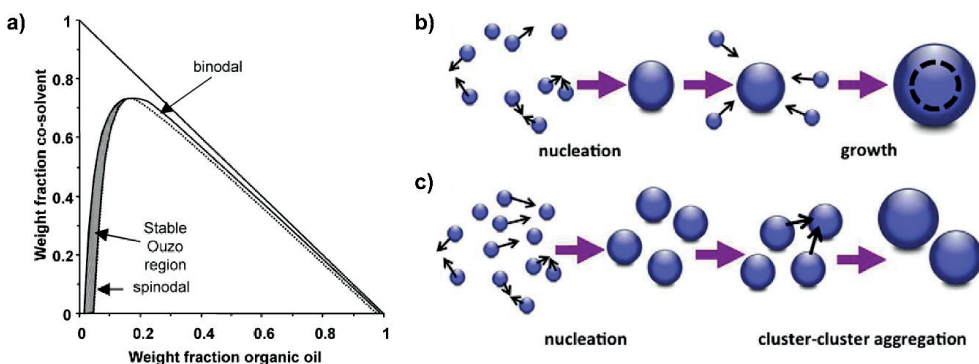


Figure 4 (a) Three-component phase diagram at constant temperature and pressure. The weight fraction of a solute on the solvent is represented on the abscissa, and the weight fraction of the solvent on the ordinate. The weight fraction of the non-solvent is found by difference. (b) Schematic representing nucleation growth limited by diffusion of solutes and supersaturation. (c) Schematic representing nucleation growth based on cluster-cluster aggregation. Reprinted with permission from ref. [184, 186].

The further growth of these NPs upon diffusion of dissolved solute may take place on a longer time scale driven by the Ostwald ripening, which defines that the total energy of the two-phase system can be decreased via an increase in the size scale of the second phase, and thus, a decrease in total interfacial area [189]. This can be prevented by the addition of

stabilizers. However, surfactants are often not necessary if the NPs contain hydrophilic moieties or non-neutral charge that promote the NPs' stability [190].

In addition to the initial concentration of polymer in the solvent, and the solvent/non-solvent ratio, there are other relevant parameters to control the size of the NPs produced by the “Ouzo effect”, such as the diffusion coefficient of the solvent and non-solvent, the viscosity, and the speed of the mixing process; factors that determine the mixing time of both liquids, since faster mixing has been reported to lead to smaller NP size [33, 191, 192]. Nanoprecipitation generates kinetically frozen NPs, meaning that the NPs grow until the energy barrier for the insertion of a chain becomes high enough, and this energy is dependent on the magnitude of the solvent quality change, being lower when the solvents diffusion is not complete and allowing the growth of the NPs. Thus, for a mixing time greater than the aggregation time ($\tau_{\text{mix}} > \tau_{\text{agg}}$), the size of the NPs is dictated by the mixing time and the initial polymer concentration, while for $\tau_{\text{mix}} < \tau_{\text{agg}}$, the NPs size is expected to be independent on the polymer concentration [192, 193].

For the above mentioned reason, different designs have been explored to ensure a fast and reproducible mixing pattern of the solvents [193-195]. One of the mixing techniques exploited and also applied in this thesis is based on microfluidics [33, 196]. The mixing process in microfluidics channels can be laminar or turbulent. Laminar mixing is achieved through hydrodynamic flow-focusing, in which an inner stream is narrowed and focused enabling the rapid diffusion of solvent and non-solvent inside and outside the stream, and thus, the nanoprecipitation of the solute (**Figure 5a**) [191]. In this respect, a study reported that the size and polydispersity, as well as the drug loading and release of NPs consisting of PLGA-PEG produced in this fashion, could be controlled by varying the flow rates, the polymer composition, and the polymer concentration [191]. Another study systematically screened the influence of the Reynolds number (Re) on the resulting NPs produced by microvortices-based mixing (**Figure 5b**) [33, 34]. The Re defines the flow pattern under different fluid flow situations and can be represented by the following **Equation 1**:

$$Re = \frac{\rho U L_0}{\mu} = \frac{\rho Q}{\mu E} \quad (\text{Eq. 1})$$

where ρ represents the viscosity of the fluid, U the average velocity of the fluids, L_0 the diameter of the pipe, μ the density of the fluid, Q the flow rate, and E the channel inner diameter.

For a given microfluidic setup, by increasing the viscosity of the liquids or the flow rate, or by decreasing the density of the fluids, a higher Re is achieved. Transitioning from low to high Re dictates changes in the mixing patterns of the fluids inside a microfluidic device from laminar flow to microvortices, to unsteady jetting [33]. Accordingly, NPs prepared from PLGA, hydrophobic chitosan, and acetalated dextran showed smaller sizes at higher Re [33, 34]. Moreover, NP size has been shown to be even more sensitive to Re than to the solute composition, which is indicative of the important of the mixing speed in the formation of NPs [34].

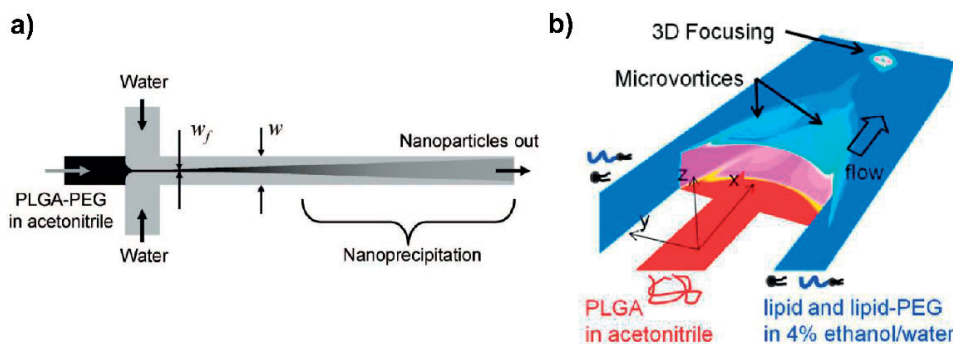


Figure 5 *Schematic representation of the nanoprecipitation process in a microfluidic device by (a) hydrodynamic flow focusing and (b) microvortices. Reprinted with permission from ref. [34, 191].*

2.1.3.2 Progress in lipid- and polymer-based DDS

To continue with the progress achieved in the last decades regarding novel approaches to control the delivery of drugs, current research focuses on the targeting of the DDS to the absorption or disease site where drug release is then triggered. Often, the carriers used for this tasks are lipid- or polymer-based DDS. Other tumor-specific strategies using DDS will be discussed in *Section 2.3.2*.

Active targeting of the lipid and polymer DDS is based on the functionalization of their surfaces to promote the affinity towards specific receptors/markers expressed by certain tissues/cells or under certain physiological conditions. Functional ligands decorating the DDS might be peptides, antibodies, sugars, lectins, etc. [197]. However, active targeting of DDS generally does not account for conformational changes or chemical instability that the ligands may suffer, or for the colloidal aggregation of particles, which hinders the exposure of the ligand [198]. Moreover, drug targeting in this fashion is a stochastic process that relies on the primary random contact of the particle with the target site to trigger the targeting mechanism [199].

In addition, other approaches are used for the targeted drug delivery of DDS. This is the case of DDS targeted by external stimuli, such as magnetic field, or ultrasound, which allow real-time targeting even to deep-seated tissues, remote triggering of drug release, and, additionally, simultaneous imaging and therapy [197]. For example, local heating of tumors by microwave or ultrasound superficial hyperthermia, used to trigger the release of DOX from liposomes by transition temperature of the liposomes, is already in clinical trials [200]. In addition, focused ultrasound has been found to reversibly disrupt and create gaps in the epithelial cell layers of the blood brain barrier (BBB) and blood-tumor barrier, allowing drugs and drug nanocarriers to escape the blood vessels into the target tissues [201]. Hyperthermia treatment of tumors can also be promoted by irradiating metallic NPs that absorb light and convert it into heat. For example, heat sensitive poly(N-isopropylacrylamide) and a poly(N-isopropylacrylamide)-co-poly(acrylamide), have been designed to present low critical solution temperatures of 32 and 39 °C, and, when coating

hollow porous gold nanostructures and upon near-infra red laser irradiation, the polymers shrink uncovering the pores and allowing drug efflux [202].

Moreover, other complex systems have been reported for the targeting of DDS. For example, communication between gold nanorods, magnetofluorescent iron oxide nanoworms, and DOX-loaded liposomes *in vivo* has been achieved, promoting tumor targeting of the liposomes through the activation of the machinery of an endogenous multistep biological cascade [203]. Tumor-targeted gold nanorods converted external electromagnetic energy into heat to locally disrupt tumor vessels, resulting in the activation of the coagulation cascade. In addition, coagulation was activated by circulating peptides that targeted coagulation enzymes activity by acting as a substrate for the coagulation transglutaminase factor XIII. Circulating iron oxide nanoworms and DOX-loaded liposomes coated with peptides capable of recognizing fibrin were therefore recruited by their interaction with the fibrin produced in the coagulation cascade at the tumor.

Another challenge faced by lipid- and polymer-based DDS is the insufficient drug loading and off-target drug release. Different approaches have been used to overcome this issues, such as the fabrication of crosslinked polymeric NPs to avoid degradation and premature drug release in the body fluids [204], or particles formed from lipid or polymer drug conjugates. For example, the natural lipid squalene, capable of forming NPs in its folded conformation has been conjugated to drugs, achieving 5 times more drug loading than liposomes [205].

Other strategies aim to endow lipid- and polymer-based DDS with the capacity to overcome biological barriers, such as the BBB. For example, NPs with certain properties are capable of interacting with the BBB-forming cells at a molecular level achieving the transport of drugs across the cell barrier [206]. In this regard, poly(butyl)cyanoacrylate NPs coated with Tween-80 were capable of binding apolipoprotein E, thus appearing as a low density lipoprotein for the endocytic cells of the BBB [207]. This allowed the entry of drug-loaded NPs into the cell from where the drug was effluxed into the brain parenchyma.

In some cases, even the intracellular targeting of DDS is required, when the therapeutic action of the drug is on a target within the cell, *i.e.*, intracellular peptides, enzymes, nucleic acids (DNA/RNA) [197]. Intracellular targeting involves the access of the DDS through the endocytic pathway into an endosome which further becomes a lysosome. Lysosomes are acidic and contain hydrolytic enzymes that degrade the material inside it; therefore, it is crucial that the active molecules escape to the cytosol intact. DDS used for intracellular targeting are usually stimulus responsive carriers that initiate their release into the cytoplasm via endosome or lysosome-disruption. Generally, cationic lipidic or polymers are used due to their proton-sponge properties. These molecules protonate upon acidification of the endosomal compartment creating an osmotic flow from the cytoplasm to the endosomes or lysosomes, increasing the pressure on the organelle that leads to its disruption [208]. Some of the lipids or polymers with proton sponge capabilities are molecules containing primary, secondary, tertiary or quaternary amines, or other positively charged groups. In this respect, lipids or polymers containing histidine or imidazole rings [209], polyethylenimine, polyamidoamine, polylysine, etc., have been used for intracellular drug delivery [208].

2.2 Nanomedicines for tumor therapy

2.2.1 Biological barriers for nanomedicines in tumor therapy

To efficiently reach the tumor site, newly developed nanomedicines have to face multiple barriers. Among them, there are the body's natural barriers and the tumor pathological barriers (**Figure 6**). The first hindrance that the nanomedicines face after i.v. injection is the rapid clearance from the blood circulation by direct renal filtration or by the MPS [12, 13]. The filtration cut-off of the kidney has been reported to be of 5.5 nm, demonstrated by the fact that particles smaller than this size were directly excreted with the urine [12]. In addition, non-stealth NPs are rapidly opsonized by the blood serum proteins, which promotes their phagocytosis by the MPS [210] via attachment of the phagocyte to the NP through surface bound opsonins [211]. Non-biodegradable NPs that fail to be completely degraded by the phagocyte machinery will further accumulate in the associated MPS organs, liver and spleen [13]. Therefore, ideally, NPs should have stealth properties in order to prolong their circulation time and to increase their chances to extravasate at the tumor site [16, 212].

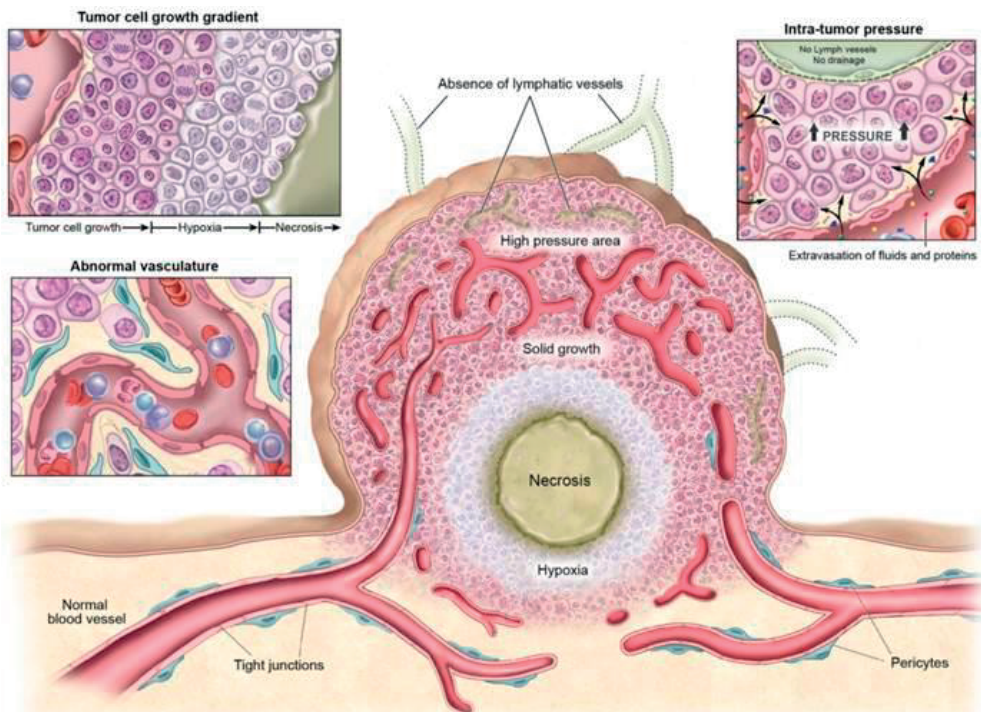


Figure 6 *Physiological characteristics of the tumor tissue and vasculature relevant for the development of DDS for tumor therapy. Reprinted from ref. [14]*

There are characteristic properties of the solid tumors that in principle help to the progression of the disease, but that can also serve to engineer nanomedicines that, taking advantage of these properties, specifically reach the tumor site [213]. These are the structure and architecture of the tumors, the cell surface, and the molecular targets. Cancerous cells are characterized by uncontrolled proliferation due to their replicative immortality, resistance to cell death, sustained proliferative signals, and metastatic capacity. Moreover, cancer cells are capable of evading growth suppression signals and immune system recognition [214]. Because of the rapid proliferation of cancer cells, the vessel density supplying oxygen to the tumor mass might drop generating hypoxic conditions [215]. In turn, cancer cells respond by reducing oxygen consumption and, if continued, adapting their metabolism by increasing glycolysis to maintain ATP production [216]. In addition, hypoxic and necrotic conditions induce the production of vascular endothelial growth factors, which promotes angiogenesis [214, 215]. In general, the balance of pro- and anti-angiogenic signals in tumors is not balanced, leading to a constant endothelial cell growth [215]. This situation causes the tumor vessels to fail forming defined structural features of arterioles, venules, or capillaries, and instead they grow caothically [215, 217]. Moreover, perivascular cells, encountered in close contact with endothelial cells in normal tissues, and in charge of controlling their proliferation, are found loose and in lower amount in tumor angiogenic blood vessels [218, 219]. As a result, some tumor vessels present a defective endothelial monolayer with disorganized, and loosely connected, branched, and overlapping endothelial cells [213]. In a study by Hashizume *et al.* [213] it was shown by scanning electron microscopy (SEM) the defective endothelial monolayer of vessels irrigating mouse mammary carcinomas, which are known to be leaky. They found out that 14% of the luminal vessel's surface presented poorly connected and overlapping endothelial cells with intercellular openings with a mean diameter of 1.7 μm , and also some transcellular openings of 0.6 μm mean diameter. Besides the widely explored tumoral leaky vasculature, a novel discovery has been reported [220]. Using intravital confocal laser scanning microscopy, stochastic bursts were observed in the tumor vasculature that led to dynamic vents through which a brief and vigorous outward flow of fluid and NPs extravasated to the tumor interstitial space. In this respect, long circulating NPs could better take advantage of this phenomenon, which also would allow the extravasation of large particles.

In addition to the enhanced tumor permeation, the interstitium of the tumor is characterized by deficient lymphatic drainage which promotes high interstitial pressure [221, 222]. In combination with the high permeability of the tumoral endothelial blood vessels, they render the so-called enhanced permeability and retention (EPR) effect, which is invariably found in all the solid tumors [51, 222]. This effect promotes the permanence of the therapeutic agents that extravasate the tumor blood vessels passively at the tumor interstitium [51]. However, the high intratumoral pressure may hinder the passive extravasation of therapeutic agents through the leaky vasculature, and may also tend to push the extravasated therapeutic agents to the margins of the tumor, resulting in their inefficient uptake [223]. In addition to the high interstitial pressure, poor lymphatic drainage, together with the propensity of tumors for glycolytic metabolism of glucose to lactate, render the tumor tissue slightly acidic [224, 225].

2.2.2 Strategies for nanomedicines in tumor therapy

Understanding the biological barriers and tumor physiopathology has led to the rational design and development of multistage and multifunctional advanced nanomedicines for antitumoral applications attaining predictable properties *in vivo* (Figure 7).

To begin with, opsonization of particles defines whether or not these will be recognized by the MPS and cleared from the body. Accordingly, some parameters of the particles can be engineered to reduce or slow down opsonization, such as the size, surface charge, and surface hydrophobicity/hydrophilicity [226], although no definitive rules exist for completely blocking it [13]. Regarding the size of the DDS, NPs with diameters smaller than 5.5 nm are quickly excreted by the kidneys [12]; however, particles with diameters larger than 200–300 nm tend to accumulate to a greater extent into the MPS cells in the spleen and liver [14, 227]. In addition, hydrophilic non-ionic NPs have been found to prevent opsonization by steric stabilization, compared to hydrophobic NPs, which present enhanced adsorption of serum proteins on their surfaces [226, 228-230]. In terms of charge, neutral particles have demonstrated lower opsonization rates than positively or negatively charged ones, likely due to the inhibition of the electrostatic interactions between proteins and particles [231, 232]; however, slightly negatively charged NPs *in vivo* have shown reduced liver accumulation and enhanced tumor accumulation compared to highly positively or negatively charged particles [233]. Therefore, to slow down opsonization hydrophilic polymers and non-ionic surfactants, such as polysaccharides, polyacrylamide, poly(vinyl alcohol), poly(N-vinyl-2-pyrrolidone), PEG, and PEG-containing copolymers, are often adsorbed or grafted to the surface of NPs [13]. To date, PEG is the most widely used polymer to provide NPs with long circulation capacity [16, 49, 234, 235]. Although recent studies have suggested the immunogenicity of PEG after repeated injections followed by accelerated blood clearance, this issue still holds controversy, since administered doses, animal species tested, and the type of PEGylated NPs, among others, seem to play a key role on the blood clearance [236].

Many of the engineered NPs for tumor therapy rely solely on the EPR effect to extravasate to the tumor [47, 237-239], and have even reached the market, such as Doxil [143], a PEG-based DOX liposomal formulation that shows a long circulation time in plasma, enhanced accumulation in murine tumors, and superior therapeutic activity over free DOX [49]. However, to further promote the extravasation and tumor penetration of therapeutic agents, these have been coupled to a variety of ligands that detect specific or overexpressed markers present on the endothelial cells' surface of blood vessels irrigating the tumors [15, 240]. Although this approach has demonstrated to be more advantageous than simply targeting to tumor cells, which suffer from poor extravasation to the tumor tissue, more advanced systems have arisen. In order to ensure the efficient extravasation and tumor penetration of nanosystems, tumor-penetrating peptides have recently been developed for targeting endothelial and tumor cells simultaneously, while being capable of penetrating into the tumor tissue [15]. Usually, the tumor penetrating peptides are developed by *in vivo* phage display [240], consisting of the screening of tumor molecular targets with phage random peptide libraries that specifically bind to them [240, 241]. Among others, examples of tumor-penetrating peptides are given by LyP-1 [242] and iRGD [241], which demonstrated *in vivo* to mediate the extravasation and tumor tissue penetration of intact

particles coated with these peptides, therefore increasing the efficiency of the drugs transported. In particular, iRGD, a cyclic peptide (CRGDK/RGPD/EC), has shown great advantages for tumor accumulation of NPs *in vivo* [243, 244]. iRGD and iRGD-coated NPs demonstrated to efficiently extravasate from the blood vessels, and accumulate at the tumor parenchyma, spreading around the tumor tissue in a metastatic tumor model [241]. This peptide specifically binds to $\alpha\beta3$ and $\alpha\beta5$ integrins upregulated in angiogenic endothelial cells and certain tumor cells [245]. Following, the sequence is proteolytically cleaved exposing a C-terminal CRGDK motif that losses affinity for the integrins while gaining affinity for the receptor Neuropilin-1, which mediates tumor cells and tissue penetration [241].

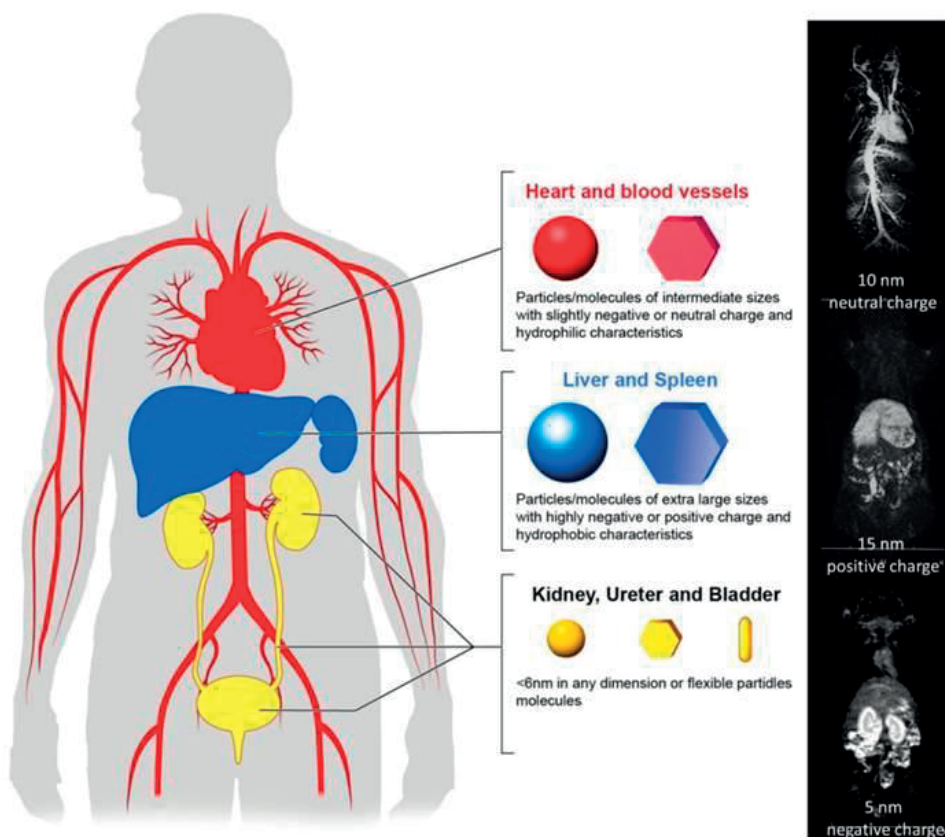


Figure 7 *Pharmacokinetics of particles administered i.v. Tumor extravasation of particles is aided by the prolonged blood circulation time. Reprinted from ref. [14].*

Despite all the advances, the battle for achieving tumor extravasation of NPs has gone further by tuning the geometry of the DDS in order to facilitate the adhesion to abnormal endothelium relying on the vascular blood flow patterns [198]. NPs follow intravascularly three steps: (1) lateral drift to the margins of the vessels, or margination; (2) firm adhesion to the endothelium; and (3) internalization [198]. Margination can be promoted by the

rational design of particles to achieve their accumulation in the vicinity of the endothelial cells, where laminar blood flow is observed. While classical spherical NPs rely on lateral external forces to marginate, such as gravitation [246], non-spherical particles tumble and roll, which can be used to control their margination dynamics without the need for external forces. Hence, larger discoidal, quasi-hemispherical and ellipsoidal particles are expected to adhere more efficiently to the endothelium of the vasculature than small spherical particles, due to a larger surface for adhesive interactions and greater margination propensity [247, 248].

NP-based cancer theranostics has emerged as the next-generation tool for personalized medicine, consisting of the combination of therapeutic and diagnostic agents on a single entity [249-251]. Theranostic NPs can simultaneously be applied to non-invasive diagnosis and treatment monitoring of solid tumors in patients by *in vivo* imaging techniques, such as computed tomography, magnetic resonance imaging (MRI), positron emission tomography, single-photon emission computed tomography, and fluorescence imaging [252]. On one hand, since diagnosis or treatment monitoring is not necessary with every administered dose, two identical platforms can be used independently or combined for therapy and imaging; on the other if using safe and inexpensive imaging agents, a single NP could be utilized as well [253]. In this respect, DDS have been combined with a variety of imaging agents in order to obtain data on their accumulation at the target site. For example, radiolabeled PEGylated liposomes were monitored on the treatment of a patient with Kaposi sarcoma, observing accumulation and prolonged retention of the liposomes at the place of the lesions [254]. Paramagnetic and superparamagnetic NPs, such as gadolinium [255], iron oxide [256], or manganese [257], have also been used for theranostic applications of NPs, because of their properties as MRI contrast agents. In addition, they have been utilized for magnetic guidance of DDS at the target sites by strong external magnetic fields and hyperthermia treatment of tumors [255, 258].

In addition to the satisfactory NP extravasation at the tumor site, efficient tumor treatment also relies on the stability of the NPs in the circulation and release of drug cargo intratumorally. In this way, it is possible to minimize undesirable off-target side effects of chemotherapeutic agents, while maximizing the therapeutic efficacy of the drug. One of the classical triggers exploited for the spatial delivery of drugs from lipid and polymer DDS is the pH. The characteristic pH values found at the tumors or metastases make a good example of it, and were already predicted as a potential trigger for drug release from pH-sensitive liposomes over 30 years ago [259]. Other designs make use of different stimuli as the trigger for drug delivery. These can be classified as intratumoral stimuli, such as interstitial or intracellular pH [260, 261], enzymatic actuation [262, 263], and reductive intracellular environment [264, 265]; and external stimuli, as described in *Section 2.1.3.2*, such as heat [266, 267], radiation [268, 269], magnetism [270, 271], and ultrasound [272].

3 Aims of the study

Despite the advances in the field of controlled drug delivery in the last decades, great efforts are still dedicated to the formulation of poorly water-soluble molecules into DDS in order to improve their pharmacological properties. PSi has long been demonstrated beneficial properties for these purposes; however, the efficient control of drug release from this platform is still being explored. Moreover, other approaches are applied to modify the therapeutic activity of drug molecules, such as their conjugation with polymers.

In this dissertation, lipids and polymers in combination with PSi, and a polymer-drug conjugate, were utilized to fabricate advanced DDS by bulk methods or using the microfluidics technology.

The specific objectives of this dissertation are:

1. To investigate the loading and release properties of drugs with different solubility characteristics into PSi and further develop protective lipid- and polymer-based structures to achieve controlled drug release. **(I–III)**
2. To evaluate different modalities of the microfluidics technology for the fabrication of PSi-based micro- and nano-composites, including single and double emulsion droplet microfluidics, as well as mixing-based microfluidics. **(I–III)**
3. To develop a smart PSi-based hybrid nanocomposite for antitumoral applications with triggered drug release and stealth properties, and for reduced macrophage detection *in vitro*. **(III)**
4. To explore other methods for the drug loading and preparation of multi-stimuli responsive DDS based on a polymer-drug conjugate, including ligands for active targeting, and to test their potential for antitumoral applications *in vitro*. **(IV)**

4 Experimental

4.1 Fabrication of glass capillary microfluidic chips (I-III)

4.1.1 Single emulsion flow-focusing (I) and nanoprecipitation co-flow (III) glass capillary devices

The microfluidic co-flow and flow-focusing devices were made by assembling borosilicate glass capillaries on a glass slide. One end of the cylindrical capillary (World Precision Instruments, Inc.), with inner and outer diameters of around 580 and 1000 μm respectively, was tapered using a micropipette puller (P-97, Sutter Instrument Co., USA) to a diameter of 20 μm ; this diameter was further enlarged to ~ 80 μm by carefully sanding the tip. This cylindrical tapered capillary was inserted into a square capillary with inner dimension of around 1000 μm (Vitrocom, USA), and coaxially aligned with it. A transparent epoxy resin (5 minute[®] Epoxy, Devcon) was used to seal the capillaries where required. For the single emulsion flow-focusing device, the collection capillary was treated with 2-[methoxy(polyethyleneoxy)propyl]trimethoxy silane, to render a hydrophilic tip and prevent wetting of the oil phase on the wall of the capillary. The fluids were injected separately into the microfluidics device through polyethylene tubes attached to syringes at constant flow rates, controlled by automatic injection pumps (PHD 2000, Harvard Apparatus, USA).

4.1.2 Double emulsion glass capillary device (II)

The double emulsion glass capillary device consisted of two cylindrical capillaries of inner and outer diameter of 580 and 1000 μm , tapered and carefully sanded to a tip diameter of 80 and 120 μm for injection and collection, respectively, inserted into the opposite ends of a square capillary of inner diameter 1000 μm (II). An additional capillary inserted into the injection capillary allowed the inner water and middle oil phases to co-flow within the injection capillary. The injection capillary was hydrophobically pre-treated with n-octadecyl-trimethoxy silane, to favor the contact of the middle oil phase with its wall; and the collection capillary was pre-treated with 2-[methoxy(polyethyleneoxy)propyl]-trimethoxy silane to render a hydrophilic tip in order to prevent wetting of the oil shell of the emulsion on the wall of the collection capillary. The fluids were injected separately into the microfluidic device through polyethylene tubes attached to syringes at constant flow rates controlled by automatic injection pumps.

4.2 Fabrication of the DDS (I-IV)

4.2.1 Fabrication of PSi micro- and nano-particles (I-III)

PSi MPs were prepared by anodizing a Si wafer (100) of p+-type with resistivity values of 0.01–0.02 Ω cm in a HF (38%):ethanol mixture (HF:EtOH 1:1, v:v) using a current density of 50 mA/cm² for 40 min, in order to obtain a porosity of ~65%. [85]. PSi MPs were produced by dry ball milling (Pulverisette 7, Fritsch GmbH) in an agate grinding jar and the particle size fraction of 1 to 38 μ m was sorted by wet sieving with ethanol. The MPs were then immersed in a HF:EtOH solution to remove the oxidized surface layer and refresh the surface hydride species, and further dried at 65 °C for several hours to evaporate the electrolyte [88]. In order to improve the stability of the PSi surface towards oxidation, PSi MPs were thermally hydrocarbonized by placing the MPs in a quartz tube under continuous N₂ flow (1 L/min) and acetylene flush (1 L/min) for 15 min, and thermally treated in an oven for 10 min at 500 °C. Then the sample was cooled down at room temperature under a N₂ flow [77, 85].

Alternatively, PSi NPs were produced by three current pulses, the first of which is common to the production of the MPs, to render a porosity of the Si wafer of 65%. The second consisted of a shorter and higher current pulse to produce a highly porous and mechanically fragile layer. The third was a zero-current pulse to remove possible electrolyte concentration gradients created in the pores during the high current pulse. Subsequently, the porous films were dried and thermally hydrocarbonized following the same protocol as the one described for the MPs. Then the PSi film was ball milled using liquid to improve the grinding efficacy. The liquid used was 1-decene, which reduced the oxidation of the non-thermally hydrocarbonized surfaces produced during ball milling due to the high grinding forces, which created enough heat to render the thermal hydrosilylation of aliphatic alkenes exposed [73, 85].

4.2.2 Single emulsion-based fabrication of solid lipid microcomposites (SLMCs) (I)

The THCPsi–solid lipid microcomposites (THCPsi–SLMCs) were produced with the single-emulsion glass-capillary microfluidic flow-focusing device described in the *Section 4.1.1 (I)*. The inner oil phase consisted of stearic acid (20 mg/mL, w/v) and egg phosphatidylcholine (40 mg/mL, w/v) dissolved in ethyl acetate, and bearing THCPsi MPs (10 mg/mL) that were dispersed by continuous stirring. The outer water phase consisted of a Poloxamer 188 aqueous solution (1%, w/v), which efficiently stabilized the oil/ water interface. The inner oil phase was pumped through the inner capillary at a rate of 2 mL/h and focused by the outer water phase pumped in the opposite direction at 40 mL/h, which ultimately broke-up the oil phase in droplets, induced by the shear forces. The SLMCs were prepared following exactly the same procedure, but without THCPsi MPs in the inner phase.

The SLMCs and THCPsi–SLMCs produced were collected and the organic solvent from the inner oil phase removed by placing the particles in a water bath at 60 °C for 30 min.

Lastly, all the collected MPs or microcomposites were solidified on ice for following characterization.

Drug loaded THCPSi MPs and THCPSi–SLMCs (I)

Different drugs were loaded into the THCPSi MPs using an immersion method [64]. For all the four drugs tested, a drug concentration of 30 mg/mL at a ratio of 3:1 (drug:THCPSi MPs w:w) and loading time of 2 h, were used. Methotrexate was dissolved in phosphate buffer (pH 8.0), ranitidine was dissolved in an ethanol:water solution (1:1), and both furosemide and fenofibrate were dissolved in acetone. After the loading, all the suspensions were centrifuged at 10000 rpm (5415D, Eppendorf, Germany) for 3 min and the supernatant removed with the excess of free drugs. Thereafter, drug-loaded THCPSi MPs were used to prepare the THCPSi–SLMCs with the microfluidics flow-focusing device.

4.2.3 Double emulsion-based fabrication of P*Si*–lipid vesicles (II)

To fabricate lipid-stabilized double emulsion drops with ultrathin shells and simultaneously encapsulate THCPSi MPs within their cores, we used the double emulsion glass-capillary microfluidic device described in *Section 4.1.2*. The inner water phase containing the THCPSi MPs with typical sizes of the order of 15 μm , was pumped into the innermost capillary inserted in the injection capillary. To facilitate the dispersion of the THCPSi MPs, they were pre-wetted with ethanol and suspended into an aqueous solution that contained 8 wt-% PEG (6 kDa) and 2 wt-% polyvinyl alcohol (PVA, 13–23 kDa) at a final concentration of 3 mg/mL. The suspension was sonicated and poured into a syringe together with a magnetic bar that allowed vigorous shaking of the suspension, thereby avoiding MP aggregation and sedimentation during the injection of the suspension within the microfluidic chip. The middle oil phase containing 4.6 mg/mL of 1,2-dioleoyl-sn-glycero-3-phosphocholine (Avanti) was dissolved in a mixture of chloroform and hexane at a volume ratio of 1:1.8, containing 0.25 mol-% of 1,2-dioleoyl-sn-glycero-3-phosphoethanolamine-N-(lissamine rhodamine B sulfonyl) (DHPE-Rh Molecular Probes) to fluorescently label the lipid bilayer, which was then pumped through the hydrophobically treated injection capillary, co-flowing with the inner water phase. At the tip of the innermost capillary inserted on the injection capillary large plug-like water drops containing the THCPSi MPs were formed, which were broken-up at the tip of the injection capillary into double emulsion drops by the shear forces induced by the outer water phase consisting of a 10 wt-% PVA (13–23 kDa) aqueous solution. The collection capillary was hydrophilic, which prevented the wetting of the oil shell of the emulsion on the wall of the collection capillary.

Importantly, this microfluidic approach provided 100% encapsulation efficiency since the particles in the inner water phase ended-up in the cores of the double emulsions as shown in publication **II**.

The double emulsion droplets were collected in an aqueous solution of sucrose with the same osmolarity as the inner water phase (100 mOsm/L) to avoid any osmotic destabilization of the double emulsion droplets. Under these conditions, the chloroform in

the middle oil phase easily evaporated from the shell of the double emulsions, thereby increasing the ratio of hexane, which is a poor solvent for the lipids in the oil shell of the double emulsion. This reduction in solvent quality induced the attraction between the two monolayers of lipids at the o/w interfaces of the double emulsion, which lead to the dewetting of the hexane from the inner cores of the double emulsion droplets, and ultimately resulted in the formation of the lipid bilayer. The dewetting process occurred in about two minutes [163]. The small amount of residual solvent present in the vesicles after dewetting remained concentrated in a very small region of the bilayer, allowing the bilayer to behave similarly to vesicles produced by conventional approaches [163]. Moreover, the organic solvent evaporated further in the next days.

Drug loaded THCPSi MPs and THCPSi–lipid vesicles (II)

The THCPSi MPs were loaded with piroxicam, which belongs to the Biopharmaceutical Classification System class II, *i.e.*, the dissolution rate is the limiting factor in the permeability across biological membranes. To load piroxicam, an immersion method was used [27]. The THCPSi MPs were stirred in an acetone solution of piroxicam at 15 mg/mL for 2 h. Then, the suspension was centrifuged at 11,300g for 4 min and the pellet was washed 3 times with 0.5 mL of MilliQ-water. The water allowed to remove the excess of piroxicam from the surface of the particles, while avoiding a premature release of the drugs from the pores. Finally, the loaded MPs were suspended into the inner water phase and the production proceeded as described previously.

4.2.4 Nanoprecipitation-based fabrication of PSi–Polymer composite (PSi–PC) (III)

The PSi–PC was produced by on-chip nanoprecipitation using the flow-focusing glass capillary device described in *Section 4.1.1 (III)*. The inner fluid was prepared by mixing the PSi NPs with the polymers in solution. Poly(ethylene) glycol-*block*-polylactide methyl ether (PEG–PLA) (0.625 mg) was dissolved in 7.5 mL of ethanol, and poly(ethylene) glycol-*block*-poly(L-histidine) (PEG–PHIS) (1.875 mg) was dissolved in 2.5 mL of 0.1 M of hydrochloric acid containing 0.3 mM of citric acid and 0.2% (w/v) of F127. PSi was added to the aqueous solution and dispersed by 30 seconds tip sonication at 30% amplitude. Then, it was mixed with the ethanolic solution and sonicated again for 30 seconds at 30% amplitude. The final concentration of PSi NPs was 100 µg/mL. The outer fluid consisted of a F127 in Milli-Q water solution (0.2% w/v) adjusted to pH 12.8. Both fluids were pumped inside the microfluidic chip at a rate of 10 and 100 mL/h for the inner and outer fluids, respectively, and forced to co-flow and rapidly mix inside the microfluidic channels. While both the fluids were mixed, the solvent quality was decreased, leading to the nanoprecipitation and formation of the PSi–PC. The empty compound micelles were obtained by the exact same procedure, without including PSi NPs into the inner phase.

Drug loaded PSi NPs and PSi-PC (III)

Sorafenib (SFN), a drug that inhibits cell proliferation and angiogenesis in tumors, was loaded into the PSi NPs using an immersion method [64]. The drug was dissolved in acetone (2 mg/mL) and PSi was added to the solution in a ratio of SFN:PSi of 6.7:1. The suspension was stirred for 90 min to allow the loading of the drug within the pores of PSi. After stirring, the suspension was centrifuged at 15000 rpm for 5 min and the supernatant with excess of free drug was removed. Consequently, the particles were washed with 20% (v/v) acetone in Milli-Q water (500 μ L) to wash out the free drug on the surface of the PSi NPs. The samples were then centrifuged, the supernatant removed, and the pellet resuspended in the medium of interest. Subsequently, the loaded PSi NPs were used to produce the SFN-loaded nanocomposites

4.2.5 pH-switch nanoprecipitation of IO@PNP (IV)

The NPs were produced by an organic solvent-free pH-switch nanoprecipitation method [273]. For that, methoxy-terminated PEG-PHIS (mPEG-PHIS) and amino-terminated PEG-PHIS (NH₂-PEG-PHIS) were dissolved to a concentration of 10 mg/mL in 10 mM of acetic acid. Both the solutions were subsequently mixed in a ratio of 9:1, mPEG-PHIS to NH₂-PEG-PHIS. To this polymeric solution, PEG-coated SPION with a size of 5 nm (Sigma-Aldrich) were added to a final concentration of 100 μ g/mL. Thereafter, the polymer solution containing SPION was added dropwise to an equal volume of Na₂HPO₄ (50 mM) and citric acid (25 mM) buffer (pH 5) under stirring for 30 min. Then, the NPs were pelleted by centrifugation for 5 min at 13.200 rpm and resuspended in 10 mM of 4-(2-Hydroxyethyl)-1-piperazineethanesulfonic acid (HEPES) pH 7.4.

Fabrication of IO@PNP-DOX (IV)

For the preparation of the polymer-drug conjugate-based IO@PNP, first the DOX free base was conjugated to the C-terminal side of mPEG-PHIS by an 1-Ethyl-3-(3-dimethylaminopropyl) carbodiimide/N-Hydroxysuccinimide (EDC/NHS) coupling reaction (IV), linking both the molecules through an amide bond. The mPEG-PHIS-DOX produced was dissolved in 10 mM of acetic acid (10 mg/mL) and mixed with NH₂-PEG-PHIS also dissolved in 10 mM of acetic acid (10 mg/mL) in a ratio of 9 to 1. Then the IO@PNP-DOX were produced as described above.

In order to follow the intracellular fate of IO@PNP-DOX *in vitro*, NH₂-PEG-PHIS was used instead of mPEG-PEG-PHIS, to attach Alexa fluor 647 (AF) and DOX simultaneously. First, NH₂-PEG-PHIS was labelled with NHS-AF, by direct coupling in 10 mM of 2-(N-morpholino) ethanesulfonic acid (MES) buffer pH 6 (2 mg/mL) for 12 h. The product was purified by centrifugal filtration using a spinning tube with a membrane with a molecular weight cut-off of 3 kDa (Spectrum Laboratories, Inc.). The washing process was repeated five times using deionized water. Then, DOX was conjugated to AF-NH-PEG-

PHIS as described above. NPs were prepared with the resulting AF-NH-PEG-PHIS-DOX, rendering the formation of IO@AF-PNP-DOX.

Decoration of the NPs with iRGD homing-peptide (IV)

The iRGD cyclic peptide was conjugated with the amine groups of NH₂-PEG-PHIS present on the surface of either IO@PNP or IO@PNP-DOX using a cross-linker, which represented 10% of the total polymer conferring the NPs. The cyclic peptide iRGD fluorescein isothiocyanate-labeled (FITC-Ahx-CCRGDKGPDC, C2-C10), was purchased from United BioSystems Inc., and sulfosuccinimidyl 4-(N-maleimidomethyl) cyclohexane-1-carboxylate (Sulfo-SMCC), and the cross-linker containing NHS and maleimide reactive groups, was purchased from (Thermo Fisher Scientific Inc.). First, the NPs were suspended after centrifugation in 10 mM of HEPES solution (pH 7.5) to a concentration of 5 mg/mL, equivalent to 0.5 mg/mL of the amine terminated polymer. A 10 mg/mL solution of sulfo-SMCC was freshly prepared in the same medium, added to the NPs' suspension in a 60 molar excess with respect to the amine terminated PEG-PHIS, and stirred for 30 min. Then, the non-reacted crosslinker was washed out by centrifugation, followed by dispersion of the NPs in 10 mM of HEPES solution (pH 7.5) to a concentration of 5 mg/mL. Next, 20 molar excess of the peptide, with respect to the amine terminated PEG-PHIS, was added to the NPs' suspension. The reaction was allowed to proceed for 30 min and then the IO@iRGD-PNP and IO@iRGD-PNP-DOX were collected and washed twice with the same medium.

4.3 Characterization of the DDS (I-III)

The properties of THCPsi MPs (**I** and **II**) were characterized with N₂ sorption at 77 K using TriStar 3000 gas sorption apparatus (Micromeritics Inc., Norcross, USA). The specific surface area and pore volume was calculated from the isotherm using the Brunauer-Emmett-Teller theory [274]. The average pore diameter was estimated using the obtained values of the specific surface area and the total volume at a relative pressure of $p/p_0 = 0.97$ by assuming the pores as cylindrical. The particle size distribution of the THCPsi MPs after sieving was determined using Sympatec Helos laser diffractometer, equipped with a Cuvette wet disperser system (Sympatec GmbH, Clausthal-Zellerfeld, Germany). For the measurements, the MPs were dispersed in ethanol and stirred at 400 rpm.

The morphology and size of all the drug carriers developed in this project were also studied. According to the size range of the carrier, either confocal fluorescence microscopy (**I** and **II**) or light scattering and electron microscopy (**III** and **IV**), were used to address these features.

The microcarriers (**I** and **II**) were imaged by confocal fluorescence microscopy and the size of the MPs analyzed based on these images (Image J). Thereupon, THCPsi MPs encapsulated within the solid lipid MPs (**I**) were fluorescently labelled with Rhodamine 123 (Sigma-Aldrich) in order to ease the visualization of the THCPsi MPs within the lipidic structure using confocal fluorescence microscopy. In the case of the THCPsi-lipid vesicles

(II), the membranes of the vesicles were fluorescently labeled with DHPE-Rh (Molecular Probes). THCPsi MPs and THCPsi-SLMCs were suspended in the aqueous outer phase, and the PSi-lipid vesicles were suspended in a 100 mOsm/ L sucrose water solution, collected onto a glass slide and then observed by Leica SP2 inverted confocal microscope with a HCX Plan Apochromat 63×/1.2-0.6 oil immersion objective (Leica Microsystems, Germany) equipped with argon (488 nm) and DPSS (561 nm) lasers.

The size and polydispersity index (PDI) of the nanocarriers was studied by light scattering. PSi-PC (III) were suspended in Milli-Q water adjusted to pH around 7.4 to preserve the NPs' structure and analyzed by multiangular dynamic light scattering (DLS) using a Brookhaven Instruments BI-200SM goniometer, with the detector set at different scattering angles, *i.e.*, 45°, 60°, 90°, and 135°. The polydispersity was estimated using the 2nd order cumulant fit to represent the size distribution width of the NPs' population [275]. IO@PNP (IV) were dispersed in 10 mM HEPES (pH 7.5) prior to analyzing their size and PDI by DLS with a detector set at an angle of 173°.

The morphology of the nanocarriers was identified by transmission electron microscopy (TEM, Tecnai 12, FEI Company, USA) at an acceleration voltage of 120 kV. In addition, the nanocarriers were imaged using SEM (Quanta 250 FEG; FEI Company, USA) (II, III, and IV).

For the last work of this thesis (IV) the amount of SPION encapsulated in the polymeric NPs (IO@PNP) and the magnetic properties were evaluated. The amount of SPION encapsulated in IO@PNP was quantified by UV absorbance (UV-1600 PB Spectrophotometer, VWR). About 1 mg of IO@PNP was prepared and the NPs pelleted, washed with 10 mM of HEPES solution (pH 7.5) to remove free SPION, and finally the polymer was dissolved in 10 mM of acetic acid. Spectra of PEG-PHIS and SPION in 10 mM of acetic acid were obtained independently, and a calibration curve of the absorbance of different concentrations of SPION at 290 nm was performed. Then, the spectra of the solution was obtained and the amount of SPION calculated. Consequently, a suspension of IO@PNP was prepared and put in a 6-well plates and the magnetic NPs were guided and accumulated around the magnetic field of the magnet. In addition, the hysteresis loop of the SPION and IO@PNP was determined using a magnetometer (MicroMag 3900 VSM; Lake Shore Cryotronics, Inc.). For this, 36.7 µg of SPION or 3.96 mg IO@PNP containing the same amount of SPION were dried and placed in a gelatin capsule for the measurements. The magnetic moment ($A\ m^2$) obtained versus the applied magnetic field (T) was normalized with the amount of SPION in the sample and corrected for dia/paramagnetic component in order to obtain the magnetization value (Am^2/kg)

In addition, the amount of iRGD conjugated to the IO@PNPs was quantified by fluorescence (IV). For this, a calibration curve of the FITC-labelled iRGD dissolved in 10 mM of HEPES (pH 7.5) was made and the fluorescence intensity value of the IO@iRGD-PNP in the same buffer medium was interpolated using the calibration curve.

4.4 Loading degree and drug release studies (I-III)

The PSi micro- and nano-particles used in this thesis (I–III) were loaded with various drugs by an immersion method [64], and the drug-loaded PSi particles were used to produce the composites, as described in the *Sections 4.2.1, 4.2.2, and 4.2.3*. However, for the last work presented in this thesis (IV), the loading of the drug was achieved by the production of NPs based on a polymer-drug conjugate (*Section 4.2.5*).

4.4.1 Loading degree (I-III)

The loading degree of the bare PSi particles and the PSi composites was assessed by disassembling the polymers or lipids encapsulating the PSi particles when applicable, and completely releasing the drug payload from PSi particles with a suitable solvent for the release of the drug. The drug was then analyzed by high pressure liquid chromatography (HPLC) and the drug loading calculated as the percentage in weight of the drug to the carrier.

The conjugation efficiency of DOX to the mPEG–PHIS chains that were further used to produce IO@PNP-DOX (IV) was evaluated by analyzing the fluorescence intensity of DOX in dimethylsulfoxide (DMSO). For that, a calibration curve of DOX free base in DMSO was prepared and the intensity values of the DOX-polymer conjugates interpolated in the calibration curve. The conjugation efficiency of DOX free base to mPEG–PHIS was 40% (mol/mol). Subsequently, mPEG–PHIS-DOX and NH₂-PEG–PHIS in a 9:1 ratio were used to produce IO@PNP-DOX, yielding a final DOX loading of 36% (mol/mol) (polymer/DOX)

4.4.2 *In vitro* drug release (I-IV)

In vitro drug release was assessed for the bare PSi particles and the corresponding composites (I–III). For studies I and II, the drug loaded, the THCPSi MPs, THCPSi–SLMC, and THCPSi–lipid vesicles were added into dialysis bags with a molecular weight cut off of 1 kDa, and placed in the release buffers maintaining sink conditions for the drug. For the study III, PSi–PC were directly added into the release medium. In all cases (I–III), a certain volume of the release medium was withdrawn at each timepoint to analyze the drug concentration by HPLC, and the withdrawn medium was then replaced.

The release of the four model drugs loaded into the THCPSi MPs and THCPSi–SLMCs (I) was determined after solvent evaporation from the SLMC structure, by placing the samples into a dialysis bag and immersing them into buffers with pH values of 1.2, 5.0, and 7.4, while shaking at 100 rpm and 37 °C. For the release of fenofibrate Tween-80 (1%, w/v) was added to the release media due to the low solubility of the drug.

Similarly, the release of piroxicam from THCPSi MPs and THCPSi–lipid vesicles (II) placed in the dialysis bags was studied in buffers at pH 7.4 and 6, while shaking at 45 rpm and 37 °C.

In the case of SFN-loaded PSi NPs (SFN-PSi) and PSi-PC (III), samples were added directly to the release medium. Owing to the very poor water solubility of SFN, dissolution was aided by adding to the release medium fetal bovine serum (FBS) proteins [121], therefore hindering the use of dialysis bag, which does not allow the free diffusion of the proteins. The release of SFN was analyzed in human plasma (pH 7.4), and buffers pH 6.8 and 5.5 enriched with 10% FBS, while stirring at 500 rpm and 37 °C.

The release and delivery of DOX (IV) was assed intracellularly using IO@AF-PNP-DOX. Amide bonds are known to be chemically stable [276], thus enzymatic cleavage of the bond was necessary to release the DOX from the polymer conjugate, which can be done by the lysosomal enzyme cathepsin-b [277]. Accordingly, the drug-NPs were incubated with a prostate cancer cell line, PC3MM2, and the intracellular fate of the NPs observed by confocal fluorescence microscopy for 1, 3, 6, 10, and 24 h. The cell nuclei were stained after fixation with 4, 6-diamidino-2-phenylindole (DAPI) for 3 min, followed by five times washing with Hank's balanced salt solution-HEPES (HBSS-HEPES) solution. More details about cell culturing and incubation are given in the *Section 4.6.3.2*.

4.5 Human plasma stability of nanocarriers (III and IV)

PSi NPs, PSi-PC (III) were dispersed in phosphate buffer saline (PBS) (150 µL) and added to human plasma (1 mL) (obtained from anonymous donor from the Finnish Red Cross Blood Service) at a concentration of 150 µg/mL. The suspension was stirred at 37 °C, and the samples were withdrawn after 1, 2, 5, 10, 20, 30, 60, 90, and 120 min. The samples were transferred and diluted into a folded capillary cell (Malvern Instruments) and the size, PDI, and ζ-potential were measured by DLS.

4.6 *In vitro* cell-based studies (I-IV)

4.6.1 Cell lines and cell culture (I-IV)

Human colon adenocarcinoma Caco-2, mucus-secreting intestinal cells HT29, and macrophage cells RAW 264.7 were obtained from American Type Culture Collection (USA); and the human prostate cancer cells PC3MM2 were kindly provided by Prof. Akseli Hemminki (Faculty of Medicine, Biomedicum Helsinki, University of Helsinki, Finland). All the cell lines were cultured in Dulbecco's Modified Eagle's Medium (DMEM) supplemented with 10% FBS, 1% non-essential amino acids, 1% L-glutamine, penicillin (100 IU/mL) and streptomycin (100 mg/ml). The cell cultures were kept in a standard incubator (16 BB gas, Heraeus Instruments GmbH, Germany) at 37 °C in an atmosphere of 5% CO₂ and 95% relative humidity. The growth media was changed every other day for all the cell lines until the day of the experiments, and the subculturing performed at 80% confluency using trypsin-PBS-EDTA solution.

4.6.2 Cytotoxicity (I–IV)

The *in vitro* cytotoxicity of the particles (I and II) and the drug loaded particles (III and IV) was assessed by an ATP-based cell viability kit, according to the manufacturer's specifications. Briefly, the cells were seeded in 96-well plates (Corning Inc., USA) at a concentration of 5×10^5 HT-29 cells/mL, 2.5×10^5 Caco-2 cells/mL, and 1×10^5 PC3MM2 cells/mL; and allowed to attach overnight. Next, the medium was replaced with different concentrations of particles dispersed in $1 \times$ HBSS–HEPES (I, II and IV) or DMEM enriched with 10% FBS (III), to allow the release of SFN. A positive (1% Triton X-100 solution) and negative control (HBSS–HEPES buffer solution) were included in each 96-well plate. After predetermined incubation times, the NPs were removed from the wells and washed with fresh HBSS–HEPES buffer. Then, 100 μ L of CellTiter-Glo[®] reagent assay (Promega Corporation, USA) were added to each well and the luminescence analyzed with a Varioskan Flash Multimode Reader (Thermo Fisher Scientific, USA). All the experiments were performed at least in triplicate ($n \geq 3$).

4.6.3 Cell–particle interactions and intracellular trafficking (III and IV)

4.6.3.1 Flow cytometry analysis (III and IV)

The internalization of NPs (III and IV) by RAW 264.7 (III), PC3MM2 (IV), and EA.hy926 cells (IV) was studied using flow cytometry. The cells were seeded in 6 well-plates (2 mL) at a concentration of 2.5×10^5 cells/mL, and incubated overnight at 37 °C to allow the attachment of the cells to the well. Next, the medium was removed from the wells and washed once with HBSS–HEPES buffer solution. About 1 mL of different concentrations of Alexa Fluor 488 (AF 488) (III) and Alexa Fluor 647 (AF 647) (IV)-labeled NPs dispersed in DMEM supplemented with 10% FBS (III) or HBSS–HEPES buffer solution (IV) were added to each well. In each experiment, a negative control of cells without treatment, incubated either with DMEM 10% FBS or HBSS–HEPES was used for comparison.

All the samples were incubated for 3 h at 37 °C, whereupon the medium was removed from the wells and washed three times with HBSS–HEPES to remove any free NPs not associated with the cells. Finally, the cells were harvested by incubating them with trypsin–PBS– ethylenediaminetetraacetic acid (trypsin–PBS–EDTA) for 5 min at room temperature, after which the cells were centrifuged for 5 min at 900 rpm, and the extracellular fluorescence of the AF 488 NPs (III) quenched with trypan blue. Then, the cells were washed and the medium replaced with 300 μ L of PBS with EDTA (5 mM). NP–cell internalization and association were quantified by flow cytometry (Galios Flow Cytometer; Beckman Coulter, Inc.; laser 642 nm) and the data was post-processed using the software FloJo X (FlowJo, LLC).

4.6.3.2 Confocal fluorescence microscopy analysis (III and IV)

The NP's intracellular localization (**III** and **IV**), lysosomal escape (**IV**), and DOX intracellular release (**IV**), were studied by confocal fluorescence microscopy with RAW 264.6 (**III**) and PC3MM2 cells (**IV**). For this, the cells were seeded in an 8-chamber slide (Nunc Lab-Tek II Chamber Slide System, Thermo scientific, Inc., USA) at a concentration of 2.5×10^5 cells/mL (200 μ L/chamber), and incubated overnight at 37 °C to allow the attachment of the cells. Next, the medium was removed from the chamber and replaced with 200 μ L of a 100 μ g/mL suspension of FITC-labeled (**III**) and AF 647-labeled (**IV**) NPs in DMEM supplemented with 10% FBS (**III**) or HBSS–HEPES buffer solution (**IV**). A negative control of the cells without treatment, incubated with either DMEM containing 10% FBS or HBSS–HEPES buffer solution was included in each chamber.

The NPs were then incubated with the cells, whereupon the NP suspensions were removed and the NPs not associated with the cells washed out with HBSS–HEPES buffer solution. Then, the different cell components were stained according to the needs of each study. For RAW 264.7 cells (**III**), the cell membrane was stained with CellMask Deep Red (Life Technologies, USA), according to the manufacturer's instructions. In the case of PC3MM2 (**IV**), either the lysosomes to study the lysosomal escape or the nuclei to study intracellular release of DOX, were stained. The lysosomes were stained by incubating the cells with LysoTracker Red for 30 min at 37 °C. The nuclei were stained with DAPI after fixation of the cell culture, by incubating the cells with 300 μ M DAPI in 1 \times PBS for 3 min. All the cell cultures were fixed with 2.5% glutaraldehyde solution in HBSS–HEPES buffer solution for 30 min at room temperature followed by five times washing with HBSS–HEPES buffer solution. PBS was finally added to the chambers and then the cells were visualized with a confocal fluorescence microscope (Leica inverted confocal microscope SP5 II HCS A) using HeNe (633 nm), DPSS (561 nm), Ar (488 nm), and UV-diode (405 nm) as the laser sources, and a water immersion objective HCX PL APO 63 \times .

4.7 Hemotoxicity (IV)

RBCs were purified from human blood extracted from anonymous donors at the Finnish Red Cross Blood Service. Blood was stabilized with heparin and used within 2 h.

For the isolation of RBCs, 5 mL of the blood sample were mixed with 10 mL of sterile Dulbecco's PBS pH 7.4 (D-PBS) and centrifuged for 6 min at 3000 rpm in order to separate the RBCs from the serum. RBCs were then washed five times, and finally diluted twenty times with D-PBS. About 60 μ L aliquots of this suspension were added to 240 μ L of the IO@PNP and IO@iRGD-PNP to a final concentration of 25, 50, 100, and 200 μ g/mL. The suspension was mixed and incubated for 1, 4, 6, and 24 h. Subsequently, at each time point, the sample was homogenized and 50 μ L were transferred to an Eppendorf. The sample was then centrifuged for 3 min at 13000 rpm and the supernatant transferred to a 96-well plate to measure the absorbance intensity of hemoglobin at 577 nm using a microplate reader. D-PBS and water were used as negative and positive controls, respectively.

For the timepoint corresponding to 4 h, the morphology of the RBCs was also investigated by SEM. For this, the pellet of RBCs was re-dispersed in 2.5% glutaraldehyde

and incubated for 1.5 h in order to fix the membrane of the cells. After the incubation time, the RBCs were washed three times with D-PBS and post-fixed in 1% osmium tetroxide in 0.1 M of sodium cacodylate buffer (pH 7.4) for 1 h. The cells were then dehydrated in increasing concentrations of 50, 70, 96, and 100% of ethanol for 5, 10, 20, and 15 min, respectively [278]. Finally, the cell's suspensions were dropped onto plastic coverslips, dried, and sputter coated with platinum prior to SEM imaging.

4.8 Ex vivo studies (IV)

All experimental protocols with animals were approved by the Laboratory Animal Center of the University of Helsinki and the National Animal Experiment Board of Finland, in conformity with the EU's Guidelines for Accommodation and Care of Animals, following the Act (497/2013) and the Decree (564/2013) on Animal Experimentation approved by the Finnish Ministry of Agriculture and Forestry and the EU Directive (2010/63/EU). Adult Wistar rats were sacrificed and the liver and kidney removed and kept in 1× PBS placed in ice. The tissues were then cut into small pieces and the RBCs were washed out with cold 1× PBS. The tissues were mechanically disaggregated by mincing and forcing them through a 70 µm cell strainer to a 6 well-plate with 1× PBS placed in ice. The cell suspensions were transferred to a 15 mL Falcon tube and filled-up to 10 mL with cold 1× PBS. Subsequently, the suspensions were centrifuged at 900 rpm for 5 min at 4 °C and the supernatant discarded in order to remove any remaining RBCs from the surface of the pellet. The liver or kidney cells were then resuspended in HBSS–HEPES buffer solution, containing 10% of FBS, and then the cells were counted. The cells were seeded in 96-well plates (4×10^5 cells/mL, 50 µL), and 50 µL of the particles prepared at different concentrations, ranging from 50 to 200 µg/mL in HBSS–HEPES buffer solution were added to each well. After 6 h of incubation, the ATP activity was assessed with CellTiter-Glo[®] Reagent (Promega Corporation, USA), according to the manufacturer's protocol. The luminescence was measured with a Varioskan Flash Fluorometer (Thermo Fisher Scientific, USA). All the experiments were performed at least in triplicate ($n \geq 3$).

5 Results and discussion

5.1 Single-emulsion microfluidic templated THCPsi MPs–SLMCs for sustained drug delivery (I)

In the first work of this thesis, it was developed a single-emulsion microfluidics production method of THCPsi MPs encapsulated in a solid lipid matrix, which allowed to obtain stable and reproducible composites to overcome the major drawbacks that THCPsi particles present for drug delivery applications, such as premature drug release and poor aqueous stability. The solid lipid matrix efficiently capped the pores of the THCPsi MPs, controlling the release of both hydrophilic and hydrophobic molecules while improving the surface properties of the THCPsi MPs by enhancing their stability and biocompatibility.

5.1.1 Characterization and cytocompatibility

THCPsi MPs presented irregular shapes and an average particle size of 16 μm measured by a laser diffractometer when dispersed in ethanol. However, when dispersed in aqueous medium (**Figure 8a**), their size looked larger. This phenomenon could be ascribed to the poor dispersibility of PSi MPs in aqueous medium and their tendency to aggregate as a result of hydrophobic interactions [28].

Thereafter, the successful encapsulation of THCPsi MPs within the solid lipid matrix was confirmed by fluorescently labelling the THCPsi MPs (Rhodamine 123-labelled PSi MPs) and observing the obtained composite by confocal fluorescence microscopy (**Figure 8a**). The composite had a typical diameter of about 24.9 μm , with a variation coefficient of 15.4%, and were around 17.8% smaller than the droplets used as templates due to the solvent evaporation process. In addition, unlike THCPsi MPs, the microcomposites presented spherical shape and outstanding dispersibility, owed to the reduction of the surface hydrophobicity of THCPsi MPs.

As a result of their micrometric size, these vehicles could be possibly applied for oral drug delivery, and thus, their cytocompatibility with GI tract related cancer cell lines, Caco-2 and HT-29, was also evaluated (**Figure 8b**). THCPsi MPs incubated with Caco-2 cells demonstrated a concentration-dependent cytotoxic effect for 4 and 24 h incubation, with decreased cell viability of 40% as the dose of THCPsi MPs increased from 100 to 2000 $\mu\text{g/mL}$. In contrast, HT-29 cells only showed a weak particle dose-dependent viability towards the bare THCPsi MPs after 4 and 24 h incubation (**I**). Solid lipid encapsulated THCPsi MPs demonstrated greatly enhanced cytocompatibility, especially in the case Caco-2 cells incubated with the higher doses of the particles tested (2000 and 1000 $\mu\text{g/mL}$). For the concentration of 2000 $\mu\text{g/mL}$ incubated 4 and 24 h, the viability of Caco-2 cells incubated with THCPsi MPs compared to THCPsi–SLMCs increased from ~50 to 90% and 35 to 80%, respectively.

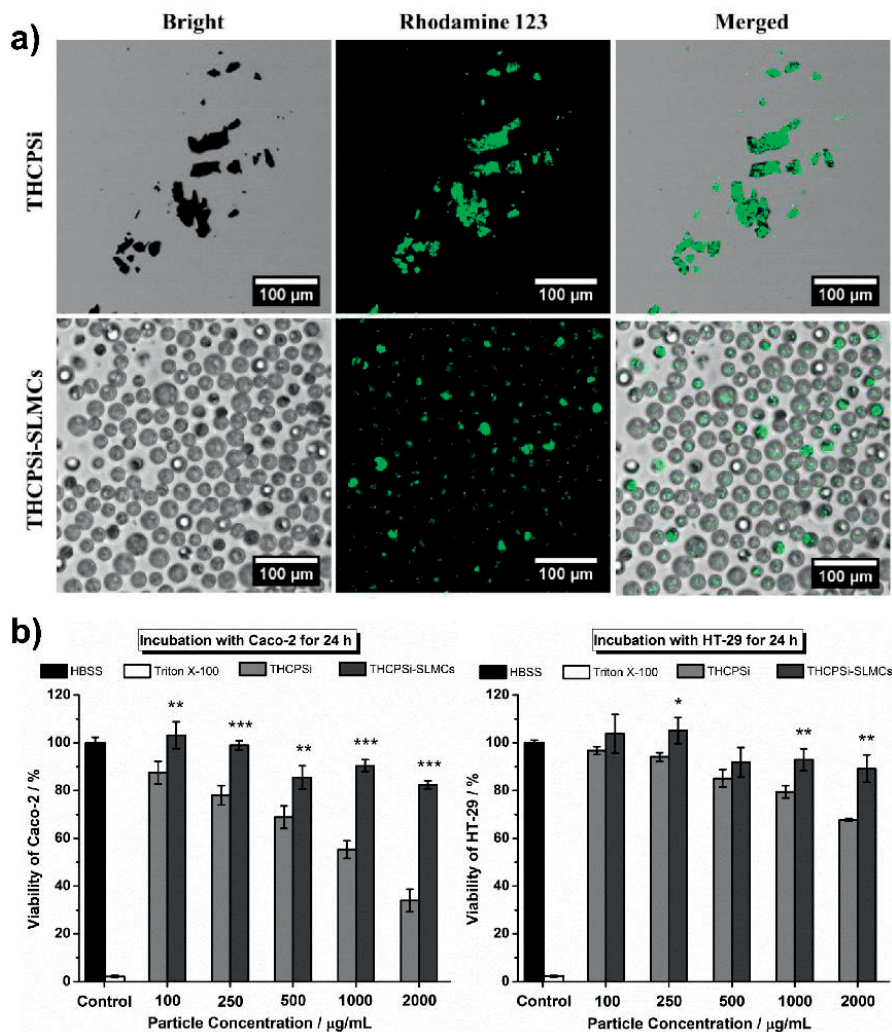


Figure 8 Characterization and cytotoxicity of THCPsSi MPs and THCPsSi-SLMCs. (a) Bright field and confocal fluorescence images of Rhodamine 123-labelled (green) THCPsSi MPs and THCPsSi-SLMCs. (b) Cytotoxicity of THCPsSi MPs and THCPsSi MPs-SLMCs incubated with GI related cancer cells lines, Caco-2 and HT-29, for 24 h. Error bars represent the mean \pm S.D ($n = 4$). The levels of significance were set at the probabilities of * $p < 0.05$, ** $p < 0.01$ and *** $p < 0.001$. Copyright © (2013) American Chemistry Society, reprinted with permission from publication (I).

The cytotoxicity induced by the MPs is a result of their interactions with the membranes of the cells, mainly determined by the nature of the surface of the particles [279-282]. Because of the similar zeta-potential values measured for both the bare THCPsSi MPs (ca. -35 mV) and the microcomposites (ca. -43 mV), the difference in cell viability cannot be attributed to their surface charge properties. Thus, the greater cytotoxicity induced by the bare THCPsSi MPs may be due to the stronger hydrophobic interactions with the cell

membranes [28, 66, 283] induced by the hydrophobic nature of THCPsi MPs,: the formation of large aggregates of MPs, and their irregular shapes. In contrast, the greater cytocompatibility observed for the THCPsi–SLMCs was likely due to the higher hydrophilicity and spherical morphology of the SLMCs compared to the THCPsi MPs, which probably resulted in a decrease in the interactions between the cells and the SLMCs [284].

5.1.2 Drug loading and release

To evaluate the loading capacity of the microcomposites and their potential to sustain the release of payloads, four model drugs with different solubilities in aqueous medium were selected: fenofibrate and furosemide, which are poorly water-soluble drugs, and methotrexate and ranitidine, which present higher water solubility than the former drugs.

The degrees of loading for the four model drugs into the P*Si* MPs and into the final microcomposites are listed in **Figure 9**. For the bare P*Si* MPs the drug loading degrees varied from about 9% for ranitidine to ~25% for furosemide. These differences can be partially ascribed to the different chemical structures and the different solubility characteristics of the drugs. The ability of the different loading solutions to wet the surface and pores of the P*Si* MPs might also have contributed to the variation in the degree of the drug loaded [285].

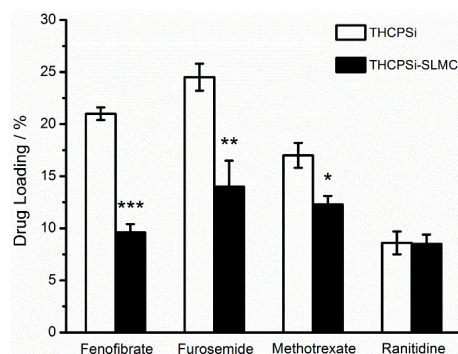


Figure 9 Drug loading degrees (%) obtained by the immersion method for THCP*Si* MPs and THCP*Si*–SLMCs after microfluidic fabrication. The levels of significance were set at a probabilities of * $p < 0.05$, ** $p < 0.01$ and *** $p < 0.001$. Copyright © (2013) American Chemistry Society, reprinted with permission from publication (1).

For the microcomposites, unlike the THCP*Si* MPs, the loading degree was lower, mostly due to the partial pre-release of the drugs when THCP*Si* was dispersed in the inner oil phase used for the microfluidic preparation of the droplet templates. This decrease was more remarkable in the cases of fenofibrate and furosemide, for which approximately half of the payload was pre-released during the templation. In contrast, for methotrexate and ranitidine, only minute amounts of drugs were pre-released during the encapsulation process. These differences were due to the different solubility of the drugs in the organic phase, ethyl

acetate, which was relatively high for fenofibrate and furosemide, but moderately low for methotrexate and ranitidine. These results indicated that a poor solubility of the drug in the solvent used as the inner fluid in the microfluidic setup is critical to preserve the degree of drug loading into the PSi MPs after their encapsulation within the SLMCs. In addition, the resultant microcomposites allowed the incorporation of rather aqueous-soluble drugs in their structure, which are usually difficult to load into traditional colloids, such as polymeric particles, o/w emulsions or micelles, due to the inherent hydrophobicity of these composites [286-288].

The release profiles of the four model drugs loaded in the THCPSi MPs (**Figure 10**) and THCPSi-SLMCs were studied in buffers with pH values of 1.2, 5.0, and 7.4, for simulating the physiological conditions of the GI tract. The dissolution rate of the less aqueous soluble drugs, fenofibrate (**Figure 10a-c**) and furosemide (**Figure 10d-f**), was enhanced when loaded in the THCPSi MPs. Furthermore, the dissolution rate of these drugs from the THCPSi MPs and THCPSi-SLMCs was dependent on the pH, showing in both cases similar trends, *i.e.*, faster dissolution or release rate at increased pH values. These results can be ascribed to the lower solubility of the payloads at lower pH conditions and to the significantly different properties of the phospholipid matrix at acidic pH conditions (<3), such as the increased phase transition temperature, gel-phase characteristics, and slight alteration of the phospholipid surface charge, which could also contribute to slow down the release rate of the payloads from the THCPSi-SLMCs at acidic pH conditions [289, 290].

For methotrexate and ranitidine, the impact of both THCPSi MPs loading and pH-value on the release profiles was less pronounced than for fenofibrate and furosemide (**Figure 10g-i**). For methotrexate, the release rate was only slightly slower at pH 5.0, whereas the release rate of ranitidine was independent of pH for all the pH values tested. Regardless of the pH-value of the media and the solubility of the four model drugs, the release rate of payloads from the microcomposites was always slower than that from the bare THCPSi MPs. For example, in the case of fenofibrate at pH 1.2, the time for the release of 50% fenofibrate from the THCPSi MPs was about 2.5 h, whereas from the microcomposite it was ~7.5 h. More importantly, these microcomposites efficiently reduced the initial 'burst release' of the drugs observed in the case of the bare PSi MPs, which was more pronounced for the aqueous-soluble drugs. For example, ~20% of ranitidine was released from the bare THCPSi MPs within the first 5 min, whereas only ~5% was released from the corresponding microcomposites, independent on the pH-value tested.

Therefore, better control over the release of the drugs was achieved with the THCPSi-SLMC than with the bare THCPSi MPs, significantly reducing both the *in vitro* release rate of the payloads and also the initial 'burst release' of the drugs.

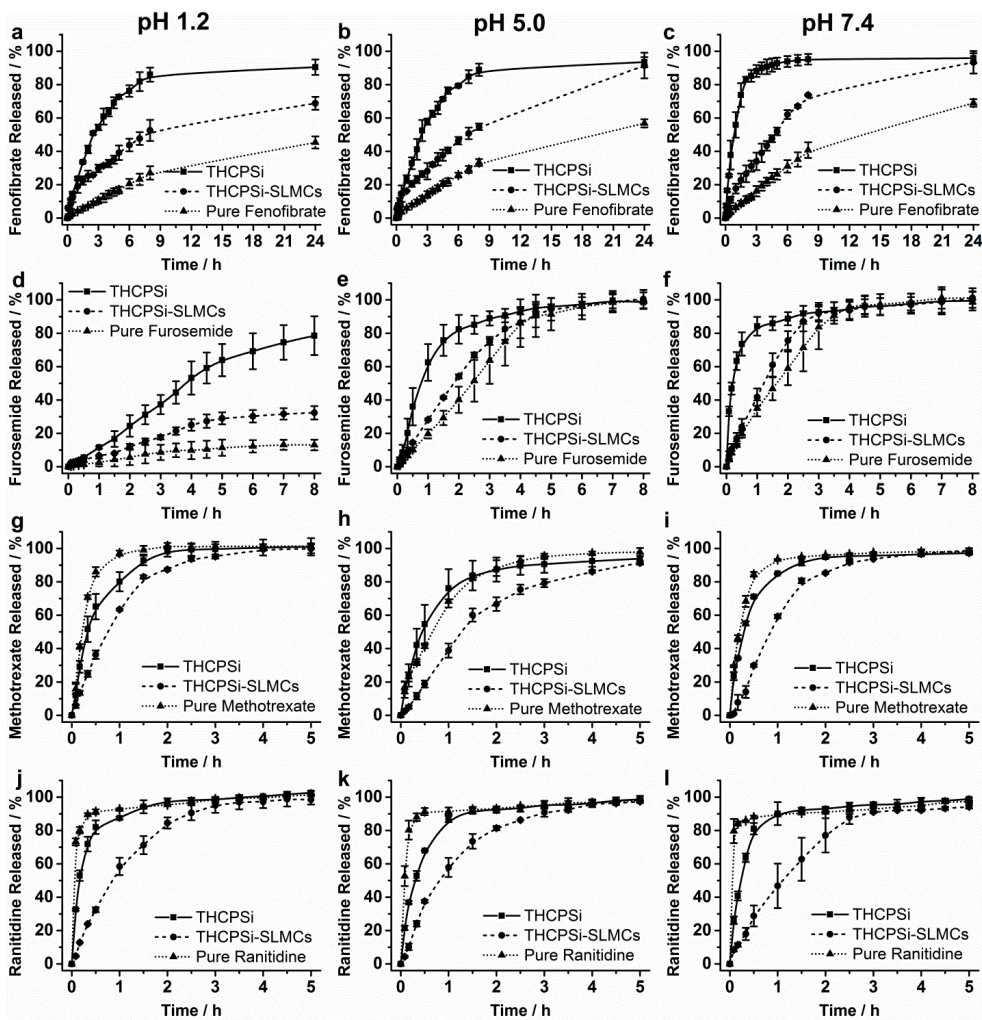


Figure 10 Release profiles of the payloads from THCPsi MPs and THCPsi-SLMCs. Fenofibrate (a, b, and c), furosemide (d, e, and f), methotrexate (g, h, and i), and ranitidine (j, k, and l) were loaded into the particles and the release profiles were measured at pH 1.2 (a, d, g and j), 5.0 (b, e, h and k), and 7.4 (c, f, i and l). The dissolution profiles of pure drugs are also shown for comparison. All experiments were conducted at 37 °C. Error bars represent the mean \pm s.d. ($n = 3$). Copyright © (2013) American Chemistry Society, reprinted with permission from publication (1).

5.2 Double-emulsion microfluidic templated THCPsi MPs–lipid vesicles for sustained drug delivery (II)

In the second study, it was investigated the combination of lipid vesicles with ultra-thin membrane around THCPsi MPs in order to overcome the limitation that these vesicles

present. The ultra-thin membranes hamper the loading of hydrophobic molecules within, and thus, the THCPsi MPs were loaded with a hydrophobic drug and encapsulated in the aqueous core of lipid vesicles to provide them with the capacity to load hydrophobic cargo. The THCPsi MP–lipid vesicles were produced by double emulsion microfluidics in a highly efficient and reproducible manner.

5.2.1 Microfluidic encapsulation of THCPsi MPs in lipid vesicles and characterization

THCPsi MPs were encapsulated in the aqueous core of ultra-thin lipid vesicles, with ~100% encapsulation efficiency (**Figure 11a**), rendering THCPsi MP–lipid vesicles with a diameter of $114 \pm 8.4 \mu\text{m}$ (**Figure 11b**). The lipid bilayer was stained with a fluorescent dye for further visualization by confocal fluorescence microscopy (**Figure 11c**). In addition, the THCPsi MPs were observed by SEM (**Figure 11d**).

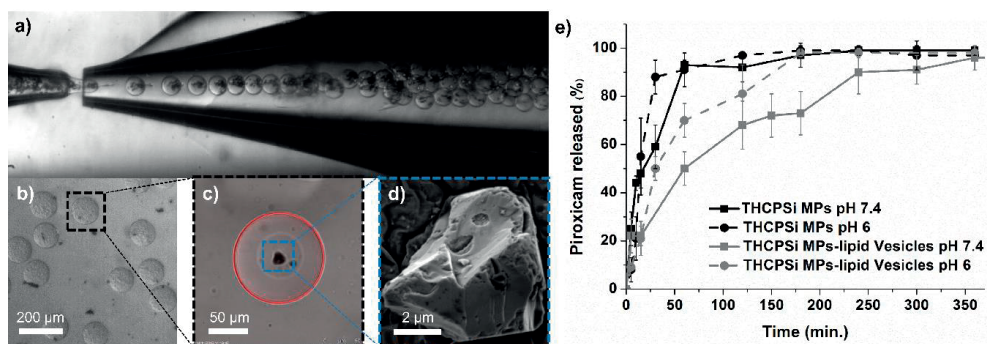


Figure 11 (a) Optical microscope image of a typical THCPsi MP–lipid vesicles production based on double emulsion microfluidics. It can be observed that all the THCPsi MPs ended-up in the inner core of the lipid vesicles. (b) Optical microscope image of THCPsi MP–lipid vesicles suspended in an aqueous solution of sucrose. (c) Optical and fluorescence confocal overlaid images of a single THCPsi MP–lipid vesicle. A THCPsi MP is pointed out by the blue region and the lipid bilayer was stained with a fluorescent dye (red). (d) SEM micrograph of a THCPsi MP. (e) Drug release profiles of piroxicam-loaded THCPsi MPs (black squares) and THCPsi–lipid vesicles (grey triangles). Release was performed at 37 °C in PBS buffer pH 7.4 (solid line) and pH 6 (slashed line). The experiments were done in triplicate and the error bars represent the mean ± s.d. at each timepoint. Copyright © (2014) Royal Chemistry Society, reprinted with permission from publication (II).

5.2.2 Cytocompatibility and sustained drug release

Owing to the size of the THCPsi MPs and THCPsi MP–lipid vesicles, one of the intended applications for these drug carriers would be the oral delivery of drugs, being advisable to test their cytocompatibility with GI tract related cancer cells. The cytotoxicity was then studied with HT-29 cancer cells and found to be concentration-dependent for both the

systems (II). However, no statistically significant differences were observed between the THCPsi MPs and THCPsi MPs–lipid vesicles ($p \leq 0.05$). Overall, this demonstrated a very good cytocompatibility of the developed DDS.

Furthermore, the model drug piroxicam, belonging to the Biopharmaceutical Classification class II, *i.e.*, poorly water-soluble drug and with high permeability through biological membranes, was loaded in the pores of THCPsi MPs. These were further encapsulated in the aqueous core of the lipid vesicles, obtaining a final drug loading degree of 19% (w/w). The drug release from both the systems was evaluated in PBS buffer at pH 6 and pH 7.4 (Figure 11e).

The drug release profiles showed that piroxicam-loaded THCPsi MPs released 90% of the payload within 50 min. In contrast, lipid-vesicles sustained the release of the piroxicam-loaded THCPsi MPs, which was dependent on the pH of the release medium. While 100% of the drug was released from the THCPsi–lipid vesicles within 3 h at pH 6, the release was further sustained at pH 7.4, being completed within 6 h. The sudden increase in the release rate of piroxicam from the THCPsi–lipid vesicles observed after 200 min. was most likely due to the significant vesicle disruption after 4 h, as confirmed by the optical microscope images (II).

Despite the unfeasibility of loading hydrophobic molecules within the bilayer of ultra-thin lipid vesicles, this study demonstrated a new approach to achieve a high loading degree of a molecule with these characteristics within the aqueous core of the vesicles, due to the introduction of THCPsi MPs as the carrier of the drug.

5.3 Microfluidic nanoprecipitation self-assembly of PSi-based hybrid nanocomposites with pH-responsive properties (III)

In the third work of this thesis, some of the hurdles that drug nanocarriers present for the treatment of tumors were faced, such as the poor water solubility of certain drug molecules, along with the fast clearance of nanocarriers from blood circulation and the spatially controlled drug delivery at the tumor site [36, 291]. To address these issues, it was designed a smart hybrid nanocomposite consisting of a blend of PEG–PHIS and PEG–PLA assembled on the surface of SFN-loaded PSi NPs, which was spontaneously formed by nanoprecipitation in a flow-focusing microfluidic chip. Importantly, the nanocarrier presented PEG on the surface that prevented macrophage recognition likely by avoiding protein opsonization.

5.3.1 Characterization

The formation of the PSi–PC and its properties were monitored by DLS and TEM. Firstly, multiangular DLS was used to analyze the angular-dependent size of the PSi–PC, as well as of the empty polymeric NPs. The results showed that the size of both the systems was dependent on the angle at which the light scattered detector was set, which suggested that the NPs did not present spherical shapes [275]. The size of the NPs was calculated for a

detection angle of at 0° , being for PSi-PC 260 nm, and for the empty NPs 200 nm, with a PDI lower than 0.2. Moreover, the size of the PSi NPs measured by DLS was 130 nm. Together, the size increment of the PSi-PC compared to bare PSi NPs and the empty NPs pointed out to a combination of the last two systems in the PSi-PC.

The non-spherical shape of the PSi-PC was further demonstrated by TEM and SEM (III). The irregular and porous structure of the PSi NPs could not be identified after the formation of the composite, revealing the efficient sealing of the pores of the PSi NPs. Moreover, it could be observed by TEM that PSi-PC avoided an extensive aggregation of the PSi NPs. SEM images of the PSi-PC provided a hint about the type of structure formed. Small micelle-like structures were observed on the surface of the PSi-PC, suggesting that the structure could be a compound micelle. This structure was formed by small aggregated reverse micelles with hydrophilic cores and hydrophobic coronas, interacting by hydrophobic forces with the surface of PSi, and further stabilized by a layer of block copolymers with their hydrophobic blocks towards the inner reverse micelles and their hydrophilic blocks towards the aqueous environment.

In addition, the surface zeta-potential of the different NPs was studied, being -14.8 mV, $+2.8$ mV, and -5 mV for the PSi NPs, compound micelles, and PSi-PC, respectively. AS a result of the assembly of the compound micelle on the surface of PSi NPs, the surface negative charges of the latter were compensated by the positive charges of the compound micelle, rendering a PSi-PC with a less negative surface charge.

5.3.2 pH-Triggered drug delivery and cell growth inhibition

PSi-PC were designed allow the delivery of the drug upon acidification of the environment, triggered by tumor extracellular microenvironment or intracellular late endosomes or lysosomes, which possess typical pH values of 5–6.8 [225, 292]. PEG-PHIS possesses a pH-responsive behavior due to the presence of an imidazole ring in each histidine unit of the polypeptide, bearing a protonable nitrogen. Under physiological conditions, the imidazole remains as the conjugated base of the amine, but upon acidification, the nitrogen protonates. Therefore, in the case of PEG-PHIS, at neutral pH the PHIS is mostly found in its unprotonated form, allowing the interaction of PHIS blocks through attractive hydrophobic forces, which leads to the self-assembly of the block polymers, rendering supramolecular structures [293]. When the pH decreases, PHIS gradually protonates, creating repulsive electrostatic forces between the positive charges, and hindering the hydrophobic interaction between the PHIS blocks. This leads to the disassembly of the structure and dissolution of the polymer. PEG-PLA was introduced in the structure as a modulator, quenching to a certain extent the electrostatic repulsive forces of the protonated chains by increasing the hydrophobic interactions, and thus, decreasing the pH value at which the electrostatic repulsive forces beat the hydrophobic interactions [294]. Based on this, the aim was to achieve pH-triggered drug release from the pores of the PSi NPs upon the rupture of the polymeric structure assembled on its surface.

SFN, a cytotoxic drug that inhibits cell proliferation and angiogenesis, was loaded in the pores of the PSi NPs by an immersion method [64], and further encapsulated into the polymeric structure. The drug loading degrees of SFN into PSi NPs and PSi-PC were 5.8%

and 4.9%, respectively. Thereupon, the SFN release profiles from both the nanocarriers and the dissolution rate of free SFN were determined in human plasma (pH 7.4) and PBS buffer enriched with 10% FBS with pH values of 6.8 and 5.5, in order to mimic the physiological tumor microenvironment and the intracellular conditions, respectively (**Figure 12a**). SFN is very poorly soluble in aqueous media, however, in the presence of surfactants, proteins, or others compounds its solubility can be enhanced. Accordingly, FBS was used to enhance the dissolution rate of SFN [121]. Anyhow, due to the remarkably low solubility of SFN, just 10% of the drug was dissolved in 6 h, for all the media tested. However, SFN-PSi greatly improved the drug's dissolution rate up to ~100%. Remarkably, SFN release from the PSi-PC in plasma at pH 7.4 was low (<5%), whereas in PBS-FBS at pH 6.8 and 5.5 burst-type release profiles were observed.

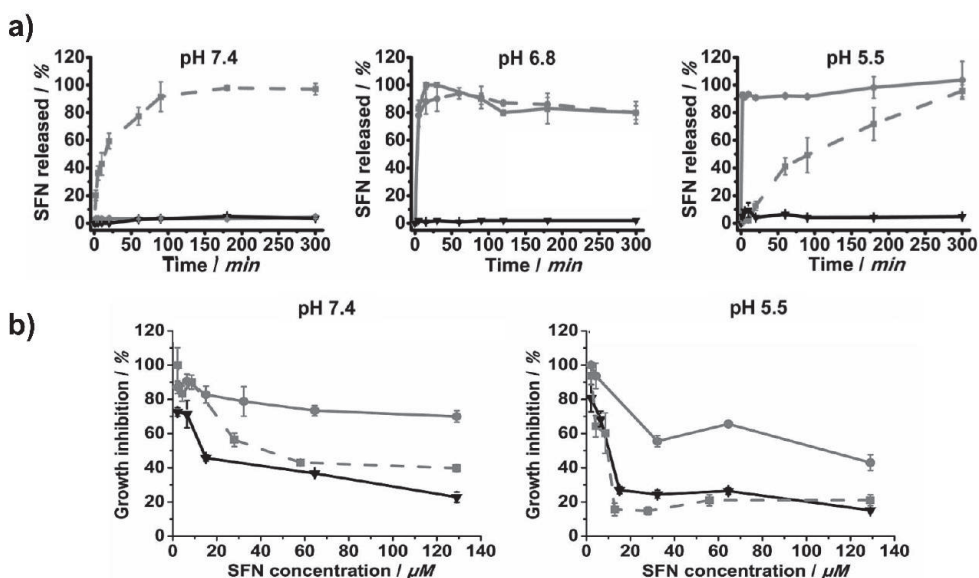


Figure 12 pH-dependent drug release and cell growth inhibition. (a) Dissolution and drug release profiles of SFN (solid black line) and SFN-PSi NPs (dashed grey line) and PSi NP-PC (solid grey line). The release was performed in plasma pH 7.4 and PBS enriched with 10% FBS at pH 6.8 and 5.5. (b) Growth inhibition of PC3MM2 cells incubated with SFN (black solid line), SFN-PSi NPs (dashed grey line), and PSi-PC (solid grey line) at pH 7.4 and 5.5 for 24 h. The experiments were done in triplicate and the error bars represent the mean \pm s.d. at each timepoint. Copyright © (2015) John Wiley & Sons, Inc., reprinted with permission from publication (II).

Overall, these experiments confirmed the potential of PSi to significantly increase the dissolution rate of SFN, and further highlighted the robustness of the nanocomposite to protect the drug inside the structure, preventing major leakage in physiological conditions (pH 7.4). To further assess if the pH could trigger the release of SFN from the PSi-PC and allow the drug to exert its therapeutic effect, the cytotoxicity effect of SFN and the SFN-loaded PSi NPs and PSi-PC (**Figure 12b**), was tested by incubating the drug and drug-

loaded NPs with the metastatic prostate cancer cell line, PC3MM2, at pH 7.4 and 5.5 for 24 h. The concentration of SFN needed to inhibit the cell population to half (IC_{50}), at both pH values was lower than 15 μ M. At pH 7.4, SFN-PSi NPs presented an IC_{50} of ~ 27 μ M, while SFN-loaded PSi-PC (SFN-PSi-PC) did not reach the IC_{50} within the concentration range tested (130 μ M). Moreover, the maximum cell growth inhibition achieved by PSi-PC at pH 7.4 was 30% and 43% lower than that of SFN-PSi and SFN, respectively. These results showed that free SFN was slightly more potent than when loaded into PSi NPs, and that the polymeric composite limited the cytotoxic effect of the drug by keeping it locked inside the nanocarrier at physiological pH. However, at pH 5.5, the IC_{50} of the composite was reduced to 32 μ M, revealing that the acidic conditions triggered the release and the effect of the drug.

In conclusion, SFN-PSi-PC effectively inhibited the effect of SFN towards PC3MM2 cells under physiological conditions, while showing greater toxicity under acidic conditions. However, the free drug was more efficient than the nanocarriers inhibiting cell growth. Therefore, to really assess the superiority of the nanocomposites over the free drug, the combination of pH-triggered drug release and passive targeted delivery of the drug should be studied *in vivo*.

5.3.3. *In vitro* stealth properties

The efficacy of PEGylation was further evaluated based on the capacity of the composite to avoid recognition and clearance by the MPS *in vitro*. With this aim, RAW 264.7 macrophage cells were incubated for 3 h in medium enriched with 10% FBS with fluorescently labelled PSi NPs and PSi-PC, and the cellular uptake was studied by confocal microscopy and flow cytometry (**Figure 13a**). The confocal results showed greater fluorescence density inside the space delimited by the membrane of the macrophages when incubated with the fluorescently labelled PSi NPs compared to the composites. These results were also supported by the flow cytometry analysis (**Figure 13b**). Overall, these results indicated that 93% of the macrophages internalized the PSi NPs, while just 23% internalized the PSi-PC. In addition, the mean fluorescence intensity (MFI) of the RAW 264.7 cells incubated with PSi NPs was four times greater than for the cells incubated with PSi-PC, meaning that the macrophages incubated with PSi NPs internalized a greater amount of the NPs compared to the macrophages incubated with PSi-PC. Thus, this corroborated that the macrophages had less tendency to interact with the PSi-PC than with bare PSi NPs, most likely due to the presence of the PEG (5 kDa) corona on the surface of the nanocomposites.

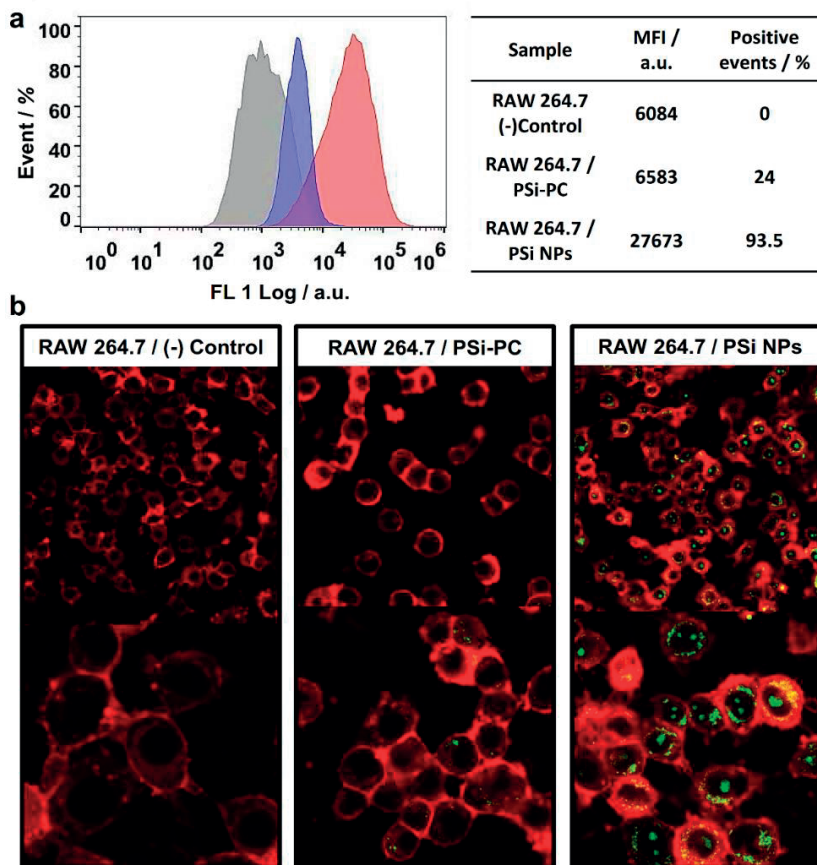


Figure 13 *Phagocytosis of PSi NPs and PSi-PC by RAW 264.7 cells after 3 h incubation at 37 °C. (a) Flow cytometry analysis. The histogram represents the percentage of positive events at a given fluorescence intensity signal. The negative control, cells without treatment, are shown in grey, and the AF 488-labelled PSi NPs and PSi-PC are shown in red and blue, respectively. The table summarizes the MFI value of each event and the percentage of positive events. (b) Confocal microscopy analysis. Cell membrane, in red, was stained with CellMask Deep Red, and the PSi NPs and PSi-PC, in green, were labelled with Tetramethylrhodamine. The first column depicts the negative control, cells without treatment. The second and third columns depict cells incubated with PSi-PC and PSi NPs, respectively. Copyright © (2015) John Wiley & Sons, Inc., reprinted with permission from publication (II).*

5.4 pH-switch nanoprecipitation of polymeric solid NPs for tumor theranostics (IV)

In the fourth work of this thesis, an advanced targeted and multi-stimuli responsive theranostic platform was developed, consisting of SPION NPs encapsulated in a PEG-PHIS

based NP, and further decorated with the tumor homing-peptide iRGD [241]. The developed nanoplatform combined intracellularly triggered drug release properties and potential for *in vivo* targeting and imaging. In addition, it was performed in this work an *in vitro* and *ex vivo* toxicity assessment, together with the evaluation of the cellular interactions, lysosomal escape, and intracellular drug delivery of the developed theranostic NPs.

5.4.1 Characterization and toxicity assessment

The size and surface charge of the NPs was characterized by DLS, and were visualized with SEM and TEM (IV). The IO@PNP and IO@iRGD-PNP dispersed in 10 mM of HEPES (pH 7.5) presented sizes of 210 and 219 nm, PDIs of 0.096 and 0.075, and a surface zeta-potentials of -0.23 and -10 mV, respectively. The presence of PEG on the surface of the NPs was responsible for both the neutral surface charge of the nanoparticle and the colloidal stabilization by steric hindrance when suspended in a good bulk medium, where PEG is well-solvated and prevents interpenetration of chains [295]. The successful encapsulation of SPION was observed by TEM. Furthermore, the loading efficiency was found to be 40% with a final concentration of $8 \mu\text{g}$ of SPION per 1 mg of polymer (IV). Importantly, the magnetization saturation (M_s) and superparamagnetism of the SPION and the polymer encapsulated SPION were characterized by assessing their hysteresis loop (Figure 14a). Superparamagnetism is a property of magnetic materials through which their magnetization is destabilized by thermal energy. For typical ferromagnets the length scale at which superparamagnetism exists has been described to be below $\sim 5\text{--}10$ nm [296]. Superparamagnetism is a desirable property for NPs to be used for drug delivery, because upon removal of the magnetic field the nanoparticles do not present attraction for each other, thus avoiding a major driving force for aggregation [296]. In this respect, results demonstrated that the superparamagnetism of SPION was preserved after encapsulation in the polymeric structure, partially revealed by the hysteresis loop, in which the coercivity was negligible, and confirmed by the TEM images of IO@PNP (Figure 14b), where SPION was found as single NPs with a size smaller than 10 nm. In addition, the M_s of the SPION was found to be $24 \text{ Am}^2/\text{kg}$, and $38 \text{ Am}^2/\text{kg}$ for IO@PNP. The observed increase in M_s for the IO@PNP compared to the SPION, may be attributed to the clustering of SPIONs in the polymeric structure [297, 298]. Overall, the M_s displayed by IO@PNP is in the range of other magnetic systems found to be useful for magnetic guided therapy *in vivo* [299, 300].

Furthermore, a prerequisite for the application of NPs *in vivo* is to demonstrate their safety. Therefore, as a preliminary study, the cytotoxicity of the system was assessed using physiologically-relevant cell types: primary rat liver and kidney cells, and human RBCs. Primary hepatic and kidney cells are often used for toxicological assessment of chemicals due to the capacity of these cells to retain their specialized functions better than by immortalized cell lines. In addition, these cells are greatly exposed to the NPs, and thus, to their toxic effects after i.v. administration *in vivo* [301]. Accordingly, the viability of these cells incubated for 6 h with IO@PNP and IO@iRGD-PNP, in the range of concentrations of 50 to $500 \mu\text{g}/\text{mL}$, was studied (Figure 14c). The results showed more than 90% viability for the hepatic cells and more than 82% viability for the kidney cells at all the concentrations tested for both the types of NPs.

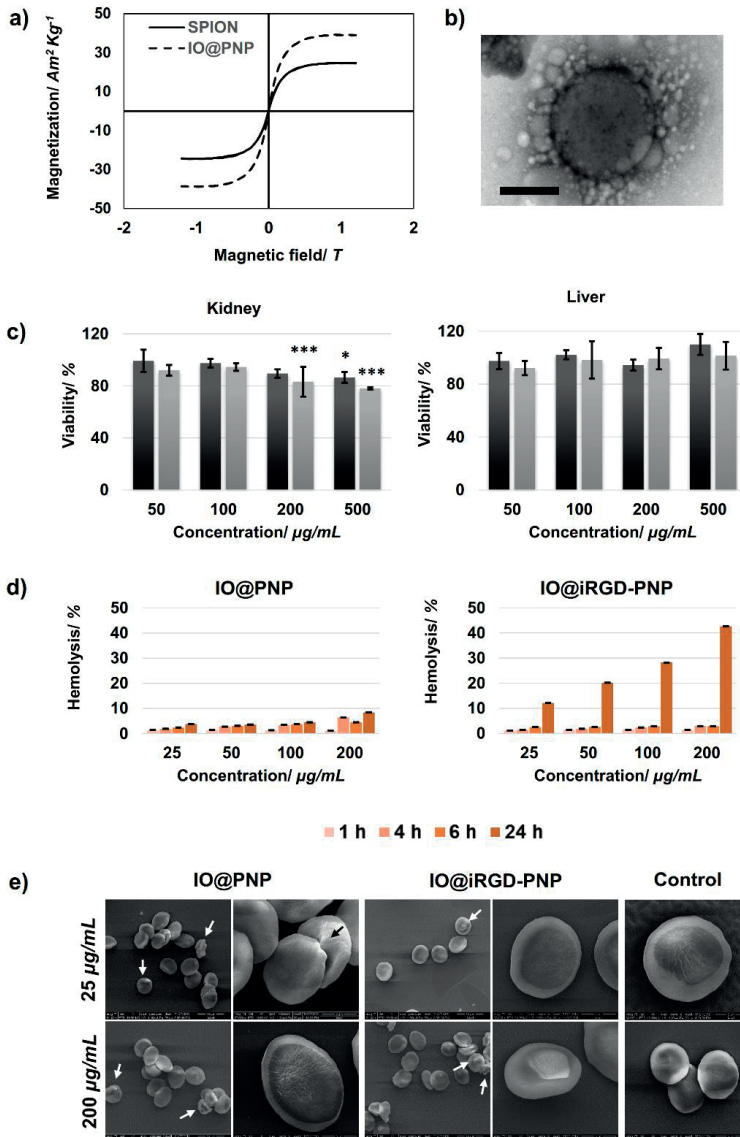


Figure 14 Characterization and in vitro toxicity assessment. (a) Hysteresis loop of SPION and IO@PNP. (b) Single IO@PNP with SPION (black dots) that can be identified inside the nanoparticle. Scale bar represents 100 nm. (c) Cytotoxicity of IO@PNP and IO@iRGD-PNP incubated for 6 h with rat kidney and liver primary cells. Black bars represent IO@PNP and grey bars IO@iRGD-PNP. Results were compared with the negative controls and the statistical significance levels were set at the probabilities of $*p \leq 0.05$, $**p \leq 0.01$, and $***p \leq 0.001$. (d, e) Effect of IO@PNP and IO@iRGD-PNP over human RBCs. (d) Percentage of RBCs lysed after 1, 4, 6 and 24 h incubated with 25, 50, 100 and 200 $\mu\text{g/mL}$ of IO@PNP and IO@iRGD-PNP. (e) SEM images of the RBCs incubated with 25 and 200 $\mu\text{g/mL}$ of IO@PNP and IO@iRGD-PNP for 4 h. Arrows indicate cells that have suffered changes in their morphology. The experiments were done in triplicate and the error bars represent the mean \pm s.d. at each timepoint.

RBCs are also very vulnerable to the toxic effects of the NPs administered intravenously, as they may suffer changes on the morphology or even lysis, with the consequent release of hemoglobin to the blood stream [278, 302]. The intrinsic oxidative nature of hemoglobin may cause damage to tissues if not efficiently quenched or metabolized, which is the case in severe hemolytic processes [303]. IO@PNP and IO@iRGD-PNP (**Figure 14d**) showed time and concentration-related hemolytic capacity, reaching overall hemolytic rates below 8.5% for concentrations up to 200 $\mu\text{g/mL}$ and 24 h of incubation, with the exception of IO@iRGD-PNP, which after 24 h incubation resulted in hemolytic rates from 12 to 42% for the range of concentrations tested. In general, any *in vitro* hemolytic value $<10\%$ is considered to be potentially non-hemolytic *in vivo*, while hemolytic values $>25\%$ are considered to be potentially hemolytic *in vivo* [304]. Furthermore, the shorter incubation times are more representative of the potential harmful effects of i.v. administered NPs, because these are distributed and cleared from the bloodstream relatively fast along the time. Morphologically, some RBCs incubated with both IO@PNP and IO@iRGD-PNP presented alterations, although apparently neither concentration- nor NP-dependent. Besides the normal discocyte-shaped RBCs, few knizocytes and codocytes were also found (**Figure 14e**) [305]. Overall, based on these results, IO@PNP and IO@iRGD-PNP can be considered to be safe for their i.v. administration.

5.4.2 iRGD-Mediated cell uptake

The iRGD homing peptide has efficiently demonstrated to mediate the extravasation of drugs and NPs from the blood circulation to the tumor site in metastatic cancer models *in vivo* through the interaction with $\alpha\text{v}\beta\text{3}$ and $\alpha\text{v}\beta\text{5}$ integrins and neuropilin-1, which are upregulated in angiogenic blood vessels [241, 306], and further spread into the tumor mass. In addition, these receptors are also expressed by other tumor cell lines and can be internalized in these cells through receptor-mediated endocytosis [241, 245]. Based on this, the previously prepared IO@PNP were decorated with iRGD and the cellular uptake *in vitro* was tested with two relevant cell lines, EA.hy926 and PC3MM2 cells, with the aim to mimic the endothelial blood vessels and a metastatic tumor, respectively. Association of the NPs was studied by flow cytometry (**Figure 15**) and subsequently confirmed by confocal microscopy (**Figure 16a**).

For both the cell lines tested, IO@PNP and IO@iRGD-PNP demonstrated extensive and concentration-dependent cellular association, with a minimum 80% of the cells containing NPs. iRGD decoration of IO@PNP showed modest improvements in the association of the NPs to EA.hy926 cells, and no improvements in the case of PC3MM2 cells. Despite the promising *in vivo* tumor homing characteristics of iRGD, these results were already reported in an *in vitro* study; however, the *in vitro* experiments did not further correlate with the *in vivo*, in the latter case the role of iRGD was more relevant [243]. This could be attributed to the lack of an unknown protease in cell cultures that cleaves iRGD after its association to the cell surface integrins to expose the CendR motif that binds to NRP-1 and would require further *in vivo* analysis [241].

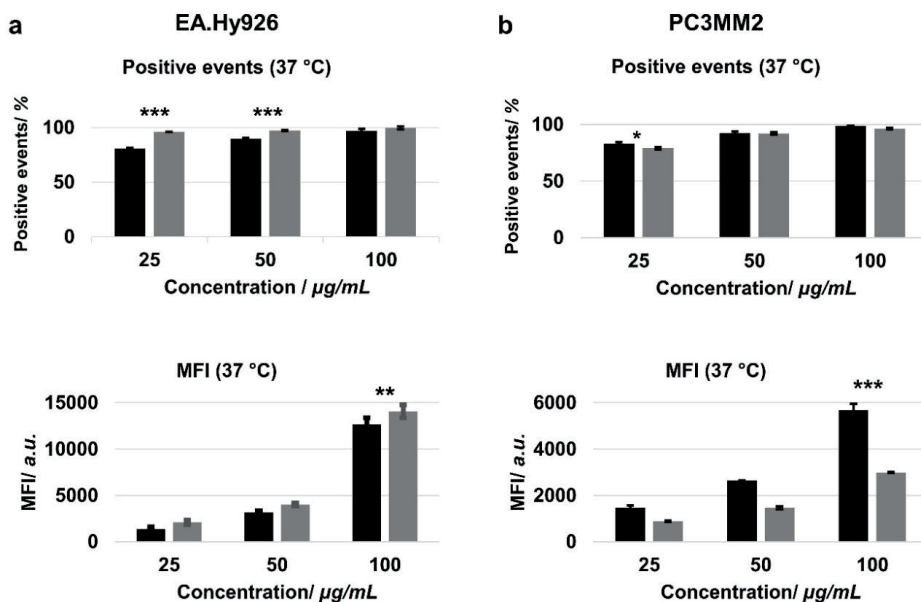


Figure 15 Cell internalization of IO@PNP and IO@iRGD-PNP incubated with (a) EA.hy926, and (b) PC3MM2 cells for 3 h at 37 °C. Results show the positive events and median fluorescence intensity (MFI). IO@PNP are represented by the black bars and IO@iRGD-PNP by the grey bars. Statistical significance was set at the probabilities of * $p \leq 0.05$, ** $p \leq 0.01$, and *** $p \leq 0.001$.

5.4.3 Lysosomal escape and intracellular drug delivery

Endocytosed NPs must escape the endocytic pathway in order to deliver the drug cargo into the cytoplasm of the cancer cells [307-309]. In this respect, the imidazole groups of PEG-PHIS can protonate upon acidification of the endosomes [307], promoting the proton-sponge effect, and thus, releasing the polymer and the cargo in the cytoplasm of the cells [209]. To confirm this, the lysosomes of the cells were labelled (red), and the cells observed after 1, 3, and 6 h of incubation with AF 647-labelled IO@PNP and IO@iRGD-PNP (IO@AF-PNP and IO@iRGD-AF-PNP, in green) (**Figure 16a**). These experiments revealed that the NPs were predominantly internalized rather than associated to the cell membrane of the PC3MM2 cells. Moreover, already after 1 h of incubation, both types of NPs were found co-localized within the lysosomes, but also extensively in the cytoplasm, demonstrating the capacity of the NPs to escape the lysosomes. The extensive fluorescence found in the cytoplasm was most likely owed to the disassembly of the NPs in the lysosomes, which were further released to the cytoplasm as block-copolymer chains.

The previous works presented in this thesis (**I**, **II**, and **III**) relied on PSi-base materials as the carrier for drug cargo, further protected from the premature release using different approaches. In contrast, in this last work (**IV**), a polymer-drug conjugate connected through an amide bond was designed, and was used to produce NPs. This approach ensures no

leaking of the drug along the delivery route due to the stable polymeric structure at physiological pH and to the chemical stability of the amide bond.

First, it is necessary to demonstrate the *in vitro* cleavage of the amide bond linking the polymer chains to the drug DOX, presumably by the action of the lysosomal enzyme cathepsin b, as reported elsewhere [277]. For this, one end of the block-copolymer was conjugated to AF, and the other to DOX, rendering IO@AF-PNP-DOX NPs. Therefore, the *in vitro* cleavage of the amide bond linking the polymer chains to the DOX would be confirmed by the absence of co-localization of both the signals intracellularly. Thus, PC3MM2 cells were incubated with IO@AF-PNP-DOX and observed by confocal microscopy after 1, 3, 6, 10, and 24 h (**Figure 16b**). It was found that DOX and AF were mostly not co-localized, being the fluorescent signal of AF localized in the cytoplasm of the cells and DOX co-localized with DAPI in the nuclei, sparingly after 1 h of incubation and extensively after 3 h of incubation, in particular in the nucleoli. After 6 and 10 h of incubation, exocytic vesicles were found, in which the fluorescent signals coming from exocytosed genetic material (stained with DAPI) and DOX, were co-localized. After 24 h of incubation, the damage to the cell culture was undisguised, cell debris, exocytic vesicles, apoptotic, and living cells, prominently containing DOX co-localized with their nucleoli, were found.

In general, these results pointed out that when the IO@AF-PNP-DOX NPs were endocytosed and reached the lysosomes they protonated and disassembled due to the acidic pH of this organelle [307], possibly allowing the action of the lysosomal enzyme cathepsin-b on the amide bonds [309], which cleaved the DOX from the structure, while creating internal osmotic pressure that eventually caused the burst of the lysosome and cytosolic release of the drug [307]. Thereafter, free DOX translocated into the nucleus of the cells [310] and seemingly accumulated in their nucleoli. This observation is in agreement with previous reports about the preferential location of DOX in the nucleolus and the interaction of DOX with both DNA and RNA [311, 312]. These experiments demonstrated *in vitro* the cleavage of the amide bond between DOX and the block copolymer of the NPs, and the translocation of the drug to the nucleus of the cells, which opens up the door for further mechanistic exploration of the DOX internalization and release from these nanocarriers in this fashion.

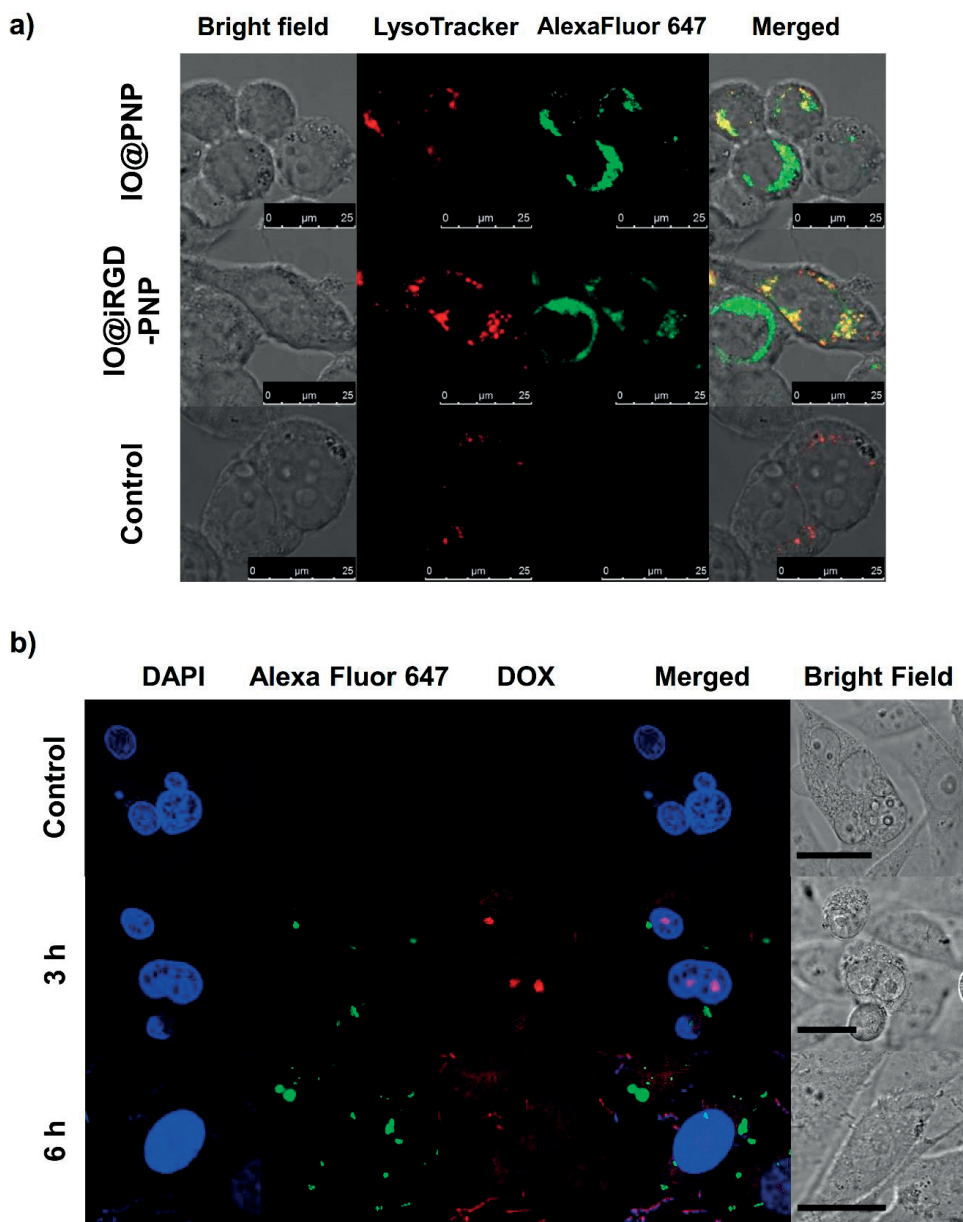


Figure 16 Intracellular trafficking and drug delivery. (a) Lysosomal escape of IO@PNP and IO@iRGD-PNP incubated with PC3MM2 cells for 1 h. Lysosomes were stained with LysoTracker[®] Red (red) and IO@PNP were labelled with AF 647 (green). Co-localized lysosomes and IO@PNP appear in yellow. (b) Confocal fluorescence microscope images of the fate of IO@PNP-DOX in PC3MM2 cells at different incubation time points. The nuclei of the cells was stained with DAPI (blue), DOX-IO@PNP were labelled with AF 647 (green), and DOX is shown in red. Co-localized DOX with DAPI and AF 647 appears in pink and yellow, respectively.

5.4.4 *In vitro* cell growth inhibition

To confirm the successful delivery of DOX intracellularly, the cytotoxicity of DOX administered in its free base form and conjugated to the NPs after 24 h incubation, was evaluated (Figure 17).

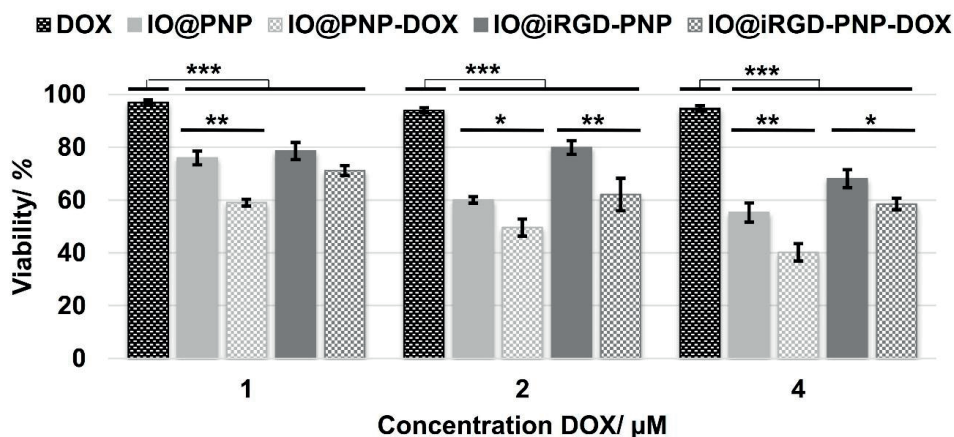


Figure 17 Cytotoxicity of DOX, IO@PNP, IO@PNP-DOX, IO@iRGD-PNP, and IO@iRGD-PNP-DOX incubated with PC3MM2 cells for 24 h. The experiments were done in triplicate and the error bars represent the mean \pm s.d. at each timepoint. Statistical significance levels were set at probabilities of * $p \leq 0.05$, ** $p \leq 0.01$, and *** $p \leq 0.001$.

For the incubation time and concentration range tested of DOX and its polymer-conjugated form, 1 to 4 μM , DOX free base did not present cytotoxic effects, while IO@PNP and the iRGD decorated NP presented certain cytotoxicity. The toxicity of the NPs was likely due the polycationic nature of PHIS, which, by promoting the proton-sponge mechanism, also causes the spillage of the lysosomal content and triggering of intracellular Ca^{2+} release leading to some toxicity [313]. However, IO@PNP-DOX showed augmented cytotoxicity compared to the free drug and the NPs, 45 and 14% greater on average, respectively. Likewise, IO@iRGD-PNP-DOX demonstrated to enhance the cytotoxic effect of DOX free base and the NPs, 31 and 12%, on average, respectively. The enhanced cytotoxicity of the DOX-NP conjugates can be ascribed to a combination of the inherent toxicity of the IO@PNP and the efficient intracellular delivery of the drug, which might be hindered for the free base form of the drug due to its poor aqueous solubility. The finding confirmed the possibility of using this type of polymer-drug conjugate NPs as a vehicle for intracellular delivery of drugs.

6 Conclusions

In this dissertation, lipids and polymers in combination with PSi particles, and a polymer-drug conjugate, were utilized to fabricate advanced DDS for the loading of hydrophilic and hydrophobic drugs in order to achieve sustained or triggered drug release and to improve the dissolution properties of poorly aqueous soluble drugs. In addition, the potential of the DDS for tumor therapy was evaluated *in vitro*.

In the first study, it was investigated the loading and release properties of PSi MPs and PSi MPs encapsulated into a solid lipid matrix, using model drugs with different solubility profiles. The microcomposites, produced by single emulsion droplet-based microfluidics, demonstrated to sustain the release of hydrophilic and hydrophobic drugs, reduce the initial ‘burst release’ observed for bare PSi, and also to modify the surface properties of PSi, making it less hydrophobic and reducing its cytotoxicity.

The second study explored, the encapsulation of a hydrophobic drug molecule within the aqueous core of lipid vesicles aided by PSi MPs. Piroxicam-loaded PSi–lipid vesicles were produced by double emulsion droplet-based microfluidics in a highly reliable, reproducible, and efficient manner; and were capable of sustaining the release of piroxicam, particularly at pH 7.4.

In the third study, a smart hybrid nanocomposite was developed for antitumoral applications with triggered release and stealth properties. The nanocomposite, produced by flow-focusing microfluidics nanoprecipitation, consisted of a pH-sensitive polymeric compound micelle assembled on the surface of PSi NPs loaded with the hydrophobic drug SFN. The release of SFN was successfully prevented in physiological conditions (pH 7.4) while fast release was observed in acidic conditions. Accordingly, the SFN-loaded nanocomposite evidenced a pH-dependent cell growth inhibition capacity of a prostate cancer cell line, resulting in more cell death at pH 5.5 than at pH 7.4, revealing the potential of the developed nanocomposite of reducing the drugs’ unspecific effect. Furthermore, the nanocomposite presented limited interaction with macrophages, indicating the potential of the DDS for prolonged blood circulation time.

In the fourth study, a targeted theranostic DDS was developed with multi-stimuli responsive properties to magnetic field and pH, consisting of a polymeric-drug conjugate NP, containing encapsulated SPION, and decorated with a tumor homing-peptide, iRGD. The DDS was fabricated by pH-switch nanoprecipitation in organic-free solvents, ideal for further biomedical applications. The DDS demonstrated reduced cytotoxicity and hemolytic effects. Moreover, the association of DDS with endothelial cells was extensive, and was moderately enhanced by iRGD. The DDS demonstrated efficient lysosomal escape *in vitro*, likely due to the proton-sponge effect exerted by the pH-sensitive polymer. In addition, the amide bond linking the polymer to the anticancer drug DOX was cleaved intracellularly, allowing the drug to translocate into the nucleus, and improving, in this fashion, the performance of the drug.

In conclusion, the developed hybrid micro- and nano-systems in this thesis represent a novel contribution to the field of drug delivery, in particular regarding PSi as a platform for advanced DDS. Moreover, the DDS systems evaluated *in vitro* for antitumoral applications hold great potential for their further *in vivo* assessment.

References

- [1] Allen T.M., Cullis P.R. Drug delivery systems: entering the mainstream. *Science*. 2004;303:1818-22.
- [2] Duncan R., Gaspar R. Nanomedicine (s) under the microscope. *Mol. Pharmaceutics*. 2011;8:2101-41.
- [3] Liechty W.B., Kryscio D.R., Slaughter B.V., Peppas N.A. Polymers for drug delivery systems. *Annu. Rev. Chem. Biomol. Eng.* 2010;1:149.
- [4] Yun Y.H., Lee B.K., Park K. Controlled Drug Delivery: Historical perspective for the next generation. *J. Control. Release*. 2015;219:2-7.
- [5] Stegemann S., Leveiller F., Franchi D., De Jong H., Lindén H. When poor solubility becomes an issue: from early stage to proof of concept. *Eur. J. Pharm. Sci.* 2007;31:249-61.
- [6] Medlicott N.J., Foster K.A., Audus K.L., Gupta S., Stella V.J. Comparison of the effects of potential parenteral vehicles for poorly water soluble anticancer drugs (organic cosolvents and cyclodextrin solutions) on cultured endothelial cells (HUV-EC). *J. Pharm. Sci.* 1998;87:1138-43.
- [7] Kumar Malik D., Baboota S., Ahuja A., Hasan S., Ali J. Recent advances in protein and peptide drug delivery systems. *Curr. Drug. Delivery*. 2007;4:141-51.
- [8] Shrestha N., Shahbazi M.-A., Araújo F., Mäkilä E., Raula J., Kauppinen E.I., Salonen J., Sarmiento B., Hirvonen J., Santos H.A. Multistage pH-responsive mucoadhesive nanocarriers prepared by aerosol flow reactor technology: A controlled dual protein-drug delivery system. *Biomaterials*. 2015;68:9-20.
- [9] Marschütz M.K., Bernkop-Schnürch A. Oral peptide drug delivery: polymer-inhibitor conjugates protecting insulin from enzymatic degradation in vitro. *Biomaterials*. 2000;21:1499-507.
- [10] Munier S., Messai I., Delair T., Verrier B., Ataman-Önal Y. Cationic PLA nanoparticles for DNA delivery: comparison of three surface polycations for DNA binding, protection and transfection properties. *Colloids Surf., B*. 2005;43:163-73.
- [11] Sahoo S., Parveen S., Panda J. The present and future of nanotechnology in human health care. *Nanomedicine*. 2007;3:20-31.
- [12] Choi H.S., Liu W., Misra P., Tanaka E., Zimmer J.P., Ipe B.I., Bawendi M.G., Frangioni J.V. Renal clearance of quantum dots. *Nat. Biotechnol.* 2007;25:1165-70.
- [13] Owens D.E., Peppas N.A. Opsonization, biodistribution, and pharmacokinetics of polymeric nanoparticles. *Int. J. Pharm.* 2006;307:93-102.
- [14] Kobayashi H., Watanabe R., Choyke P.L. Improving conventional enhanced permeability and retention (EPR) effects; what is the appropriate target. *Theranostics*. 2014;4:81-9.
- [15] Ruoslahti E., Bhatia S.N., Sailor M.J. Targeting of drugs and nanoparticles to tumors. *J. Cell Biol.* 2010;188:759-68.
- [16] Stolnik S., Illum L., Davis S. Long circulating microparticulate drug carriers. *Adv. Drug Delivery Rev.* 2012;64:290-301.
- [17] Kwon S.M., Nam H.Y., Nam T., Park K., Lee S., Kim K., Kwon I.C., Kim J., Kang D., Park J.H. In vivo time-dependent gene expression of cationic lipid-based emulsion as a stable and biocompatible non-viral gene carrier. *J. Control. Release*. 2008;128:89-97.
- [18] Xu Z., Chen L., Gu W., Gao Y., Lin L., Zhang Z., Xi Y., Li Y. The performance of docetaxel-loaded solid lipid nanoparticles targeted to hepatocellular carcinoma. *Biomaterials*. 2009;30:226-32.
- [19] Zhang Y., Chan H.F., Leong K.W. Advanced materials and processing for drug delivery: the past and the future. *Adv. Drug Delivery Rev.* 2013;65:104-20.
- [20] Nair L.S., Laurencin C.T. Biodegradable polymers as biomaterials. *Progress in polymer science*. 2007;32:762-98.
- [21] Sokolova V., Epple M. Inorganic nanoparticles as carriers of nucleic acids into cells. *Angew. Chem., Int. Ed.* 2008;47:1382-95.

- [22] Santos H.A., Mäkilä E., Airaksinen A.J., Bimbo L.M., Hirvonen J. Porous silicon nanoparticles for nanomedicine: preparation and biomedical applications. *Nanomedicine*. 2014;9:535-54.
- [23] Canham L. *Handbook of porous silicon*: Springer; 2014. 1008 pp.
- [24] Santos H.A. *Porous silicon for biomedical applications*: Elsevier; 2014. 558 pp.
- [25] Canham L. Silicon quantum wire array fabrication by electrochemical and chemical dissolution of wafers. *Appl. Phys. Lett.* 1990;57:1046-8.
- [26] Salonen J., Laitinen L., Kaukonen A., Tuura J., Björkqvist M., Heikkilä T., Vähä-Heikkilä K., Hirvonen J., Lehto V.-P. Mesoporous silicon microparticles for oral drug delivery: loading and release of five model drugs. *J. Control. Release*. 2005;108:362-74.
- [27] Salonen J., Lehto V.-P. Fabrication and chemical surface modification of mesoporous silicon for biomedical applications. *Chem. Eng. J.* 2008;137:162-72.
- [28] Liu D., Mäkilä E., Zhang H., Herranz B., Kaasalainen M., Kinnari P., Salonen J., Hirvonen J., Santos H.A. Nanostructured Porous Silicon-Solid Lipid Nanocomposite: Towards Enhanced Cytocompatibility and Stability, Reduced Cellular Association, and Prolonged Drug Release. *Adv. Funct. Mater.* 2013;23:1893-902.
- [29] A Santos H., M Bimbo L., Lehto V.-P., J Airaksinen A., Salonen J., Hirvonen J. Multifunctional porous silicon for therapeutic drug delivery and imaging. *Curr. Drug Discovery Technol.* 2011;8:228-49.
- [30] Santos H. Opinion Paper: Microfluidics Technique to Revolutionize the Drug Delivery Field: Current Developments and Applications. *Curr. Drug. Delivery*. 2015.
- [31] Fontana F., Ferreira M.P., Correia A., Hirvonen J., Santos H.A. Microfluidics as a cutting-edge technique for drug delivery applications. *J. Drug. Deliv. Sci. Technol.* 2016.
- [32] Utada A., Chu L.-Y., Fernandez-Nieves A., Link D., Holtze C., Weitz D. Dripping, jetting, drops, and wetting: the magic of microfluidics. *MRS Bull.* 2007;32:702-8.
- [33] Liu D., Cito S., Zhang Y., Wang C.F., Sikanen T.M., Santos H.A. A versatile and robust microfluidic platform toward high throughput synthesis of homogeneous nanoparticles with tunable properties. *Adv. Mater.* 2015;27:2298-304.
- [34] Kim Y., Lee Chung B., Ma M., Mulder W.J., Fayad Z.A., Farokhzad O.C., Langer R. Mass production and size control of lipid-polymer hybrid nanoparticles through controlled microvortices. *Nano Lett.* 2012;12:3587-91.
- [35] Biswas S., Vaze O.S., Movassaghian S., Torchilin V.P. *Polymeric micelles for the delivery of poorly soluble drugs*. John Wiley & Sons: New York; 2013. p. 411-76.
- [36] Wang M., Thanou M. Targeting nanoparticles to cancer. *Pharmacol. Res.* 2010;62:90-9.
- [37] Zhao K., Yuan Y., Wang H., Li P., Bao Z., Li Y. Preparation and evaluation of valsartan by a novel semi-solid self-microemulsifying delivery system using Gelucire® 44/14. *Drug Dev. Ind. Pharm.* 2016:1-30.
- [38] Vyas A., Saraf S., Saraf S. Cyclodextrin based novel drug delivery systems. *J. Incl. Phenom. Macrocycl. Chem.* 2008;62:23-42.
- [39] Vallet-Regí M., Balas F., Arcos D. Mesoporous materials for drug delivery. *Angew. Chem., Int. Ed.* 2007;46:7548-58.
- [40] Barratt G. Colloidal drug carriers: achievements and perspectives. *Cell. Mol. Life Sci.* 2003;60:21-37.
- [41] Dawidczyk C.M., Russell L.M., Searson P.C. Nanomedicines for cancer therapy: state-of-the-art and limitations to pre-clinical studies that hinder future developments. *Front. Chem.* 2014;2:69.
- [42] Coniot J., Silva J.M., Fernandes J.G., Silva L.C., Gaspar R., Brocchini S., Florindo H.F., Barata T.S. Cancer immunotherapy: nanodelivery approaches for immune cell targeting and tracking. *Front. Chem.* 2014;2:105.
- [43] Maulvi F.A., Lakdawala D.H., Shaikh A.A., Desai A.R., Choksi H.H., Vaidya R.J., Ranch K.M., Koli A.R., Vyas B.A., Shah D.O. In vitro and in vivo evaluation of novel implantation technology in hydrogel contact lenses for controlled drug delivery. *J. Control. Release*. 2016;226:47-56.
- [44] Su J., Sun H., Meng Q., Yin Q., Tang S., Zhang P., Chen Y., Zhang Z., Yu H., Li Y. Long Circulation Red-Blood-Cell-Mimetic Nanoparticles with Peptide-Enhanced Tumor

Penetration for Simultaneously Inhibiting Growth and Lung Metastasis of Breast Cancer. *Adv. Funct. Mater.* 2016.

[45] Qin Z., Zhang J., Chi H., Cao F. Organic–inorganic hybrid nanocomposites based on chitosan derivatives and layered double hydroxides with intercalated phacolysin as ocular delivery system. *J. Nanopart. Res.* 2015;17:1-15.

[46] Pradhan M., Singh D., Murthy S.N., Singh M.R. Design, characterization and skin permeating potential of Fluocinolone acetonide loaded nanostructured lipid carriers for topical treatment of psoriasis. *Steroids.* 2015;101:56-63.

[47] Gabizon A., Shmeeda H., Barenholz Y. Pharmacokinetics of pegylated liposomal doxorubicin. *Clin. Pharmacokinet.* 2003;42:419-36.

[48] Lyass O., Uziely B., Ben-Yosef R., Tzemach D., Heshing N.I., Lotem M., Brufman G., Gabizon A. Correlation of toxicity with pharmacokinetics of pegylated liposomal doxorubicin (Doxil) in metastatic breast carcinoma. *Cancer.* 2000;89:1037-47.

[49] Gabizon A., Catane R., Uziely B., Kaufman B., Safra T., Cohen R., Martin F., Huang A., Barenholz Y. Prolonged circulation time and enhanced accumulation in malignant exudates of doxorubicin encapsulated in polyethylene-glycol coated liposomes. *Cancer Res.* 1994;54:987-92.

[50] Poste G., Kirsh R., Koestler T. The challenge of liposome targeting in vivo. *Liposome Technol.* 1984;3:1-28.

[51] Maeda H., Wu J., Sawa T., Matsumura Y., Hori K. Tumor vascular permeability and the EPR effect in macromolecular therapeutics: a review. *J. Control. Release.* 2000;65:271-84.

[52] Malam Y., Loizidou M., Seifalian A.M. Liposomes and nanoparticles: nanosized vehicles for drug delivery in cancer. *Trends Pharmacol. Sci.* 2009;30:592-9.

[53] Dahan A., Hoffman A. Rationalizing the selection of oral lipid based drug delivery systems by an in vitro dynamic lipolysis model for improved oral bioavailability of poorly water soluble drugs. *J. Control. Release.* 2008;129:1-10.

[54] Sahoo S.K., Dilnawaz F., Krishnakumar S. Nanotechnology in ocular drug delivery. *Drug Discov. Today.* 2008;13:144-51.

[55] Mannermaa E., Vellonen K.-S., Urtti A. Drug transport in corneal epithelium and blood–retina barrier: emerging role of transporters in ocular pharmacokinetics. *Adv. Drug Delivery Rev.* 2006;58:1136-63.

[56] Wagner V., Dullaart A., Bock A.-K., Zweck A. The emerging nanomedicine landscape. *Nat. Biotechnol.* 2006;24:1211-7.

[57] Duncan R., Vicent M.J. Polymer therapeutics-prospects for 21st century: the end of the beginning. *Adv. Drug Delivery Rev.* 2013;65:60-70.

[58] Smith D., Adams J., Johnston S., Gordon A., Drummond M., Bennett C. A comparative economic analysis of pegylated liposomal doxorubicin versus topotecan in ovarian cancer in the USA and the UK. *Ann. Oncol.* 2002;13:1590-7.

[59] Markovskiy E., Baabur-Cohen H., Eldar-Boock A., Omer L., Tiram G., Ferber S., Ofek P., Polyak D., Scomparin A., Satchi-Fainaro R. Administration, distribution, metabolism and elimination of polymer therapeutics. *J. Control. Release.* 2012;161:446-60.

[60] Uhlir A. Electrolytic shaping of germanium and silicon. *Bell Syst. Tech. J.* 1956;35:333-47.

[61] Watanabe Y., Sakai T. Application of a thick anode film to semiconductor devices. *Rev. Electr. Commun. Lab.* 1971;19:899.

[62] Canham L.T. Bioactive silicon structure fabrication through nanoetching techniques. *Adv. Mater.* 1995;7:1033-7.

[63] Riikonen J., Salomäki M., van Wonderen J., Kemell M., Xu W., Korhonen O., Ritala M., MacMillan F., Salonen J., Lehto V.-P. Surface Chemistry, Reactivity, and Pore Structure of Porous Silicon Oxidized by Various Methods. *Langmuir.* 2012;28:10573-83.

[64] Salonen J., Kaukonen A.M., Hirvonen J., Lehto V.-P. Mesoporous silicon in drug delivery applications. *J. Pharm. Sci.* 2008;97:632-53.

[65] Wu E.C., Andrew J.S., Buyanin A., Kinsella J.M., Sailor M.J. Suitability of porous silicon microparticles for the long-term delivery of redox-active therapeutics. *Chem. Commun.* 2011;47:5699-701.

- [66] Santos H.A., Riikonen J., Salonen J., Mäkilä E., Heikkilä T., Laaksonen T., Peltonen L., Lehto V.-P., Hirvonen J. In vitro cytotoxicity of porous silicon microparticles: effect of the particle concentration, surface chemistry and size. *Acta Biomater.* 2010;6:2721-31.
- [67] Halimaoui A., Oules C., Bomchil G., Bsiesy A., Gaspard F., Herino R., Ligeon M., Muller F. Electroluminescence in the visible range during anodic oxidation of porous silicon films. *Appl. Phys. Lett.* 1991;59:304-6.
- [68] Tischler M., Collins R., Stathis J., Tsang J. Luminescence degradation in porous silicon. *Appl. Phys. Lett.* 1992;60:639-41.
- [69] Frotscher U., Rossow U., Ebert M., Pietryga C., Richter W., Berger M., Arens-Fischer R., Münder H. Investigation of different oxidation processes for porous silicon studied by spectroscopic ellipsometry. *Thin Solid Films.* 1996;276:36-9.
- [70] Mawhinney D.B., Glass J.A., Yates J.T. FTIR study of the oxidation of porous silicon. *J. Phys. Chem. B.* 1997;101:1202-6.
- [71] Jarvis K.L., Barnes T.J., Prestidge C.A. Surface chemistry of porous silicon and implications for drug encapsulation and delivery applications. *Adv. Colloid Interface Sci.* 2012;175:25-38.
- [72] Fry N.L., Boss G.R., Sailor M.J. Oxidation-induced trapping of drugs in porous silicon microparticles. *Chem. Mater.* 2014;26:2758-64.
- [73] Boukherroub R., Morin S., Wayner D., Bensebaa F., Sproule G., Baribeau J.-M., Lockwood D. Ideal passivation of luminescent porous silicon by thermal, noncatalytic reaction with alkenes and aldehydes. *Chem. Mater.* 2001;13:2002-11.
- [74] Buriak J.M. Silicon-Carbon Bonds on Porous Silicon Surfaces. *Adv. Mater.* 1999;11:265-7.
- [75] Stewart M.P., Buriak J.M. Exciton-Mediated Hydrosilylation on Photoluminescent Nanocrystalline Silicon. *J. Am. Chem. Soc.* 2001;123:7821-30.
- [76] Boukherroub R., Wojtyk J., Wayner D.D., Lockwood D.J. Thermal hydrosilylation of undecylenic acid with porous silicon. *J. Electrochem. Soc.* 2002;149:H59-H63.
- [77] Salonen J., Björkqvist M., Laine E., Niinistö L. Stabilization of porous silicon surface by thermal decomposition of acetylene. *Appl. Surf. Sci.* 2004;225:389-94.
- [78] Salonen J., Laine E., Niinistö L. Thermal carbonization of porous silicon surface by acetylene. *J. Appl. Phys.* 2002;91:456-61.
- [79] Björkqvist M., Paski J., Salonen J., Lehto V.-P. Studies on hysteresis reduction in thermally carbonized porous silicon humidity sensor. *IEEE Sens. J.* 2006;6:542-7.
- [80] Kovalainen M., Mönkäre J., Mäkilä E., Salonen J., Lehto V.-P., Herzog K.-H., Järvinen K. Mesoporous silicon (PSi) for sustained peptide delivery: effect of PSi microparticle surface chemistry on peptide YY3-36 release. *Pharm. Res.* 2012;29:837-46.
- [81] Low S.P., Voelcker N.H., Canham L.T., Williams K.A. The biocompatibility of porous silicon in tissues of the eye. *Biomaterials.* 2009;30:2873-80.
- [82] Tasciotti E., Godin B., Martinez J.O., Chiappini C., Bhavane R., Liu X., Ferrari M. Near-infrared imaging method for the in vivo assessment of the biodistribution of nanoporous silicon particles. *Mol. Imaging.* 2011;10:56.
- [83] Riikonen J., Correia A., Kovalainen M., Näkki S., Lehtonen M., Leppänen J., Rantanen J., Xu W., Araújo F., Hirvonen J. Systematic in vitro and in vivo study on porous silicon to improve the oral bioavailability of celecoxib. *Biomaterials.* 2015;52:44-55.
- [84] Tölli M.A., Ferreira M.P., Kinnunen S.M., Rysä J., Mäkilä E.M., Szabó Z., Serpi R.E., Ohukainen P.J., Välimäki M.J., Correia A.M. In vivo biocompatibility of porous silicon biomaterials for drug delivery to the heart. *Biomaterials.* 2014;35:8394-405.
- [85] Bimbo L.M., Sarparanta M., Santos H.A., Airaksinen A.J., Mäkilä E., Laaksonen T., Peltonen L., Lehto V.-P., Hirvonen J., Salonen J. Biocompatibility of thermally hydrocarbonized porous silicon nanoparticles and their biodistribution in rats. *ACS nano.* 2010;4:3023-32.
- [86] Park J.-H., Gu L., Von Maltzahn G., Ruoslahti E., Bhatia S.N., Sailor M.J. Biodegradable luminescent porous silicon nanoparticles for in vivo applications. *Nat. Mater.* 2009;8:331-6.

- [87] Reffitt D.M., Jugdaohsingh R., Thompson R.P., Powell J.J. Silicic acid: its gastrointestinal uptake and urinary excretion in man and effects on aluminium excretion. *J. Inorg. Biochem.* 1999;76:141-7.
- [88] Sarparanta M., Mäkilä E., Heikkilä T., Salonen J., Kukku E., Lehto V.-P., Santos H.A., Hirvonen J., Airaksinen A.J. 18F-labeled modified porous silicon particles for investigation of drug delivery carrier distribution in vivo with positron emission tomography. *Mol. Pharmaceutics.* 2011;8:1799-806.
- [89] Shahbazi M.-A., Hamidi M., Mäkilä E.M., Zhang H., Almeida P.V., Kaasalainen M., Salonen J.J., Hirvonen J.T., Santos H.A. The mechanisms of surface chemistry effects of mesoporous silicon nanoparticles on immunotoxicity and biocompatibility. *Biomaterials.* 2013;34:7776-89.
- [90] Araújo F., Shrestha N., Shahbazi M.-A., Liu D., Herranz-Blanco B., Mäkilä E.M., Salonen J.J., Hirvonen J.T., Granja P.L., Sarmiento B. Microfluidic assembly of a multifunctional tailorable composite system designed for site specific combined oral delivery of peptide drugs. *ACS nano.* 2015;9:8291-302.
- [91] Shrestha N., Shahbazi M.-A., Araújo F., Zhang H., Mäkilä E.M., Kauppila J., Sarmiento B., Salonen J.J., Hirvonen J.T., Santos H.A. Chitosan-modified porous silicon microparticles for enhanced permeability of insulin across intestinal cell monolayers. *Biomaterials.* 2014;35:7172-9.
- [92] Cheng L., Anglin E., Cunin F., Kim D., Sailor M., Falkenstein I., Tammewar A., Freeman W. Intravitreal properties of porous silicon photonic crystals: a potential self-reporting intraocular drug-delivery vehicle. *Br. J. Ophthalmol.* 2008;92:705-11.
- [93] Kashanian S., Harding F., Irani Y., Klebe S., Marshall K., Loni A., Canham L., Fan D., Williams K.A., Voelcker N.H. Evaluation of mesoporous silicon/polycaprolactone composites as ophthalmic implants. *Acta Biomater.* 2010;6:3566-72.
- [94] Low S.P., Voelcker N.H. Biocompatibility of Porous Silicon. *Handbook of Porous Silicon*: Springer; 2014. p. 381-93.
- [95] Shabir Q. Biodegradability of Porous Silicon. *Handbook of Porous Silicon*: Springer; 2014. p. 395-401.
- [96] Bowditch A., Waters K., Gale H., Rice P., Scott E., Canham L., Reeves C., Loni A., Cox T. In-vivo assessment of tissue compatibility and calcification of bulk and porous silicon. *MRS Proceedings*: Cambridge Univ Press; 1998. p. 149.
- [97] Sarparanta M., Bimbo L.M., Rytönen J., Mäkilä E., Laaksonen T.J., Laaksonen P.i., Nyman M., Salonen J., Linder M.B., Hirvonen J. Intravenous delivery of hydrophobin-functionalized porous silicon nanoparticles: stability, plasma protein adsorption and biodistribution. *Mol. Pharmaceutics.* 2012;9:654-63.
- [98] Shabir Q., Pokale A., Loni A., Johnson D., Canham L., Fenollosa R., Tymczenko M., Rodríguez I., Meseguer F., Cros A. Medically biodegradable hydrogenated amorphous silicon microspheres. *Silicon.* 2011;3:173-6.
- [99] Anderson S., Elliott H., Wallis D., Canham L., Powell J. Dissolution of different forms of partially porous silicon wafers under simulated physiological conditions. *Phys. Status Solidi A.* 2003;197:331-5.
- [100] Chiappini C., Liu X., Fakhoury J.R., Ferrari M. Biodegradable porous silicon barcode nanowires with defined geometry. *Adv. Funct. Mater.* 2010;20:2231-9.
- [101] Godin B., Gu J., Serda R.E., Bhavane R., Tasciotti E., Chiappini C., Liu X., Tanaka T., Decuzzi P., Ferrari M. Tailoring the degradation kinetics of mesoporous silicon structures through PEGylation. *J. Biomed. Mater. Res., Part A.* 2010;94:1236-43.
- [102] Canham L.T., Reeves C., Newey J., Houlton M., Cox T., Buriak J., Stewart M. Derivatized mesoporous silicon with dramatically improved stability in simulated human blood plasma. *Adv. Mater.* 1999;11:1505-7.
- [103] Canham L., Stewart M., Buriak J., Reeves C., Anderson M., Squire E., Allcock P., Snow P. Derivatized porous silicon mirrors: implantable optical components with slow resorbability. *Phys. Status Solidi A.* 2000;182:521-5.
- [104] Irani Y.D., Tian Y., Wang M., Klebe S., McInnes S.J., Voelcker N.H., Coffey J.L., Williams K.A. A novel pressed porous silicon-polycaprolactone composite as a dual-

- purpose implant for the delivery of cells and drugs to the eye. *Exp. Eye Res.* 2015;139:123-31.
- [105] Tong W.Y., Sweetman M.J., Marzouk E.R., Fraser C., Kuchel T., Voelcker N.H. Towards a subcutaneous optical biosensor based on thermally hydrocarbonised porous silicon. *Biomaterials.* 2016;74:217-30.
- [106] Joo J., Liu X., Kotamraju V.R., Ruoslahti E., Nam Y., Sailor M.J. Gated Luminescence Imaging of Silicon Nanoparticles. *ACS nano.* 2015;9:6233-41.
- [107] Xu W., Thapa R., Liu D., Nissinen T., Granroth S., Närvänen A., Suvanto M., Santos H.A., Lehto V.-P. Smart porous silicon nanoparticles with polymeric coatings for sequential combination therapy. *Mol. Pharmaceutics.* 2015;12:4038-47.
- [108] McInnes S.J.P., Szili E., Al-Bataineh S.A., Vasani R.B., Xu J., Alf M.E., Gleason K.K., Short R.D., Voelcker N.H. Fabrication and characterization of a porous silicon drug delivery system with an iCVD temperature-responsive coating. *Langmuir.* 2015;32:301-8.
- [109] Anglin E.J., Cheng L., Freeman W.R., Sailor M.J. Porous silicon in drug delivery devices and materials. *Adv. Drug Delivery Rev.* 2008;60:1266-77.
- [110] Wu E.C., Andrew J.S., Cheng L., Freeman W.R., Pearson L., Sailor M.J. Real-time monitoring of sustained drug release using the optical properties of porous silicon photonic crystal particles. *Biomaterials.* 2011;32:1957-66.
- [111] Lehto V., Riikonen J., Santos H. Drug loading and characterization of porous silicon materials. *Porous silicon for biomedical applications.* Woodhead Publishing, Cambridge, UK. 2014:337-55.
- [112] Prestidge C., Barnes T. Nanoporous silicon to enhance drug solubility. *Porous Silicon for Biomedical Applications.* 2014:356.
- [113] Linnell T., Santos H.A., Mäkilä E., Heikkilä T., Salonen J., Murzin D.Y., Kumar N., Laaksonen T., Peltonen L., Hirvonen J. Drug delivery formulations of ordered and nonordered mesoporous silica: Comparison of three drug loading methods. *J. Pharm. Sci.* 2011;100:3294-306.
- [114] Nieto A., Hou H., Moon S.W., Sailor M.J., Freeman W.R., Cheng L. Surface Engineering of Porous Silicon Microparticles for Intravitreal Sustained Delivery of Rapamycin. *Intravitreal Porous Silicon for Delivery of Rapamycin.* Invest. Ophthalmol. Visual Sci. 2015;56:1070-80.
- [115] Kaukonen A.M., Laitinen L., Salonen J., Tuura J., Heikkilä T., Linnell T., Hirvonen J., Lehto V.-P. Enhanced in vitro permeation of furosemide loaded into thermally carbonized mesoporous silicon (TCPSi) microparticles. *Eur. J. Pharm. Biopharm.* 2007;66:348-56.
- [116] Bimbo L.M., Mäkilä E., Laaksonen T., Lehto V.-P., Salonen J., Hirvonen J., Santos H.A. Drug permeation across intestinal epithelial cells using porous silicon nanoparticles. *Biomaterials.* 2011;32:2625-33.
- [117] Linnell T., Riikonen J., Salonen J., Kaukonen A.M., Laitinen L., Hirvonen J., Lehto V.P. Surface chemistry and pore size affect carrier properties of mesoporous silicon microparticles. *Int. J. Pharm.* 2007;343:141-7.
- [118] Heikkilä T., Salonen J., Tuura J., Kumar N., Salmi T., Murzin D.Y., Hamdy M., Mul G., Laitinen L., Kaukonen A. Evaluation of mesoporous TCPSi, MCM-41, SBA-15, and TUD-1 materials as API carriers for oral drug delivery. *Drug delivery.* 2007;14:337-47.
- [119] Wang F., Hui H., Barnes T.J., Barnett C., Prestidge C.A. Oxidized mesoporous silicon microparticles for improved oral delivery of poorly soluble drugs. *Mol. Pharmaceutics.* 2009;7:227-36.
- [120] Kinnari P., Mäkilä E., Heikkilä T., Salonen J., Hirvonen J., Santos H.A. Comparison of mesoporous silicon and non-ordered mesoporous silica materials as drug carriers for itraconazole. *Int. J. Pharm.* 2011;414:148-56.
- [121] Wang C.-F., Mäkilä E.M., Kaasalainen M.H., Liu D., Sarparanta M.P., Airaksinen A.J., Salonen J.J., Hirvonen J.T., Santos H.A. Copper-free azide-alkyne cycloaddition of targeting peptides to porous silicon nanoparticles for intracellular drug uptake. *Biomaterials.* 2014;35:1257-66.

- [122] Vale N., Mäkilä E., Salonen J., Gomes P., Hirvonen J., Santos H.A. New times, new trends for ethionamide: In vitro evaluation of drug-loaded thermally carbonized porous silicon microparticles. *Eur. J. Pharm. Biopharm.* 2012;81:314-23.
- [123] Bimbo L.M., Denisova O.V., Mäkilä E., Kaasalainen M., De Brabander J.K., Hirvonen J., Salonen J., Kakkola L., Kainov D., Santos H.I.A. Inhibition of influenza A virus infection in vitro by saliphenylhalamide-loaded porous silicon nanoparticles. *ACS nano.* 2013;7:6884-93.
- [124] Maniya N.H., Patel S.R., Murthy Z. Controlled delivery of acyclovir from porous silicon micro-and nanoparticles. *Appl. Surf. Sci.* 2015;330:358-65.
- [125] Secret E., Maynadier M., Gallud A., Gary-Bobo M., Chaix A., Belamie E., Maillard P., Sailor M.J., Garcia M., Durand J.-O. Anionic porphyrin-grafted porous silicon nanoparticles for photodynamic therapy. *Chem. Commun.* 2013;49:4202-4.
- [126] Wu E.C., Park J.-H., Park J., Segal E., Cunin F., Sailor M.J. Oxidation-triggered release of fluorescent molecules or drugs from mesoporous Si microparticles. *ACS nano.* 2008;2:2401-9.
- [127] Wang C.-F., Mäkilä E.M., Kaasalainen M.H., Hagström M.V., Salonen J.J., Hirvonen J.T., Santos H.A. Dual-drug delivery by porous silicon nanoparticles for improved cellular uptake, sustained release, and combination therapy. *Acta Biomater.* 2015;16:206-14.
- [128] Zhang H., Liu D., Shahbazi M.A., Mäkilä E., Herranz-Blanco B., Salonen J., Hirvonen J., Santos H.A. Fabrication of a Multifunctional Nano-in-micro Drug Delivery Platform by Microfluidic Templated Encapsulation of Porous Silicon in Polymer Matrix. *Adv. Mater.* 2014;26:4497-503.
- [129] Gu L., Park J.H., Duong K.H., Ruoslahti E., Sailor M.J. Magnetic luminescent porous silicon microparticles for localized delivery of molecular drug payloads. *Small.* 2010;6:2546-52.
- [130] Correia A., Shahbazi M.-A., Mäkilä E., Almeida S., Salonen J., Hirvonen J., Santos H.A. Cyclodextrin-Modified Porous Silicon Nanoparticles for Efficient Sustained Drug Delivery and Proliferation Inhibition of Breast Cancer Cells. *ACS Appl. Mater. Interfaces.* 2015;7:23197-204.
- [131] Nath S.D., Linh N.T., Sadiasa A., Lee B.T. Encapsulation of simvastatin in PLGA microspheres loaded into hydrogel loaded BCP porous spongy scaffold as a controlled drug delivery system for bone tissue regeneration. *J. Biomater. Appl.* 2014;28:1151-63.
- [132] Nan K., Ma F., Hou H., Freeman W.R., Sailor M.J., Cheng L. Porous silicon oxide-PLGA composite microspheres for sustained ocular delivery of daunorubicin. *Acta Biomater.* 2014;10:3505-12.
- [133] Liu D., Zhang H., Mäkilä E., Fan J., Herranz-Blanco B., Wang C.-F., Rosa R., Ribeiro A.J., Salonen J., Hirvonen J. Microfluidic assisted one-step fabrication of porous silicon@acetalated dextran nanocomposites for precisely controlled combination chemotherapy. *Biomaterials.* 2015;39:249-59.
- [134] Mann A.P., Tanaka T., Somasunderam A., Liu X., Gorenstein D.G., Ferrari M. E-Selectin-Targeted Porous Silicon Particle for Nanoparticle Delivery to the Bone Marrow. *Adv. Mater.* 2011;23.
- [135] Shen H., Rodriguez-Aguayo C., Xu R., Gonzalez-Villasana V., Mai J., Huang Y., Zhang G., Guo X., Bai L., Qin G. Enhancing chemotherapy response with sustained EphA2 silencing using multistage vector delivery. *Clin. Cancer Res.* 2013;19:1806-15.
- [136] Chiappini C., Tasciotti E., Serda R.E., Brousseau L., Liu X., Ferrari M. Mesoporous silicon particles as intravascular drug delivery vectors: fabrication, in-vitro, and in-vivo assessments. *Phys. Status Solidi C.* 2011;8:1826-32.
- [137] Decuzzi P., Godin B., Tanaka T., Lee S.-Y., Chiappini C., Liu X., Ferrari M. Size and shape effects in the biodistribution of intravascularly injected particles. *J. Control. Release.* 2010;141:320-7.
- [138] Van De Ven A.L., Kim P., Fakhoury J.R., Adriani G., Schmulen J., Moloney P., Hussain F., Ferrari M., Liu X., Yun S.-H. Rapid tumortropic accumulation of systemically injected plateloid particles and their biodistribution. *J. Control. Release.* 2012;158:148-55.

- [139] Kinnari P.J., Hyvönen M.L.K., Mäkilä E.M., Kaasalainen M.H., Rivinoja A., Salonen J.J., Hirvonen J.T., Laakkonen P.M., Santos H.A. Tumour homing peptide-functionalized porous silicon nanovectors for cancer therapy. *Biomaterials*. 2013;34:9134-41.
- [140] Secret E., Smith K., Dubljevic V., Moore E., Macardle P., Delalat B., Rogers M.L., Johns T.G., Durand J.O., Cunin F. Antibody-Functionalized Porous Silicon Nanoparticles for Vectorization of Hydrophobic Drugs. *Adv. Healthc. Mater.* 2013;2:718-27.
- [141] Wang C.-F., Sarparanta M.P., Mäkilä E.M., Hyvönen M.L., Laakkonen P.M., Salonen J.J., Hirvonen J.T., Airaksinen A.J., Santos H.A. Multifunctional porous silicon nanoparticles for cancer theranostics. *Biomaterials*. 2015;48:108-18.
- [142] Näkki S., Rytönen J., Nissinen T., Florea C., Riikonen J., Ek P., Zhang H., Santos H.A., Närvänen A., Xu W. Improved stability and biocompatibility of nanostructured silicon drug carrier for intravenous administration. *Acta Biomater.* 2015;13:207-15.
- [143] Barenholz Y.C. Doxil®—the first FDA-approved nano-drug: lessons learned. *J. Control. Release*. 2012;160:117-34.
- [144] Jain A.S., Shah S.M., Nagarsenker M.S., Nikam Y., Gude R.P., Steiniger F., Thamm J., Fahr A. Lipid colloidal carriers for improvement of anticancer activity of orally delivered quercetin: formulation, characterization and establishing in vitro–in vivo advantage. *J. Biomed. Nanotechnol.* 2013;9:1230-40.
- [145] Date A.A., Nagarsenker M. Parenteral microemulsions: an overview. *Int. J. Pharm.* 2008;355:19-30.
- [146] Date A.A., Nagarsenker M.S., Patere S., Dhawan V., Gude R., Hassan P., Aswal V., Steiniger F., Thamm J., Fahr A. Lecithin-based novel cationic nanocarriers (Leciplex) II: improving therapeutic efficacy of quercetin on oral administration†. *Mol. Pharmaceutics*. 2011;8:716-26.
- [147] Dhumal R., Soni M., Devarajan P., Samad A., Gaikwad R., Vanage G. Evaluation of safety of lipomer doxycycline hydrochloride (lipomer DH). *J. Biomed. Nanotechnol.* 2011;7:146-7.
- [148] Pandey R., Sharma S., Khuller G. Oral solid lipid nanoparticle-based antitubercular chemotherapy. *Tuberculosis*. 2005;85:415-20.
- [149] Chen M.-L. Lipid excipients and delivery systems for pharmaceutical development: a regulatory perspective. *Adv. Drug Delivery Rev.* 2008;60:768-77.
- [150] Cullis P.R., Hope M.J., Bally M.B., Madden T.D., Mayer L.D., Fenske D.B. Influence of pH gradients on the transbilayer transport of drugs, lipids, peptides and metal ions into large unilamellar vesicles. *BBA-Rev. Biomembranes*. 1997;1331:187-211.
- [151] Bolotin E.M., Cohen R., Bar L.K., Emanuel N., Ninio S., Barenholz Y., Lasic D.D. Ammonium sulfate gradients for efficient and stable remote loading of amphiphilic weak bases into liposomes and ligandoliposomes. *J. Liposome. Res.* 1994;4:455-79.
- [152] Chowdhary R.K., Shariff I., Dolphin D. Drug release characteristics of lipid based benzoporphyrin derivative. *J. Pharm. Pharm. Sci.* 2003;6:13-9.
- [153] Akbarzadeh A., Rezaei-Sadabady R., Davaran S., Joo S.W., Zarghami N., Hanifehpour Y., Samiei M., Kouhi M., Nejati-Koshki K. Liposome: classification, preparation, and applications. *Nanoscale Res Lett.* 2013;8:102.
- [154] Mai Y., Eisenberg A. Self-assembly of block copolymers. *Chem. Soc. Rev.* 2012;41:5969-85.
- [155] Johnson B.K., Prud'homme R.K. Mechanism for rapid self-assembly of block copolymer nanoparticles. *Phys. Rev. Lett.* 2003;91:118302.
- [156] Blanazs A., Armes S.P., Ryan A.J. Self-assembled block copolymer aggregates: from micelles to vesicles and their biological applications. *Macromol. Rapid Commun.* 2009;30:267-77.
- [157] Whitesides G., Stroock A. Flexible methods for microfluidics [J]. *Phys. Today*. 2001;54:42-8.
- [158] Tähkä S.M., Bonabi A., Nordberg M.-E., Kanerva M., Jokinen V.P., Sikanen T.M. Thiol-ene microfluidic devices for microchip electrophoresis: Effects of curing conditions and monomer composition on surface properties. *J. Chromatogr. A*. 2015;1426:233-40.
- [159] Keng P.Y., Chen S., Ding H., Sadeghi S., Shah G.J., Dooraghi A., Phelps M.E., Satyamurthy N., Chatziioannou A.F., van Dam R.M. Micro-chemical synthesis of

- molecular probes on an electronic microfluidic device. *Proc. Natl. Acad. Sci.* 2012;109:690-5.
- [160] Psaltis D., Quake S.R., Yang C. Developing optofluidic technology through the fusion of microfluidics and optics. *Nature.* 2006;442:381-6.
- [161] Vincent M.E. Microfluidics for creating spatially structured environments for single cells and microbial communities: THE UNIVERSITY OF CHICAGO; 2011. 158 pp.
- [162] Shintu L., Baudoin R.g., Navratil V., Prot J.-M., Pontoizeau C.m., Defernez M., Blaise B.J., Domange C.I., Péry A.R., Toulhoat P. Metabolomics-on-a-chip and predictive systems toxicology in microfluidic bioartificial organs. *Anal. Chem.* 2012;84:1840-8.
- [163] Arriaga L.R., Datta S.S., Kim S.H., Amstad E., Kodger T.E., Monroy F., Weitz D.A. Ultrathin shell double emulsion templated giant unilamellar lipid vesicles with controlled microdomain formation. *Small.* 2014;10:950-6.
- [164] Manz A., Harrison D.J., Verpoorte E.M., Fettingner J.C., Paulus A., Lüdi H., Widmer H.M. Planar chips technology for miniaturization and integration of separation techniques into monitoring systems: capillary electrophoresis on a chip. *J. Chromatogr. A.* 1992;593:253-8.
- [165] Ye C., Chen A., Colombo P., Martinez C. Ceramic microparticles and capsules via microfluidic processing of a preceramic polymer. *J. R. Soc., Interface.* 2010;13:1-13.
- [166] Sander J.S., Isa L., Rühs P.A., Fischer P., Studart A.R. Stabilization mechanism of double emulsions made by microfluidics. *Soft Matter.* 2012;8:11471-7.
- [167] Shum H.C., Zhao Y.j., Kim S.H., Weitz D.A. Multicompartment polymersomes from double emulsions. *Angew. Chem.* 2011;123:1686-9.
- [168] Tan Y.-C., Cristini V., Lee A.P. Monodispersed microfluidic droplet generation by shear focusing microfluidic device. *Sens. Actuators, B.* 2006;114:350-6.
- [169] Stachowiak J.C., Richmond D.L., Li T.H., Liu A.P., Parekh S.H., Fletcher D.A. Unilamellar vesicle formation and encapsulation by microfluidic jetting. *Proc. Natl. Acad. Sci.* 2008;105:4697-702.
- [170] Kim S.-H., Kim J.W., Cho J.-C., Weitz D.A. Double-emulsion drops with ultra-thin shells for capsule templates. *Lab Chip.* 2011;11:3162-6.
- [171] Lee J.N., Park C., Whitesides G.M. Solvent compatibility of poly (dimethylsiloxane)-based microfluidic devices. *Anal. Chem.* 2003;75:6544-54.
- [172] Utada A.S., Fernandez-Nieves A., Stone H.A., Weitz D.A. Dripping to jetting transitions in coflowing liquid streams. *Phys. Rev. Lett.* 2007;99:094502.
- [173] Polenz I., Weitz D.A., Baret J.-C. Polyurea microcapsules in microfluidics: surfactant control of soft membranes. *Langmuir.* 2015;31:1127-34.
- [174] Powers T.R., Zhang D., Goldstein R.E., Stone H.A. Propagation of a topological transition: The Rayleigh instability. *Phys. Fluids.* 1998;10:1052-7.
- [175] Duncanson W.J., Lin T., Abate A.R., Seiffert S., Shah R.K., Weitz D.A. Microfluidic synthesis of advanced microparticles for encapsulation and controlled release. *Lab Chip.* 2012;12:2135-45.
- [176] Amstad E., Kim S.H., Weitz D.A. Photo-and thermoresponsive polymersomes for triggered release. *Angew. Chem.* 2012;124:12667-71.
- [177] Stainmesse S., Fessi H., Devissaguet J.-P., Puisieux F., Theis C. Process for the preparation of dispersible colloidal systems of a substance in the form of nanoparticles. Google Patents; 1992.
- [178] Fessi H., Puisieux F., Devissaguet J.P., Ammoury N., Benita S. Nanocapsule formation by interfacial polymer deposition following solvent displacement. *Int. J. Pharm.* 1989;55:R1-R4.
- [179] Chorny M., Fishbein I., Danenberg H.D., Golomb G. Lipophilic drug loaded nanospheres prepared by nanoprecipitation: effect of formulation variables on size, drug recovery and release kinetics. *J. Control. Release.* 2002;83:389-400.
- [180] Leroueil-Le Verger M., Fluckiger L., Kim Y.-I., Hoffman M., Maincent P. Preparation and characterization of nanoparticles containing an antihypertensive agent. *Eur. J. Pharm. Biopharm.* 1998;46:137-43.

- [181] Betancourt T., Brown B., Brannon-Peppas L. Doxorubicin-loaded PLGA nanoparticles by nanoprecipitation: preparation, characterization and in vitro evaluation. *2007*;2:219-32.
- [182] Farokhzad O.C., Cheng J., Tepy B.A., Sherifi I., Jon S., Kantoff P.W., Richie J.P., Langer R. Targeted nanoparticle-aptamer bioconjugates for cancer chemotherapy in vivo. *Proc. Natl. Acad. Sci.* 2006;103:6315-20.
- [183] Cheng J., Tepy B.A., Sherifi I., Sung J., Luther G., Gu F.X., Levy-Nissenbaum E., Radovic-Moreno A.F., Langer R., Farokhzad O.C. Formulation of functionalized PLGA-PEG nanoparticles for in vivo targeted drug delivery. *Biomaterials.* 2007;28:869-76.
- [184] Vitale S.A., Katz J.L. Liquid droplet dispersions formed by homogeneous liquid-liquid nucleation: "The ouzo effect". *Langmuir.* 2003;19:4105-10.
- [185] Ganachaud F., Katz J.L. Nanoparticles and Nanocapsules Created Using the Ouzo Effect: Spontaneous Emulsification as an Alternative to Ultrasonic and High-Shear Devices. *ChemPhysChem.* 2005;6:209-16.
- [186] Lepeltier E., Bourgaux C., Couvreur P. Nanoprecipitation and the "Ouzo effect": Application to drug delivery devices. *Adv. Drug Delivery Rev.* 2014;71:86-97.
- [187] Horn D., Rieger J. Organic nanoparticles in the aqueous phase—theory, experiment, and use. *Angew. Chem., Int. Ed.* 2001;40:4330-61.
- [188] Aubry J., Ganachaud F., Cohen Addad J.-P., Cabane B. Nanoprecipitation of polymethylmethacrylate by solvent shifting: I. Boundaries. *Langmuir.* 2009;25:1970-9.
- [189] Voorhees P.W. The theory of Ostwald ripening. *J. Stat. Phys.* 1985;38:231-52.
- [190] Rajagopalan R., Hiemenz P.C. Principles of colloid and surface chemistry. Marcel Dekker, New-York. 1997;8247:8.
- [191] Karnik R., Gu F., Basto P., Cannizzaro C., Dean L., Kyei-Manu W., Langer R., Farokhzad O.C. Microfluidic platform for controlled synthesis of polymeric nanoparticles. *Nano Lett.* 2008;8:2906-12.
- [192] Stepanyan R., Lebouille J., Slot J., Tuinier R., Stuart M.C. Controlled nanoparticle formation by diffusion limited coalescence. *Phys. Rev. Lett.* 2012;109:138301.
- [193] Johnson B.K., Prud'homme R.K. Chemical processing and micromixing in confined impinging jets. *AIChE J.* 2003;49:2264-82.
- [194] D'Addio S.M., Prud'homme R.K. Controlling drug nanoparticle formation by rapid precipitation. *Adv. Drug Delivery Rev.* 2011;63:417-26.
- [195] Jun H., Fabienne T., Florent M., Coulon P.-E., Nicolas M., Olivier S. Understanding of the size control of biocompatible gold nanoparticles in millifluidic channels. *Langmuir.* 2012;28:15966-74.
- [196] Kim S.H., Kim J.W., Kim D.H., Han S.H., Weitz D.A. Polymersomes containing a hydrogel network for high stability and controlled release. *Small.* 2013;9:124-31.
- [197] Pattni B.S., Torchilin V.P. Targeted drug delivery systems: strategies and challenges. *Targeted Drug Delivery: Concepts and Design: Springer;* 2015. p. 3-38.
- [198] Decuzzi P., Ferrari M. Design maps for nanoparticles targeting the diseased microvasculature. *Biomaterials.* 2008;29:377-84.
- [199] Crommelin D.J., Florence A.T. Towards more effective advanced drug delivery systems. *Int. J. Pharm.* 2013;454:496-511.
- [200] Zagar T.M., Vujaskovic Z., Formenti S., Rugo H., Muggia F., O'Connor B., Myerson R., Stauffer P., Hsu I.-C., Diederich C. Two phase I dose-escalation/pharmacokinetics studies of low temperature liposomal doxorubicin (LTLTD) and mild local hyperthermia in heavily pretreated patients with local regionally recurrent breast cancer. *Int. J. Hyperthermia.* 2014;30:285-94.
- [201] Park E.-J., Zhang Y.-Z., Vykhodtseva N., McDannold N. Ultrasound-mediated blood-brain/blood-tumor barrier disruption improves outcomes with trastuzumab in a breast cancer brain metastasis model. *J. Control. Release.* 2012;163:277-84.
- [202] Yavuz M.S., Cheng Y., Chen J., Cobley C.M., Zhang Q., Rycenga M., Xie J., Kim C., Song K.H., Schwartz A.G. Gold nanocages covered by smart polymers for controlled release with near-infrared light. *Nat. Mater.* 2009;8:935-9.

- [203] Von Maltzahn G., Park J.-H., Lin K.Y., Singh N., Schwöppe C., Mesters R., Berdel W.E., Ruoslahti E., Sailor M.J., Bhatia S.N. Nanoparticles that communicate in vivo to amplify tumour targeting. *Nat. Mater.* 2011;10:545-52.
- [204] O'Reilly R.K., Hawker C.J., Wooley K.L. Cross-linked block copolymer micelles: functional nanostructures of great potential and versatility. *Chem. Soc. Rev.* 2006;35:1068-83.
- [205] Couvreur P., Stella B., Reddy L.H., Hillaireau H., Dubernet C., Desmaële D., Lepêtre-Mouelhi S., Rocco F., Dereuddre-Bosquet N., Clayette P. Squalenoyl nanomedicines as potential therapeutics. *Nano Lett.* 2006;6:2544-8.
- [206] Barbu E., Molnár É., Tsiouklis J., Górecki D.C. The potential for nanoparticle-based drug delivery to the brain: overcoming the blood–brain barrier. *Expert Opin. Drug Delivery.* 2009;6:553-65.
- [207] Gulyaev A.E., Gelperina S.E., Skidan I.N., Antropov A.S., Kivman G.Y., Kreuter J. Significant transport of doxorubicin into the brain with polysorbate 80-coated nanoparticles. *Pharm. Res.* 1999;16:1564-9.
- [208] Pack D.W., Hoffman A.S., Pun S., Stayton P.S. Design and development of polymers for gene delivery. *Nat. Rev. Drug Discovery.* 2005;4:581-93.
- [209] Midoux P., Pichon C., Yaouanc J.J., Jaffrès P.A. Chemical vectors for gene delivery: a current review on polymers, peptides and lipids containing histidine or imidazole as nucleic acids carriers. *Br. J. Pharmacol.* 2009;157:166-78.
- [210] Mitchell R. Innate and adaptive immunity: the immune response to foreign materials. *Biomaterials Science: An Introduction to Materials in Medicine.* Elsevier Academic Press, Amsterdam. 2004:304-18.
- [211] Frank M.M., Fries L.F. The role of complement in inflammation and phagocytosis. *Immunol. Today.* 1991;12:322-6.
- [212] Moghimi S.M., Hunter A.C., Murray J.C. Long-circulating and target-specific nanoparticles: theory to practice. *Pharmacol. Rev.* 2001;53:283-318.
- [213] Hashizume H., Baluk P., Morikawa S., McLean J.W., Thurston G., Roberge S., Jain R.K., McDonald D.M. Openings between defective endothelial cells explain tumor vessel leakiness. *Am. J. Pathol.* 2000;156:1363-80.
- [214] Hanahan D., Weinberg R.A. Hallmarks of cancer: the next generation. *cell.* 2011;144:646-74.
- [215] Bergers G., Benjamin L.E. Tumorigenesis and the angiogenic switch. *Nat. Rev. Cancer.* 2003;3:401-10.
- [216] Semenza G.L. HIF-1 and tumor progression: pathophysiology and therapeutics. *Trends Mol. Med.* 2002;8:S62-S7.
- [217] McDonald D.M., Foss A.J. Endothelial cells of tumor vessels: abnormal but not absent. *Cancer Metastasis Rev.* 2000;19:109-20.
- [218] Benjamin L.E., Golijanin D., Itin A., Pode D., Keshet E. Selective ablation of immature blood vessels in established human tumors follows vascular endothelial growth factor withdrawal. *J. Clin. Invest.* 1999;103:159-65.
- [219] Hirschi K.K., D'Amore P.A. Pericytes in the microvasculature. *Cardiovasc. Res.* 1996;32:687-98.
- [220] Matsumoto Y., Nichols J.W., Toh K., Nomoto T., Cabral H., Miura Y., Christie R.J., Yamada N., Ogura T., Kano M.R. Vascular bursts enhance permeability of tumour blood vessels and improve nanoparticle delivery. *Nat. Nanotechnol.* 2016.
- [221] Heldin C.-H., Rubin K., Pietras K., Östman A. High interstitial fluid pressure—an obstacle in cancer therapy. *Nat. Rev. Cancer.* 2004;4:806-13.
- [222] Matsumura Y., Maeda H. A new concept for macromolecular therapeutics in cancer chemotherapy: mechanism of tumoritropic accumulation of proteins and the antitumor agent smancs. *Cancer Res.* 1986;46:6387-92.
- [223] Jain R.K. Transport of molecules across tumor vasculature. *Cancer Metastasis Rev.* 1987;6:559-93.
- [224] Warburg O. On respiratory impairment in cancer cells. *Science.* 1956;124:269-70.
- [225] Stubbs M., McSheehy P.M., Griffiths J.R., Bashford C.L. Causes and consequences of tumour acidity and implications for treatment. *Mol. Med. Today.* 2000;6:15-9.

- [226] Storm G., Belliot S.O., Daemen T., Lasic D.D. Surface modification of nanoparticles to oppose uptake by the mononuclear phagocyte system. *Adv. Drug Delivery Rev.* 1995;17:31-48.
- [227] Jain R.K., Stylianopoulos T. Delivering nanomedicine to solid tumors. *Nat. Rev. Clin. Oncol.* 2010;7:653-64.
- [228] Müller R.H., Wallis K.H., Troester S.D., Kreuter J. In vitro characterization of poly (methyl-methacrylate) nanoparticles and correlation to their in vivo fate. *J. Control. Release.* 1992;20:237-46.
- [229] Brigger I., Dubernet C., Couvreur P. Nanoparticles in cancer therapy and diagnosis. *Adv. Drug Delivery Rev.* 2012;64:24-36.
- [230] Cao Z., Jiang S. Super-hydrophilic zwitterionic poly (carboxybetaine) and amphiphilic non-ionic poly (ethylene glycol) for stealth nanoparticles. *Nano Today.* 2012;7:404-13.
- [231] Roser M., Fischer D., Kissel T. Surface-modified biodegradable albumin nano- and microspheres. II: effect of surface charges on in vitro phagocytosis and biodistribution in rats. *Eur. J. Pharm. Biopharm.* 1998;46:255-63.
- [232] Sheng Y., Liu C., Yuan Y., Tao X., Yang F., Shan X., Zhou H., Xu F. Long-circulating polymeric nanoparticles bearing a combinatorial coating of PEG and water-soluble chitosan. *Biomaterials.* 2009;30:2340-8.
- [233] Xiao K., Li Y., Luo J., Lee J.S., Xiao W., Gonik A.M., Agarwal R.G., Lam K.S. The effect of surface charge on in vivo biodistribution of PEG-oligocholic acid based micellar nanoparticles. *Biomaterials.* 2011;32:3435-46.
- [234] Termsarasab U., Yoon I.-S., Park J.-H., Moon H.T., Cho H.-J., Kim D.-D. Polyethylene glycol-modified arachidyl chitosan-based nanoparticles for prolonged blood circulation of doxorubicin. *Int. J. Pharm.* 2014;464:127-34.
- [235] Klibanov A.L., Maruyama K., Torchilin V.P., Huang L. Amphiphilic polyethyleneglycols effectively prolong the circulation time of liposomes. *FEBS Lett.* 1990;268:235-7.
- [236] Saadati R., Dadashzadeh S., Abbasian Z., Soleimanjahi H. Accelerated blood clearance of PEGylated PLGA nanoparticles following repeated injections: effects of polymer dose, PEG coating, and encapsulated anticancer drug. *Pharm. Res.* 2013;30:985-95.
- [237] O'Neal D.P., Hirsch L.R., Halas N.J., Payne J.D., West J.L. Photo-thermal tumor ablation in mice using near infrared-absorbing nanoparticles. *Cancer Lett.* 2004;209:171-6.
- [238] Iyer A.K., Greish K., Seki T., Okazaki S., Fang J., Takeshita K., Maeda H. Polymeric micelles of zinc protoporphyrin for tumor targeted delivery based on EPR effect and singlet oxygen generation. *J. Drug. Deliv.* 2007;15:496-506.
- [239] Matsumura Y., Hamaguchi T., Ura T., Muro K., Yamada Y., Shimada Y., Shirao K., Okusaka T., Ueno H., Ikeda M. Phase I clinical trial and pharmacokinetic evaluation of NK911, a micelle-encapsulated doxorubicin. *Br. J. Cancer.* 2004;91:1775-81.
- [240] Pasqualini R., Arap W., McDonald D.M. Probing the structural and molecular diversity of tumor vasculature. *Trends Mol. Med.* 2002;8:563-71.
- [241] Sugahara K.N., Teesalu T., Karmali P.P., Kotamraju V.R., Agemy L., Girard O.M., Hanahan D., Mattrey R.F., Ruoslahti E. Tissue-penetrating delivery of compounds and nanoparticles into tumors. *Cancer cell.* 2009;16:510-20.
- [242] Karmali P.P., Kotamraju V.R., Kastantin M., Black M., Missirlis D., Tirrell M., Ruoslahti E. Targeting of albumin-embedded paclitaxel nanoparticles to tumors. *Nanomedicine.* 2009;5:73-82.
- [243] Puig-Saus C., Rojas L., Laborda E., Figueras A., Alba R., Fillat C., Alemany R. iRGD tumor-penetrating peptide-modified oncolytic adenovirus shows enhanced tumor transduction, intratumoral dissemination and antitumor efficacy. *Gene Ther.* 2014;21:767-74.
- [244] Wang C., Wang X., Zhong T., Zhao Y., Zhang W.-Q., Ren W., Huang D., Zhang S., Guo Y., Yao X. The antitumor activity of tumor-homing peptide-modified thermosensitive liposomes containing doxorubicin on MCF-7/ADR: in vitro and in vivo. *Int. J. Nanomed.* 2015;10:2229.

- [245] Ruoslahti E. Specialization of tumour vasculature. *Nat. Rev. Cancer.* 2002;2:83-90.
- [246] Decuzzi P., Lee S., Bhushan B., Ferrari M. A theoretical model for the margination of particles within blood vessels. *Ann. Biomed. Eng.* 2005;33:179-90.
- [247] Müller K., Fedosov D.A., Gompper G. Margination of micro-and nano-particles in blood flow and its effect on drug delivery. *Sci. Rep.* 2014;4.
- [248] Gentile F., Chiappini C., Fine D., Bhavane R., Peluccio M., Cheng M.M.-C., Liu X., Ferrari M., Decuzzi P. The effect of shape on the margination dynamics of non-neutrally buoyant particles in two-dimensional shear flows. *J. Biomech.* 2008;41:2312-8.
- [249] Lee G.Y., Qian W.P., Wang L., Wang Y.A., Staley C.A., Satpathy M., Nie S., Mao H., Yang L. Theranostic nanoparticles with controlled release of gemcitabine for targeted therapy and MRI of pancreatic cancer. *ACS nano.* 2013;7:2078-89.
- [250] Zhou H., Qian W., Uckun F.M., Wang L., Wang Y.A., Chen H., Kooby D., Yu Q., Lipowska M., Staley C.A. IGF1 Receptor Targeted Theranostic Nanoparticles for Targeted and Image-Guided Therapy of Pancreatic Cancer. *ACS nano.* 2015;9:7976-91.
- [251] Xie J., Lee S., Chen X. Nanoparticle-based theranostic agents. *Adv. Drug Delivery Rev.* 2010;62:1064-79.
- [252] Santos H.A., Bimbo L.M., Herranz B., Shahbazi M.-A., Hirvonen J., Salonen J. Nanostructured porous silicon in preclinical imaging: moving from bench to bedside. *J. Mater. Res.* 2013;28:152-64.
- [253] Davis M.E., Shin D.M. Nanoparticle therapeutics: an emerging treatment modality for cancer. *Nat. Rev. Drug Discovery.* 2008;7:771-82.
- [254] Harrington K.J., Mohammadtaghi S., Uster P.S., Glass D., Peters A.M., Vile R.G., Stewart J.S.W. Effective targeting of solid tumors in patients with locally advanced cancers by radiolabeled pegylated liposomes. *Clin. Cancer Res.* 2001;7:243-54.
- [255] de Smet M., Heijman E., Langereis S., Hijnen N.M., Grüll H. Magnetic resonance imaging of high intensity focused ultrasound mediated drug delivery from temperature-sensitive liposomes: an in vivo proof-of-concept study. *J. Control. Release.* 2011;150:102-10.
- [256] Kim D.-H., Nikles D.E., Johnson D.T., Brazel C.S. Heat generation of aqueously dispersed CoFe₂O₄ nanoparticles as heating agents for magnetically activated drug delivery and hyperthermia. *J. Magn. Magn. Mater.* 2008;320:2390-6.
- [257] Viglianti B.L., Abraham S.A., Michelich C.R., Yarmolenko P.S., MacFall J.R., Bally M.B., Dewhirst M.W. In vivo monitoring of tissue pharmacokinetics of liposome/drug using MRI: illustration of targeted delivery. *Magn. Reson. Med.* 2004;51:1153-62.
- [258] Ma X., Tao H., Yang K., Feng L., Cheng L., Shi X., Li Y., Guo L., Liu Z. A functionalized graphene oxide-iron oxide nanocomposite for magnetically targeted drug delivery, photothermal therapy, and magnetic resonance imaging. *Nano Res.* 2012;5:199-212.
- [259] Yatvin M., Kreutz W., Horwitz B., Shinitzky M. pH-sensitive liposomes: possible clinical implications. *Science.* 1980;210:1253-5.
- [260] Kanamala M., Wilson W.R., Yang M., Palmer B.D., Wu Z. Mechanisms and biomaterials in pH-responsive tumour targeted drug delivery: A review. *Biomaterials.* 2016;85:152-67.
- [261] Zhang C.Y., Chen Q., Wu W.S., Guo X.D., Cai C.Z., Zhang L.J. Synthesis and evaluation of cholesterol-grafted PEGylated peptides with pH-triggered property as novel drug carriers for cancer chemotherapy. *Colloids Surf., B.* 2016.
- [262] Hansen A.H., Mouritsen O.G., Arouri A. Enzymatic action of phospholipase A₂ on liposomal drug delivery systems. *Int. J. Pharm.* 2015;491:49-57.
- [263] Liu Y., Ding X., Li J., Luo Z., Hu Y., Liu J., Dai L., Zhou J., Hou C., Cai K. Enzyme responsive drug delivery system based on mesoporous silica nanoparticles for tumor therapy in vivo. *Nanotechnology.* 2015;26:145102.
- [264] Bae J., Maurya A., Shariat-Madar Z., Murthy S.N., Jo S. Novel Redox-Responsive Amphiphilic Copolymer Micelles for Drug Delivery: Synthesis and Characterization. *AAPS J.* 2015;17:1357-68.

- [265] Wen H.-Y., Dong H.-Q., Xie W.-j., Li Y.-Y., Wang K., Pauletti G.M., Shi D.-L. Rapidly disassembling nanomicelles with disulfide-linked PEG shells for glutathione-mediated intracellular drug delivery. *Chem. Commun.* 2011;47:3550-2.
- [266] Needham D., Anyarambhatla G., Kong G., Dewhirst M.W. A new temperature-sensitive liposome for use with mild hyperthermia: characterization and testing in a human tumor xenograft model. *Cancer Res.* 2000;60:1197-201.
- [267] Dabbagh A., Mahmoodian R., Abdullah B.J.J., Abdullah H., Hamdi M., Abu Kasim N.H. Low-melting-point polymeric nanoshells for thermal-triggered drug release under hyperthermia condition. *Int. J. Hyperthermia.* 2015:1-10.
- [268] Fomina N., McFearin C., Sermsakdi M., Edigin O., Almutairi A. UV and near-IR triggered release from polymeric nanoparticles. *J. Am. Chem. Soc.* 2010;132:9540-2.
- [269] You J., Zhang G., Li C. Exceptionally high payload of doxorubicin in hollow gold nanospheres for near-infrared light-triggered drug release. *ACS nano.* 2010;4:1033-41.
- [270] Oliveira H., Pérez-Andrés E., Thevenot J., Sandre O., Berra E., Lecommandoux S. Magnetic field triggered drug release from polymersomes for cancer therapeutics. *J. Control. Release.* 2013;169:165-70.
- [271] Kim J., Lee J.E., Lee S.H., Yu J.H., Lee J.H., Park T.G., Hyeon T. Designed fabrication of a multifunctional polymer nanomedical platform for simultaneous cancer-targeted imaging and magnetically guided drug delivery. *Adv. Mater.* 2008;20:478-83.
- [272] Yu F.T., Chen X., Wang J., Qin B., Villanueva F.S. Low Intensity Ultrasound Mediated Liposomal Doxorubicin Delivery Using Polymer Microbubbles. *Mol. Pharmaceutics.* 2015;13:55-64.
- [273] Chen T., D'Addio S.M., Kennedy M.T., Swietlow A., Kevrekidis I.G., Panagiotopoulos A.Z., Prud'homme R.K. Protected peptide nanoparticles: experiments and brownian dynamics simulations of the energetics of assembly. *Nano Lett.* 2009;9:2218-22.
- [274] Brunauer S., Emmett P.H., Teller E. Adsorption of gases in multimolecular layers. *J. Am. Chem. Soc.* 1938;60:309-19.
- [275] Schärtl W. Light scattering from polymer solutions and nanoparticle dispersions: Springer Science & Business Media; 2007. 191 pp.
- [276] Smith R.M., Hansen D.E. The pH-rate profile for the hydrolysis of a peptide bond. *J. Am. Chem. Soc.* 1998;120:8910-3.
- [277] Etrych T., Šubr V., Laga R., Říhová B., Ulbrich K. Polymer conjugates of doxorubicin bound through an amide and hydrazone bond: Impact of the carrier structure onto synergistic action in the treatment of solid tumours. *Eur. J. Pharm. Sci.* 2014;58:1-12.
- [278] Zhao Y., Sun X., Zhang G., Trewyn B.G., Slowing I.I., Lin V.S.-Y. Interaction of mesoporous silica nanoparticles with human red blood cell membranes: size and surface effects. *ACS nano.* 2011;5:1366-75.
- [279] Verma A., Stellacci F. Effect of surface properties on nanoparticle–cell interactions. *Small.* 2010;6:12-21.
- [280] Karmali P.P., Simberg D. Interactions of nanoparticles with plasma proteins: implication on clearance and toxicity of drug delivery systems. *Expert Opin. Drug Delivery.* 2011;8:343-57.
- [281] Nel A.E., Mädler L., Velegol D., Xia T., Hoek E.M., Somasundaran P., Klaessig F., Castranova V., Thompson M. Understanding biophysicochemical interactions at the nano-bio interface. *Nat. Mater.* 2009;8:543-57.
- [282] Jiang W., Kim B.Y., Rutka J.T., Chan W.C. Nanoparticle-mediated cellular response is size-dependent. *Nat. Nanotechnol.* 2008;3:145-50.
- [283] Bimbo L.M., Mäkilä E., Raula J., Laaksonen T., Laaksonen P., Strommer K., Kauppinen E.I., Salonen J., Linder M.B., Hirvonen J. Functional hydrophobin-coating of thermally hydrocarbonized porous silicon microparticles. *Biomaterials.* 2011;32:9089-99.
- [284] Mahmoudi M., Lynch I., Ejtehadi M.R., Monopoli M.P., Bombelli F.B., Laurent S. Protein–nanoparticle interactions: opportunities and challenges. *Chem. Rev.* 2011;111:5610-37.
- [285] Riikonen J., Mäkilä E., Salonen J., Lehto V.-P. Determination of the physical state of drug molecules in mesoporous silicon with different surface chemistries. *Langmuir.* 2009;25:6137-42.

- [286] Liu D., Ge Y., Tang Y., Yuan Y., Zhang Q., Li R., Xu Q. Solid lipid nanoparticles for transdermal delivery of diclofenac sodium: preparation, characterization and in vitro studies. *J. Microencapsulation*. 2010;27:726-34.
- [287] Almeida A.J., Souto E. Solid lipid nanoparticles as a drug delivery system for peptides and proteins. *Adv. Drug Delivery Rev.* 2007;59:478-90.
- [288] Liu D., Jiang S., Shen H., Qin S., Liu J., Zhang Q., Li R., Xu Q. Diclofenac sodium-loaded solid lipid nanoparticles prepared by emulsion/solvent evaporation method. *J. Nanopart. Res.* 2011;13:2375-86.
- [289] Zhou Y., Raphael R.M. Solution pH alters mechanical and electrical properties of phosphatidylcholine membranes: relation between interfacial electrostatics, intramembrane potential, and bending elasticity. *Biophys. J.* 2007;92:2451-62.
- [290] Träuble H., Eibl H. Electrostatic effects on lipid phase transitions: membrane structure and ionic environment. *Proc. Natl. Acad. Sci.* 1974;71:214-9.
- [291] Zhang L., Gu F., Chan J., Wang A., Langer R., Farokhzad O. Nanoparticles in medicine: therapeutic applications and developments. *Clin. Pharmacol. Ther.* 2008;83:761-9.
- [292] Spitzer K.W., Vaughan-Jones R.D. Regulation of intracellular pH in mammalian cells. *The Sodium-Hydrogen Exchanger*: Springer; 2003. p. 1-15.
- [293] Lee E.S., Shin H.J., Na K., Bae Y.H. Poly (L-histidine)-PEG block copolymer micelles and pH-induced destabilization. *J. Control. Release*. 2003;90:363-74.
- [294] Yin H., Lee E.S., Kim D., Lee K.H., Oh K.T., Bae Y.H. Physicochemical characteristics of pH-sensitive poly (L-histidine)-b-poly (ethylene glycol)/poly (L-lactide)-b-poly (ethylene glycol) mixed micelles. *J. Control. Release*. 2008;126:130-8.
- [295] Studart A.R., Amstad E., Gauckler L.J. Colloidal stabilization of nanoparticles in concentrated suspensions. *Langmuir*. 2007;23:1081-90.
- [296] Krishnan K.M. Biomedical nanomagnetism: a spin through possibilities in imaging, diagnostics, and therapy. *Magnetics, IEEE Transactions*. 2010;46:2523-58.
- [297] Amiri H., Mahmoudi M., Lascialfari A. Superparamagnetic colloidal nanocrystal clusters coated with polyethylene glycol fumarate: a possible novel theranostic agent. *Nanoscale*. 2011;3:1022-30.
- [298] Nguyen D.H., Lee J.S., Choi J.H., Park K.M., Lee Y., Park K.D. Hierarchical self-assembly of magnetic nanoclusters for theranostics: Tunable size, enhanced magnetic resonance imaging, and controlled and targeted drug delivery. *Acta Biomater.* 2016;35:109-17.
- [299] Zheng D.-W., Lei Q., Chen S., Qiu W.-X., Liu M.-Y., Chen X., Ding Y.-X., Li P.-H., Zhang Q.-Y., Xu Z.-S. Supermolecular theranostic capsules for pH-sensitive magnetic resonance imaging and multi-responsive drug delivery. *Journal of Materials Chemistry B*. 2015;3:8499-507.
- [300] Carenza E., Barceló V., Morancho A., Levander L., Boada C., Laromaine A., Roig A., Montaner J., Rosell A. In vitro angiogenic performance and in vivo brain targeting of magnetized endothelial progenitor cells for neurorepair therapies. *Nanomedicine*. 2014;10:225-34.
- [301] Bourdeau P., Sommers E., Mark Richardson G., Hickman J. Short-term toxicity tests for non-genotoxic effects. 1990.
- [302] Domański D., Klajnert B., Bryszewska M. Influence of PAMAM dendrimers on human red blood cells. *Bioelectrochemistry*. 2004;63:189-91.
- [303] Schaer D.J., Buehler P.W., Alayash A.I., Belcher J.D., Vercellotti G.M. Hemolysis and free hemoglobin revisited: exploring hemoglobin and heme scavengers as a novel class of therapeutic proteins. *Blood*. 2013;121:1276-84.
- [304] Amin K., Dannenfelser R.M. In vitro hemolysis: guidance for the pharmaceutical scientist. *J. Pharm. Sci.* 2006;95:1173-6.
- [305] Ciccoli L., De Felice C., Paccagnini E., Leoncini S., Pecorelli A., Signorini C., Belmonte G., Guerranti R., Cortelazzo A., Gentile M. Erythrocyte shape abnormalities, membrane oxidative damage, and β -actin alterations: an unrecognized triad in classical autism. *Mediators Inflammation*. 2013;2013:432616:1-11.
- [306] Ruoslahti E. Specialization of tumour vasculature. *Nat. Rev. Cancer*. 2002;2:83-90.

- [307] Barua S., Mitragotri S. Challenges associated with penetration of nanoparticles across cell and tissue barriers: a review of current status and future prospects. *Nano Today*. 2014;9:223-43.
- [308] Marcucci F., Lefoulon F. Active targeting with particulate drug carriers in tumor therapy: fundamentals and recent progress. *Drug Discov. Today*. 2004;9:219-28.
- [309] Zhao F., Zhao Y., Liu Y., Chang X., Chen C., Zhao Y. Cellular uptake, intracellular trafficking, and cytotoxicity of nanomaterials. *Small*. 2011;7:1322-37.
- [310] Thorn C.F., Oshiro C., Marsh S., Hernandez-Boussard T., McLeod H., Klein T.E., Altman R.B. Doxorubicin pathways: pharmacodynamics and adverse effects. *Pharmacogenet. Genomics*. 2011;21:440.
- [311] Muggia F.M., Young, C. W., & Carter, S. K. (Eds.). *Anthracycline Antibiotics in Cancer Therapy: Proceedings of the International Symposium on Anthracycline Antibiotics in Cancer Therapy*, New York, New York, 16–18 September 1981 1985;10:566.
- [312] Muggia F.M. *Cancer Chemotherapy 1*: Springer Science & Business Media; 1983.
- [313] Xia T., Kovochich M., Liang M., Mädler L., Gilbert B., Shi H., Yeh J.I., Zink J.I., Nel A.E. Comparison of the mechanism of toxicity of zinc oxide and cerium oxide nanoparticles based on dissolution and oxidative stress properties. *ACS nano*. 2008;2:2121-34.

Recent Publications in this Series

14/2016 Sanna Mäkelä

Activation of Innate Immune Responses by Toll-like Receptors and Influenza Viruses

15/2016 Mari Hirvinen

Immunological Boosting and Personalization of Oncolytic Virotherapies for Cancer Treatment

16/2016 Sofia Montalvão

Screening of Marine Natural Products and Their Synthetic Derivatives for Antimicrobial and Antiproliferative Properties

17/2016 Mpindi John Patrick

Bioinformatic Tools for Analysis, Mining and Modelling Large-Scale Gene Expression and Drug Testing Datasets

18/2016 Hilla Sumanen

Work Disability among Young Employees Changes over Time and Socioeconomic Differences

19/2016 Oyediran Olulana Akinrinade

Bioinformatic and Genomic Approaches to Study Cardiovascular Diseases

20/2016 Prasanna Sakha

Development of Microfluidic Applications to Study the Role of Kainate Receptors in Synaptogenesis

21/2016 Neha Shrestha

Mesoporous Silicon Systems for Oral Protein/Peptide-Based Diabetes Mellitus Therapy

22/2016 Tanja Holopainen

Targeting Endothelial Tyrosine Kinase Pathways in Tumor Growth and Metastasis

23/2016 Jussi Leppilähti

Variability of Gingival Crevicular Fluid Matrix Metalloproteinase -8 Levels in Respect to Point-of-Care Diagnostics in Periodontal Diseases

24/2016 Niina Markkula

Prevalence, Predictors and Prognosis of Depressive Disorders in the General Population

25/2016 Katri Kallio

The Roles of Template RNA and Replication Proteins in the Formation of Semliki Forest Virus Replication Spherules

26/2015 Hanna Paatela

Role of Dehydroepiandrosterone in High-Density Lipoprotein-Mediated Vasodilation and in Adipose Tissue Steroid Biosynthesis

27/2016 Johanna Mäkelä

Neuroprotective Effects of PGC-1 α Activators in Dopaminergic Neurons

28/2016 Sandra Söderholm

Phosphoproteomic Characterization of Viral Infection

29/2016 Mariann Lassenius

Bacterial Endotoxins in Type 1 Diabetes

30/2016 Mette Ilander

T and NK Cell Mediated Immunity in Chronic Myeloid Leukaemia

31/2016 Ninja Karikoski

The Prevalence and Histopathology of Endocrinopathic Laminitis in Horses

32/2016 Michael Backlund

Regulation of Angiotensin II Type 1 Receptor by Its Messenger RNA-Binding Proteins

33/2016 Stanislav Rozov

Circadian and Histaminergic Regulation of the Sleep-Wakefulness Cycle

